NUMERICAL MODELLING OF GLASS FIBER REINFORCED POLYMER (GFRP) CROSSARM IN TRANSMISSION TOWER SUBJECTED TO STATIC LOADING

AFIQAH NADHIRAH BINTI ROSLI

COLLEGE OF GRADUATE STUDIES
UNIVERSITI TENAGA NASIONAL

2020

NUMERICAL MODELLING OF GLASS FIBER REINFORCED POLYMER (GFRP) CROSSARM IN TRANSMISSION TOWER SUBJECTED TO STATIC LOADING

AFIQAH NADHIRAH BINTI ROSLI

A Thesis Submitted to the College of Graduate Studies, Universiti Tenaga Nasional in Fulfilment of the Requirements for the Degree of

Master of Civil Engineering

SEPTEMBER 2020

DECLARATION

I hereby declare that the thesis is my original work except for quotations and citations which have been duly acknowledged. I also declare that it has not been previously, and is not concurrently submitted for any other degree at Universiti Tenaga Nasional or at any other institutions. This thesis may be made available within the university library and may be photocopies and loaned to other libraries for the purpose of consultation.

_____

AFIQAH NADHIRAH BINTI ROSLI

Date :

ABSTRACT

Nowadays, the utilization of glass fiber reinforced polymer (GFRP) composite is being largely used in different structures. The knowledge to understand the mechanical behavior of fiberglass are extremely essential in the design and analysis of composite fiberglass. Composite materials have the ability to reduce cost especially in construction and maintenance. In Malaysia, glass fiber reinforced polymer (GFRP) was utilized as composite material in crossarm of transmission tower. However, due to some failure of GFRP crossarm, an investigation was carried out to analyze the behaviour of GFRP crossarm. Experimental testing was conducted to find out the physical and mechanical properties of existing crossarm. The results indicated that Brand A crossarm has display a superior performance in terms of physical and mechanical properties if compared with the other brands of crossarm. Maximum load capacity of GFRP was investigated by using full scale testing and numerical modelling. Numerical modelling using ANSYS software was used throughout this study to analyze the behavior of GFRP crossarm subjected to static loading. The numerical analysis then was compared with experimental testing as to validate the experimental results. It was discovered that percentage difference between experimental and numerical analysis results for all brands of GFRP crossarm falls below 5%. During the experimental testing, the Brand A sample was not failed even the load has been exceed until 80 kN which proves that Brand A sample has the ability to withstand highest working load. Parametric study for determining Factor of Safety (FOS) of GFRP crossarm for normal and broken wire condition were investigated. Strength over stress calculation was used to calculate the FOS. The result indicated that the Brand A crossarm was able to support up to 5 times Working Load (WL) for normal condition with minimum FOS of 1.08 for normal condition. Meanwhile, Brand A crossarm also able to support up to 3 times Working Load (WL) with minimum FOS of 1.10 in broken wire condition. Brand A have the highest factor of safety among all brand of crossarm. Based on depth understanding of the behaviour of GFRP crossarm, Brand A crossarm showed a high potential to utilize as composite material in crossarm of transmission tower that have a high mechanical and physical properties, high maximum load capacity and high factor of safety.

ACKNOWLEDGMENT

First and foremost, praises and thanks to Almighty ALLAH S.W.T for the gracious kindness in all the endeavours, I have taken up in my life.

I would like to express my sincere gratitude appreciation and thanks to my supervisor, Dr. Agusril Syamsir for the guidance, insight, helpful advice, and continuous encouragement provided throughout this research. His vision, sincerity and motivation have deeply inspired me. He has clearly guide me to carry out the methodology and clearly present the research work. It was a great privilege and honour to do research under his guidance.

Sincere words of thanks must also go to all team members of TNB Seeding Fund, "Optimization of Fiberglass Crossarms in Transmission Line Towers" : Daud Mohamad, Ir. Zakaria Che Muda, Dr. Salmia Beddu, Nazirul Mubin, Helmi Mansor, Dr. Zarina Itam, Nurliyana Kamal, Dr. Md Ashraful Alam, Mahyun Zainoodin, and Siti Nabihah for their encouragement assistance during the testing of the specimens and for their support throughout my research. I also would like to thank Grid Solution Expertise Department in Tenaga Nasional Berhad for providing the GFRP crossarm.

My admiration and respect goes to my family (Rosli bin Ahmad, Zarina binti Nusi, Syafiqah 'Izzati, Aqilah Fatinah, Athirah Najihah, Muhammad Sayyid Asyraf, and Saiyidah Najibah) for their endless support, love, encouragement and prayers for me. My sincere gratitude and appreciation also goes to the Institute of Energy Infrastructure (IEI) and Centre of Graduate Studies (COGS) for giving me opportunities to complete this research. Finally, to those whom I failed to mention but have been a great part of this endeavour, thank you very much.

TABLE OF CONTENTS

LIST OF TABLES

LIST OF FIGURES

LIST OF SYMBOLS

σ_1, σ_{12}	Stress in plane
Xt	Longitudinal tensile strength
Xc	Longitudinal compressive strength
Yt	Tensile strength in transverse direction
Yc	Compressive strength in transverse direction
S_1	Longitudinal shear strength
$\varepsilon_1, \varepsilon_{12}$	Strain in Plane
$\varepsilon_{1t}^f, \varepsilon_{2t}^f$	Tensile strength
$\varepsilon_{1c}^f, \varepsilon_{2c}^f$	Compressive strength
ε_{12}	Ultimate shear strain in 1,2 planes
S_L	Longitudinal shear strength
S_T	Transverse shear strength
F	Force
A	Area
dL	Deformation
L	Original length
T	Tension
C	Compression
f, S	Interaction perimeter between normal stresses σ_1 and σ_2
°C	Celcius
Mm	Millimeter
N	Newton
Kg/m^3	Kilogram Per Cubic Metre

LIST OF ABBREVIATIONS

GFRP	Glass fiber reinforced polymer
TNB	Tenaga Nasional Berhad
UV	Ultraviolet
RC	Reinforced concrete
QDs	Quantum dots
UTS	Ultimate tensile stress
HGFRP	Hollow glass fiber reinforced polymer
ILSS	Interlaminar shear strength
ASTM	American standard testing method
ACP	Ansys Composite Prepost
CSM	Chopped Strand Mat
FOS	Factor of Safety
WL	Working Load

LIST OF GLOSSARIES

GFRP	Glass fiber reinforced polymer
TNB	Tenaga Nasional Berhad
UV	Ultraviolet
RC	Reinforced concrete
QDs	Quantum dots
UTS	Ultimate tensile stress
HGFRP	Hollow glass fiber reinforced polymer
ILSS	Interlaminar shear strength
ASTM	American standard testing method
ACP	Ansys Composite Prepost
CSM	Chopped Strand Mat
FOS	Factor of Safety
WL	Working Load

LIST OF PUBLICATIONS

1. Nadhirah, A., Beddu, S., Mohamad, D., Zainoodin, M., Nabihah, S., Zahari, N. M., ... & Muda, Z. C., "Properties of fiberglass crossarm in transmission tower-a review", International Journal of Applied Engineering Research, vol. 12, no. 24, pp. 15228-15233, 2017.

2. Syamsir, A., Ishak, Z. A. M., Yusof, Z. M., Salwi, N., & Nadhirah, A., November), "Durability control of UV radiation in glass fiber reinforced polymer (GFRP)-A review", In AIP Conference Proceedings (Vol. 2031, No. 1, p. 020033). AIP Publishing, 2018.

CHAPTER 1

INTRODUCTION

1.1 Background

The main structure of the transmission line is the transmission tower. Transmission towers design must endure the weight of the transmission conductor at a certain height from the ground. Transmission tower also must be able to sustain all kinds of natural disasters. Hence, building up a transmission tower needs a large involvement from all three basic engineering concepts which are mechanical, civil, and electrical engineering concepts which are evenly applicable [1]. An electricity transmission tower consists of many parts. One of the main structures in an electricity transmission tower is the crossarm. Crossarm of the transmission tower supports the transmission conductor. Normally, the materials used for crossarms in transmission tower are wood, steel, and fiberglass [2]. There are three main materials commonly used as the structures in transmission tower which are wood, steel concrete, and Fiberglass Reinforced Polymers (GFRP).

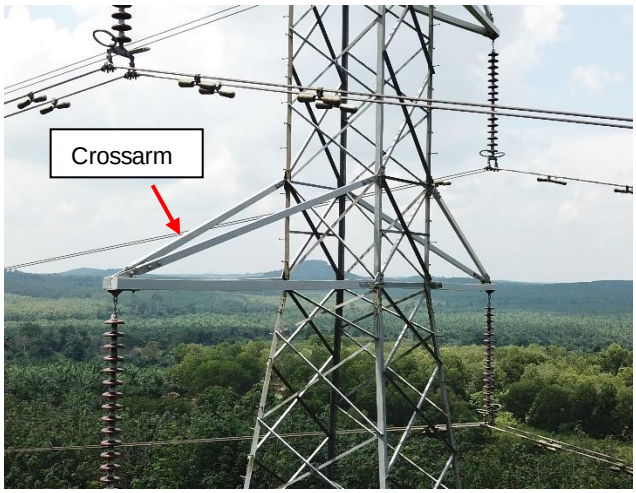

Figure 1.1 Crossarm of transmission tower

Historically, wood is the first material used as the structures in transmission line. Tenaga Nasional Berhad has utilized Chengal wood as crossarms on 132 kV suspension tower in 1963 after a successful performance on 66 kV transmission tower in 1929 [3]. Wood is a resourceful material for structural purposes and has been used

for a very long time. Wood selected as one of the structures that is economical whereas the cost of wood production is quite low when compared with the other two materials. However, wood need extra inspections after exposure to attack by natural enemies such as woodpeckers, termites, and rotting. However, the availability of large quantities of good quality of wood is limited since it is difficult to find adequate suppliers. Furthermore, wood crossarm is difficult to transport due to its heavy weight.

Steel was then selected to become an alternative material to replace wooden crossarms. Steel has flexible design, so it can be designed to its required shape. Steel is also lightweight and does not biodegrade. However, rusting could not be prevented from spreading in steel which caused by aggressive environments, chemicals and pollution which can significantly decrease its lifespan. Based on past studies by , it was observed that steel transmission structures have good track records and some of them can withstand for more than 100 years [4]. However, steel is electrically conductive and induction can also create currents which causes hazardous for the installing personnel making live, energized structural work will be more dangerous.

Hence, alternative materials were applied for a better improvement of transmission line. A comparison was made by I. Mohamed Rawi between three alternatives where Fiberglass Reinforced Polymer (GFRP) crossarm were selected to replace wood crossarm [3]. GFRP crossarm became the most favourable solution between those other two materials because it enables direct replacement on existing tower without adjustment on tower attachment fittings [3]. Fiberglass is a recent material used in the market and has a lowest life cycle costs and longest expected lifespan up to 80 years compared to wood crossarm. Furthermore, it can be easily installed and transported to areas with difficult access which can saving on installation costs. Fiberglass has greater composition compared to the other two materials. This is because fiberglass is electrically nonconductivity and has higher mechanical strength to weight ratio, making live line energized work much safer. These properties make fiberglass crossarm has a great potential to replace steel and wood crossarm [2].

However, lightning overvoltage is the major cause of the transmission line interruption in Malaysia [5]. Malaysia is one of highest region that experiencing a tremendously high number of lightning strikes every year. The impact from this lightning causes

defects on GFRP crossarms after a few years it was installed. A case study was carried out to investigate the electrical properties only along the crossarm surface during the existence of lightning based on defects found on 132 kV member crossarm [3]. This study will develop parametric studies to provide optimum design of composite GFRP crossarm. Apart from that, ultimate strength of existing crossarms will be determined. An experimental testing is carried out to find the material physical composition and material characterization of GFRP to be used as input parameter in numerical studies.

1.2 Problem Statement

Traditionally, transmission line structures have utilized treated lumber, steel, or concrete as a construction material. Recently, the latest technology of crossarm is using Fiberglass Reinforced Polymer (GFRP). The GFRP cross arm cannot be used as a single component in the insulation system. It has to be installed with insulators as a multi-insulation system to improve the lightning insulation strength of distribution and transmission lines. GFRP crossarm was found to be the most suitable materials that can be used to replace wood cross arm due to its properties which is non-conductivity and high mechanical strength-to-weight ratio [2].

However due to the Malaysian weather, many newly installed GFRP crossarms failed within a short time due to heavy rain, lightning, and wind as well as under dry and wet conditions. Based on previous analysis on defects crossarm, it was observed that the resin was found burnt and formed a charred path which revealed the internal glass structure [3]. Therefore, several assumptions arise regarding the failure of GFRP crossarm at transmission tower which is include the possibility of the failure due to the composition of fiberglass and resin itself or due to the design of the crossarm itself. These issues become crucial since it affects the production of electricity and increases costs for reparation and maintenance.

1.3 Objective

This aim of this research is to study the behaviour of glass fiber reinforced polymer (GFRP) crossarms subjected to static loading through laboratory testing and numerical modelling. In order to achieve this research, the following objectives are:

i) To determine the mechanical and physical properties of GFRP crossarms through experimental testing.

ii) To determine the maximum load capacity of glass fiber reinforced polymer (GFRP) crossarms through experimental work and finite element modelling.

iii) To determine Factor of Safety (FOS) of GFRP crossarm in normal and broken wire conditions.

iv) To determine the failure criteria of GFRP crossarms.

1.4 Scope of study

The scope of this research covers the behaviour of glass fiber reinforced polymer (GFRP) crossarm with a 4832 mm long and 127 mm width for main member and 4747mm and 102mm width for tie member. The laminated glass fiber has a thickess of 6.3 mm with different orientation. The mechanical and physical properties of GFRP are determined by using three experimental testing, which are standard test method for constituent content of composite materials, density and specific gravity of plastics by displacement, tensile properties of polymer matrix composite material, and the compressive properties of rigid plastics as an input parameter in numerical modelling.

Full scale testing of assembled crossarm by using vertical load is carried out to determine the maximum load capacity of the GFRP crossarm. The deformation of different brands of GFRP crossarms were recorded and compared. Simulation was developed by using SolidWorks software to design the 3D model of the GFRP crossarm. The numerical analysis was performed using ANSYS Composite Prepost where analysis of the maximum deformation with maximum working load carrying capacity was determined. Results from numerical modelling were validated with experimental testing.

The validated GFRP crossarm models was then continuously used for parametric studies with similar material properties in order to determine Factor of Safety (FOS) and the failure criteria of GFRP crossarm by using the Hashin failure criteria.

CHAPTER 2

LITERATURE REVIEW

2.1 Introduction

Composite is a combination of two or more sub-components in order to form a new material with better engineering properties. Forming a composite will improved the stiffness, strength to weight ratio, thermal properties and fatigue life of a material. [6]. Generally, fiber reinforced polymer (FRP) composites was designed with the combination of a strong fibers and resin binders [7].

2.2 Constituent of GFRP

GFRP are made of two constituent material which is known as fiber reinforcement with polymer resin or matrix. Laminate represents the stacked of a several layers of fiber reinforcement and matrix. These two-constituent materials can be produced to form a structure or profiles by going through the pultrusion process.

2.2.1 Fiber reinforcement

Fiber functions as to produce high strength and stiffness at lowest possible weight. This is because fiber carrying most of the strength and functions as the main load carrying member in FRP. There are various of material that can be used as fiber reinforcement but the most common one is glass, carbon, and aramid fiber. The material used as fiber reinforcement in this study is GFRP. The properties of GFRP extremely depending on the characteristics of constituent materials, fiber orientation, fiber content and matrix [8]. GFRP are inhomogeneous which it should be viewed and analyzed with different stages (fiber/resin, lamina, laminate and structure) and different scales (micro and macro mechanics) as shown in Figure 2.1 [7].

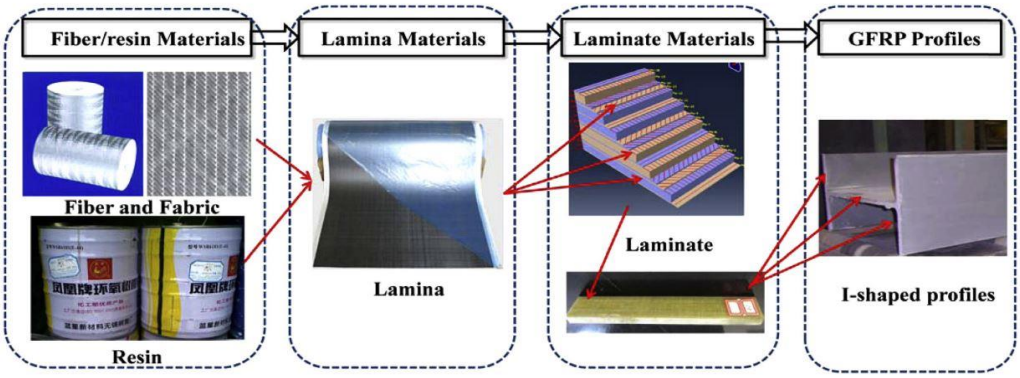

Figure 2.1 Different stages of GFRP composites [7]

2.2.2 Polymer resin

Functions of resin is to hold the fibres together, maintain the shape of the structure, protect the fibres and carry interlaminar shear between fibres. There are two categorized of resins which is thermoplastic and thermosetting resin. Generally, thermosetting resin such as epoxy, polyester, vinyl ester and phenolic is used as the binder [9].

GFRP has many applications in various of industrial areas especially in structural construction industry. In the civil engineering field, it is stated that application of composite as the main bearing components or strengthening member [7]. GFRP have been increasingly utilized because of its advantages which can ease the installation and saving production time. Pultruded GFRP will meet the suitable design criteria with reasonable cost in terms of cost efficiency. Despite of composite advantages, it still has disadvantages in serviceability and mechanical limitations [10].

2.3 Properties and behaviour of GFRP

Different types of composite have a different material properties and behaviour. GFRP composite is a lightweight composite that has a high corrosion resistance. GFRP is one of the composites that tolerant to the most aggressive environments especially in Malaysia climate and weather.

2.3.1 UV Radiation

GFRP was commonly used as external layer, and it may expose to the ultraviolet exposure and susceptible to UV radiation. The consent of the harmfulness of ultraviolet (UV) radiation to human health and polymer degradation have become an attention recently in engineering industries. The effect of UV radiation will lead to degradation of the GFRP and it will reduce the quality and performance of GFRP. Syamsir et. al. (2018), Kashi et. al. (2017), M. Giampaoli et. al. (2017), Y. Fang et al. (2017), Reis (2017) and Wong et al. (2014) have addressed problems of UV radiation towards GFRP laminate. UV radiation toward coupling steel laminates of GFRP pultruded shows increasing in the load carrying capacity of the joint due to polymerization of the adhesives [10]. UV radiation on GFRP shows the aging process of GFRP which demonstrate the signs of plasticization. The tensile strength of GFRP shows substantial descending pattern and the tensile modulus were found less affected compared to tensile strength after 6 months.

Kashi et. al. (2017) investigated the effect of marine environmental condition on durability of RC-corroded columns strengthened with GFRP sheets by using 3 methods which were directly GFRP-wrapped, GFRP-wrapped after replacing damaged concrete with repair mortar, and GFRP-wrapped after removing damaged concrete, and then repair mortar was applied around the GFRP sheet [11]. It was discovered that the method 3 has a better performance of retrofitted columns in marine environmental conditions compared with the other two methods. The increasing in stiffness obtained by coupling steel laminates to GFRP pultruded profiles was investigated. Based on past research, three different epoxy adhesives were used and compared [12]. After the UV radiations, the load carrying capacity of the joints was instead increased due to further polymerization of adhesives. It also showed better effects on the mechanical responses of the joints than those registered in the aging conditions separately analyze. Monitoring the effects of seawater ageing in GFRP composites using quantum dots (QDs) was proposed by using a simple and innovative method [13]. After 6 months exposed to seawater, the tensile strength of GFRP composite showed a substantial descending trend and the tensile modulus was less affected than tensile strength in seawater or water.

Reis (2017) discovered that for particular composite, the stiffness of the tensile specimen is not significantly affected by the ageing time, but the ultimate tensile stress (UTS) is affected by the ageing time [14]. Two types of cement-based mortar, namely polymeric and self-compacted, were applied on the GFRP sheets. A. Kashi, A. Akbar, and F. Moodi (2017) concluded that the bond strength of the polymeric mortar to GFRP sheets was more than those with self-compacted mortar [15]. Increasing use of composite especially in structures and transportation vehicles urge researchers to explore more on effect of UV resistant composites in order to minimize the harmful effect to human and degradation of polymer-based composite materials. Wong (2014) investigated the effect by using composite filled with nano-zinc oxide as UVA and UVB radiation absorbent. Appropriate amount of nano-zinc oxide filled in composite can effectively blocked the UV transmission [16].

2.3.2 Creep

Creep can be one of the method to interpret the extensive age term behaviour of unidirectional GFRP laminates and manufactured quality together with wet-lay-up practice and its constituent state [17]. Creep test is carried out in order to figure out the adhesive behaviour of the composites and their matrix and fiber phases. Paolo et al. (2017) conducted creep test to predict micromechanical behaviour for laminates and fibers of GFRP. This research shows GFRP laminates with E glass fiber reveals better rheological behaviour with percentage strain increase of resins after 3800h with range of 70% to about 100% for 6 months observation [18]. Sá et al. (2011) study shows the experimental investigations were carried out on pultruded GFRP material made of polyester and E-glass fibers at two different scales which is by laminate and full-scale profile. The experimental included flexural creep tests on 8 mm thick small-scale specimens with a span of 160mm and subjected to sustained loads corresponding to stress levels ranging from 20% to 80% of their ultimate stress [19].

Creep behaviour of pultruded GFRP showed a common reduction in instantaneous longitudinal, flexural stiffness of pultruded profile around 50% for the period of 50 years. It was predicted for the period of 1 year, the flexural stiffness will be in the range of 75 – 80% of elastic and the creep deflection will be up to 35% increase and it estimated to increase up to 100% after 50 years [19]. It was achieved through testing

concrete beams reinforced with GFRP bars which was subjected to a stress level of about 20–25% of the ultimate stress of the GFRP bars. Al-salloum and Almusallam (2007) discovered the creep effect of concrete beam reinforced with GFRP was due to loading and environment exposure. The creep effect on the concrete strain was high due to loading and environmental exposure [20].

In addition, Beddu et al. (2018) investigated the creep behaviour of GFRP on concrete footbridge resulted the reduction on the creep deformations of GFRP structures. Creep behaviour usually affected by the load level and environmental conditions which are temperature and humidity [17]. The deflection was discovered increase by approximately 40% after 5 months in flexural creep test [21]. Another study by Ascione, Berardi and Aponte (2012) presents the creep test on GFRP laminates and their constituent matrix and fiber, subjected to different stress values under constant environmental conditions [22]. It was observed that there was an increasing of the longitudinal deformation show by the polyester resin samples over time from the early hours of observation. Based on theoretical, the different rheological properties of the phases have led to a stress migration from the matrix towards the fibres. The matrix stresses have tended to be zero and the axial strains of the composites have assumed as a constant value over time due to the negligible viscous behaviour of the fibres.

2.3.3 Moisture

Major concern in outdoor applications of GFRP composites is moisture absorption. In order to recognize the mechanism of moisture absorption and the association among the microscopic structure, diffusion theory is applied which affected by moisture absorption [23]. Ray (2006) study on the cracking and flaking of polymers when exposed to elevated temperatures [24]. The study concluded that the higher temperature during hygrothermal ageing not only increases the moisture uptake rate but it also changing the local stress threshold needed for delamination nucleation. The catalyst to the diffusion of the water molecules through the composite is higher temperature. The low interlaminar shear strength (ILSS) value for high humidity absorbed level at higher temperatures may be associated with significant temperature degradation effects [24]. Other than that, Ray (2006) and Wang et al. (2015) studied ILSS of composite structure due to moisture absorption at higher temperature and

saturated in water will lead to the adverse effect which stimulate the propagation of composite damage [24][25].

There was a numerous study which have been concentrate on the variety of aggressive environments degradations in such factor of ageing of GFRP composites in general [25–27]. However, only a few studies have been identified considering the combination of moisture or water absorption as environmental agents which became the main causes of ageing mechanism that occur in GFRP structures and applications [28–32]. Zafar et al. (2012) found that the samples which have been immersed in the seawater and demineralised water has decrease their mechanical and interfacial properties. In addition, the samples slightly has gain weight due to the effect of moisture absorption [29].

Study by Sateesh et al. (2015) discovered the environmental conditions will causes the tensile strength and the degradation of GFRP composite. After a long exposure to water, the value of flexural modulus of conditioned specimens has significantly reduced [34]. M. Heshmati, R. Haghani, and M. Al-Emrani (2017) have studied the effects of environmental ageing on the mechanical properties of shear joints which made of steel and carbon GFRP or glass GFRP adherents. It was discovered that immersion at 45 °C reduce the strength and stiffness of both material and joints of GFRP [35].

Other experimental test on the effect of ageing with combination moisture and elevated temperature was conducted by Xin et al. (2016) on a perforated GFRP epoxy composite. The most influential factor of reducing flexural stiffness and bending capacity of composite structures is ageing temperature [36]. Other than that, Eslami et al. (2015) investigated on GFRP epoxy composite specimens which exposed to a humid environment. Their study includes measurement of specific temperature of moisture uptake on the mechanical degradation which results decreasing in the failure force and maximum displacement in the buckling experiments under humid conditions [37].

2.3.4 High Temperature

A comparative study by Manalo (2017) was conducted by considering longitudinal and transverse directions in order to evaluate the temperature sensitive mechanical properties of GFRP composites. Coupons sample with difference shear span-to-depth ratio tested under three-point static bending test and temperature ranging up to 200°C. The estimation of mechanical properties of the GFRP pultruded laminates for both longitudinal direction and transverse direction at varying temperature was proposed by using simplified empirical model. Manalo (2017) study shows that the mechanical properties of transversely cut specimens increased in temperature than the longitudinally cut specimens. In addition, it was found that elevated temperature has influenced the interlaminar shear and flexural strengths of GFRP composites compared to the stiffness properties [38].

Carvelli et al. (2013) study the static behaviour of concrete beams reinforced with GFRP rebars exposed to localized elevated temperatures [39]. Quasi-static three-points bending tests at room temperature were conducted to investigate the mechanical response after heating. The results discovered that the geometry of the reinforcement significantly influence on the ultimate load than on the initial stiffness of the specimens same as study by Manalo (2017) [38]. The heating temperature generates damage in concrete and partial evaporation of the matrix in the GFRP rebars without causing the disintegrate of the element.

Glass fiber reinforced polymers (GFRP) has been used as an internal reinforcement for concrete structures since corrosion of steel in reinforced concrete members became the main issue in building construction. M. Robert and B. Benmokrane (2010) evaluating the mechanical properties of sand-coated GFRP reinforcing bars subjected to the low temperatures (ranging from 0° to -100 °C) and high temperatures (ranging from 23° to 315 °C). It was concluded that mechanical properties such as tensile, shear and flexural strengths including flexural elastic modulus of GFRP bars increased while the temperature decreased [40]. Due to low temperatures, this phenomenon has increased the stiffness of the amorphous polymer matrix. Furthermore, the volume expansion of the water during the freezing contributed the initiation of microcracks

and decrease the mechanical properties if the material contained a high level of moisture, which compete with the increasing of stiffness in GFRP matrix.

Berry (2017) evaluated the effect of subfreezing temperatures on the behaviour and ultimate capacity of GFRP reinforced concrete beams [41]. Based on this study, it was concluded that the increasing of compressive and tensile strengths of the concrete is due to the decreasing in temperature. These increases are most likely due to the formation of ice within the cement matrix that attach to the concrete, and became a support in carrying the loads.

2.4 Production of GFRP

Nowadays, the most common technology used in the manufacturing industry of composite structures is the pre-impregnated method. The pre-impregnate is the method of reinforced impregnated with a specific amount of incomplete cycle of polymerisation resin, then protection film will protect one or two sides as shown in Figure 2.2. Pre-impregnates usually occurred in the form of unidirectional continuous fibres called a tape or rowing [10].

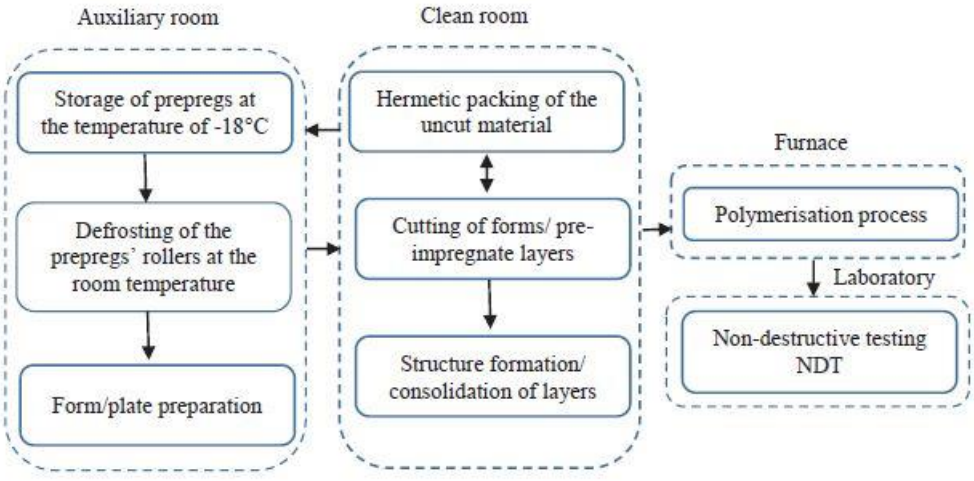

Figure 2.2 Manufacture diagram of composite [10]

Pre-impregnated method in manufacturing composites will minimize the quantity of porosity below 1% [10]. Other than that, pre-impregnated method also will increase the mechanical properties, the quality of the surface of composite and the full control

on the curing process either in temperature and pressure. The pre-impregnate is a controlled and expensive material which was sensitive to external elements. The polymerisation process is the most important stage especially during the manufacturing of composite structures. It is necessary to seal tight the element in a vacuum bag in order to avoid outside air from entering the vacuum bag and the air will diffuse inside the composite elements. This will cause voids in the composite structures in case of insufficient pressure inside the vacuum bag and resulting crack in the composite.

2.5 Composite widely used as repair material

Glass fiber reinforced polymer (GFRP) is a lightweight material that can be utilized as a repair material and retrofit material efficiently in concrete applications. Unrepaired damage of structures may cause failure on structural which lead to high cost in repairing and loss of lives. Nowadays it is important to find an alternative technique to strengthening the damage especially material that is low in cost and has shorter duration in repairing. Investigation by Bagio et al. (2014) on utilizing GFRP sheets to strengthen the reinforced concrete (RC) beams has been conducted. Various compositions to strengthening the materials can be integrated to maximize the increase in strength and repair [42]. Baggio et al. (2014) presented the effectiveness of using GFRP to boost up the shear capacity of RC shear critical beam. It was discovered that by applying the GFRP sheets will increased the overall shear capacity. The advantages of using GFRP as an anchor in repairing RC beams will improve the shear capacity and the ductility of failure and then changed the mode of failure from a shear failure to flexural failure [42]. The existence of GFRP sheet will slow down the failure of RC beams.

Research on using GFRP as repairing material were investigated by Haddad et al. (2011) on coupling effect of water recurring on concrete one-way slabs that was repaired using carbon fiber reinforced polymer (CFRP) and glass fiber reinforced polymer (GFRP) which was heated at 600°C for 2 hours. Haddad et al. (2011) discovered that upon heating then cooling the slabs, the RC slabs undergo extensive map cracking and upward cambering without spalling [43]. Other than that, it was

found that the control slab, heat-damaged slab and water recurred slabs showed a flexural failure mode with well distributed hairline cracks that was spread from the repair layers.

I. Shaw and B. Andrawes (2017) presented externally bonded GFRP laminates used as supporting shear and flexural reinforcement in RC and prestressed beam became a constructive material. Bridge girders always having a problem degradation at the ends of the beam which was exposed by the content of the salt resulting reduction in shear strength of the beam. Shaw justified that using only the mortar repair is not enough to regain back the original stiffness and strength of the beam. The mortar repair must be used with externally bonded glass and carbon FRP laminates to retrieve back the strength of the beam [44]. However, it was discovered that the GFRP laminates able to retrieve the original strength of the beam but showed no recovery in stiffness.

Many bridges and structures that are supported on steel columns or piles due to increasing load requirement and due to rusting showed an insufficient strength. An unexpected buckling of piles happens caused from the increasing in load requirement but eventually decreasing in capacity. Kaya et al. (2015) studied the effectiveness of using GFRP for retrofit of buckled steel piles or columns. Kaya et al. (2015) concluded that the installation of concrete filled GFRP jackets to quickly repair the corroded and buckled short steel columns or piles can be an effective technique to construction industry [45].

Aydin and Aktas (2015) studied to change the temporary modifications which was applied to structural element into permanent modifications using additional process. The researcher repaired the elements by gluing GFRP with heat treatment to treat the observed deficiency. It was found that by affixing the GFRP plates to steel structures after heat treatment can accomplish the objective to change the temporary to permanent repairs [46]. Other than that, Mahfouz et al. (2004) investigated the behaviour of concrete members that have been repaired using externally affixing advanced composite materials. The strength limit state for beam improving in the form of flexural and shear load when composite material bonded externally to concrete members [47]. Furthermore, the serviceability limit state also increased in the form of reduced cracks.

M. Yaqub and C. Bailey (2011) extended their research by investigating the seismic performance of repaired post-heated RC square columns with unidirectional GFRP. It was found that by wrapping the column with single layer of GFRP impressively increased the ductility, shear capacity, and the ability of energy dissipation [48]. In addition, the results also show that it will slow down the rate of strength and stiffness. Many reinforced concrete structures were experience degradation process such as spalling of concrete and extreme deflection have led to an extensive research on investigate the effects of cement based coatings when exposed to marine environments for strengthening the durability of GFRP sheets [15]. The ultimate strength of the wrapped layers of GFRP by using the polymeric mortar increase rather than the specimens without the protective mortar.

2.6 Numerical Modelling of GFRP crossarm

Unfortunately, there was a limited number of researches regarding numerical simulation on glass fiber reinforced polymer (GFRP) crossarm. Selvaraj et al. (2013) and I.M Rawi (2017) studied on finite element which mainly focus on electrical and mechanical performance on lower voltage of crossarm. Numerical modelling on GFRP crossarm was performed using SIGMA SLP and Maxwell 3D by I.M Rawi (2017) investigated the electrical properties along crossarm surface during lightning strikes. Figure 2.3 shows the current density distributed along the GFRP crossarm. It was concluded that GFRP crossarm was found to have higher dielectric strength compared to wood crossarms [3]. The study concluded that due to the lightning strike, the defects were found on crossarm member 132kV followed by surface tracking along the contaminated crossarm surface.

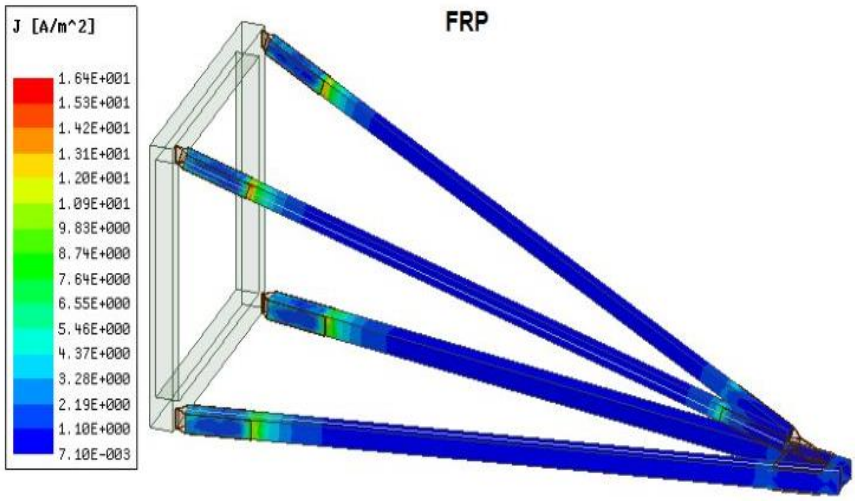

Figure 2.3 Numerical simulation on GFRP crossarm [3]

The development of a composite crossarm in a transmission line tower using GFRP pultruded profiles has been discussed by Selvaraj et al. (2013) [49]. The mechanical performance of the composite cross arm has been figured out using experimental testing and a finite element simulation as shown in Figure 2.4. Mechanical test on composite crossarm under different loads was applied in three perpendicular directions and the maximum deformation at the tip of the cross arm was recorded. The finite element (FE) model developed show the maximum stressed areas in the GFRP crossarm. The probability of using composite crossarm with steel tower body or GFRP tower body can lessen the distance of horizontal phase in order to build up more concise transmission lines.

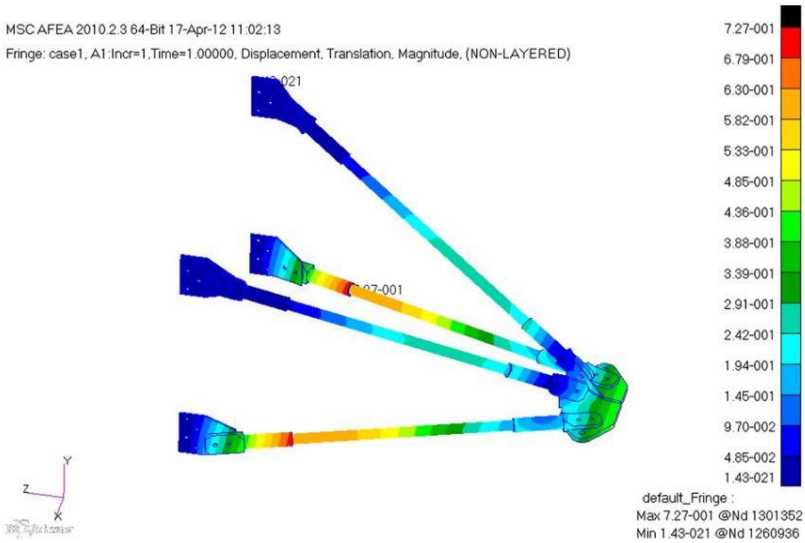

Figure 2.4 Numerical simulation of 66kV composite crossarm [49]

2.7 Factor of Safety

For the conventional materials like steel, aluminium and concrete, the strength of the material can be acknowledged as a unique value regardless its loading and dimensions. It is different for composite, composite does not have yield factor because yielding will not occur. Composite has their anisotropic nature where the physical property have different values when measured in different directions.

Factor of safety (FOS) is a fundamental measure to ensure that a structure or material does not develop any sudden failure without a presence of deformation. Smaller values of FOS will expose the design to be a failure [50]. Higher FOS also will result in higher cost on designing the structure or material. The failure of composite was measured by the minimum factor of safety which is 1.0. The laminate was safe from failure when factor of safety (FOS) is larger than 1.0 [51].

There was a study by Kaewunruen et al. (2020) discovered that by conducting full scale testing will demonstrate whether the allowable strength of the constituent materials is exceed by the service conditions or not. Determination on FOS values can be carried out by full scale testing to discover various safety aspects such as allowable deformation, brittle fracture, fatigue failure and bursting [52]. Design engineers can come up with better and suitable designs which considers whether the design is optimal, over, or under designed.

Minimum Factor of Safety for GFRP crossarm is calculated as:

$$\frac{\text{Compressive Strength (N/mm}^2\text{)}}{\text{Stress Ply of GFRP First Layer (N/mm}^2\text{)}} > 1.0 \qquad (2.1)$$

2.8 Failure Criteria

Prediction failure of GFRP composites itself is very complicated, since it is represented by a curve in their loading field rather than a point. Continuous efforts have been taken for developing failure criteria for unidirectional fiber composites and their laminates. Based on previous studies, there are numerous failure criteria which have been proposed for modelling composite materials. These include the Tsai–Hill criteria, Tsai–Wu criteria, Hashin criteria, and Puck criteria [52–55].

2.8.1 Maximum Stress Theory

Maximum stress theory is a non-interactive failure criteria which do not consider the interaction between stresses acting on the lamina. When the stress exceeds the respective allowable stress, the material will fail, as shown in Equations 2.2, 2.3 and 2.4. The maximum stress theory is more applicable for brittle modes of failure, closer to longitudinal and transverse tension. It also does not consider the stress interaction (uniaxial), hence they under predicts the strength in the presence of combined action of in plane stresses.

Fiber	$\sigma_1 \geq X_t \quad \lvert \sigma_1 \rvert \geq X_c$;	(2.2)
Matrix	$\sigma_2 \geq Y_t \quad \lvert \sigma_2 \rvert \geq Y_c$;	(2.3)
Shear	$\lvert \sigma_{12} \rvert \geq S_1$	(2.4)

where

$\sigma_{1,} \sigma_{12}$ = Stress in plane

X_t = Longitudinal tensile strength

X_c = Longitudinal compressive strength

Y_t = Tensile strength in transverse direction

Y_c = Tensile strength in transverse direction

S_1 = Longitudinal shear strength

2.8.2 Maximum Strain Theory

Maximum strain theory is the non-interactive failure criteria which do not consider the interaction between stresses acting on the lamina. When the strain exceeds the respective allowable strain, the material will fail as shown in Equation 2.5, 2.6 and 2.7. The maximum strain criteria also retain the weakness of maximum stress criteria, but the difference is it has some interaction with longitudinal and transverse direction due to poisson effect.

Fiber $$\varepsilon_1 \geq \varepsilon_{1t}^f \quad |\varepsilon_1| \geq \varepsilon_{1c}^f ; \tag{2.5}$$

Matrix $$\varepsilon_2 \geq \varepsilon_{2t}^f \quad |\varepsilon_2| \geq \varepsilon_{2c}^f ; \tag{2.6}$$

Shear $$|\varepsilon_{12}| \geq \varepsilon_{12}^f . \tag{2.7}$$

where

$\varepsilon_1, \varepsilon_{12}$ = Strain in plane

$\varepsilon_{1t}^f, \varepsilon_{2t}^f$ = Tensile strength

$\varepsilon_{1c}^f, \varepsilon_{2c}^f$ = Compressive strength

ε_{12} = Ultimate shear strain in 1,2 planes

2.8.3 Tsai-Hill, Tsai- Wu, Hashin and Puck Criteria

Tsai–Hill criteria was widely used in composite laminate analysis. Despite its disadvantages that does not considering tensile and compressive behaviour, it is acknowledged as comprehensive and historical use in composite laminate analysis [57]. Tsai-Hill criteria became a good basis for comparison between other failure criteria. Tsai-Hill criteria shows the highest error which is 19.9% by using a minimization algorithm to apply the equations of the criteria to the experimental data of the unidirectional composite laminate and multidirectional composite laminate specimens [57]. It was clearly shown that the Tsai-Hill criteria is not suitable to be used in experimental data because it does not consider tensile and compressive properties separately. Due to this limitation, other criteria were developed by Tsai and Wu in 1971 [54].

The Tsai–Wu criteria also was widely used especially in finite element modelling of composites [57]. Different with Tsai-Hill criteria, Tsai-Wu criteria considering tensile and compressive strengths. In Equation 2.9, subscripts T refer to tension and C refer to compression, respectively.

$$f_1\sigma_1 + f_2\sigma_2 + f_{22}\sigma_2^2 + f_{66}\sigma_{12}^2 + 2f_{12}\sigma_1\sigma_2 = 1.0 \quad (2.8)$$

$$f_1 = \frac{1}{S_{1T}} - \frac{1}{S_{1C}}\ ;\ f_2 = \frac{1}{S_{2T}} - \frac{1}{S_{2C}}\ ;$$
$$f_{11} = \frac{1}{S_{1T}} - \frac{1}{S_{1C}}\ ;\ f_{22} = \frac{1}{S_{2T}} - \frac{1}{S_{2C}}\ ; \quad (2.9)$$
$$f_{66} = \frac{1}{S_{12}^2}$$

where

$\sigma_1, \sigma_2, \sigma_{12}$ = Stress in plane

f, S = Interaction perimeter between normal stresses σ_1 and σ_2

T = Tension

C = Compression

Tsai-Wu criteria predicts matrix failure well with the optimal parameters, but it underestimate the fibre failures which lead to a high mean error of 15% [57]. Other than that, the optimal strength parameters found by Koh and Madsen (2018) was less than the strengths stated in past studies for natural fibre composites. Koh and Madsen (2018) concluded that Tsai-Wu criteria which use interaction parameters having difficulties in determine an experimental result. In a low-velocity impact simulation, Li et al. (2019) recommended not to use Tsai–Wu failure criteria [58]. The greatest irreversible displacement was shown by Tsai-Wu criteria due to inaccurate separation of tensile and compression damage.

The Hashin criteria was developed 9 years later after the Tsai-Wu criteria in 1980. Hashin criteria assumes that the failure criteria for transverse isotropy is separate into fiber and matrix failure modes [59]. Then, further break down into tensile and compressive failure state on each of failure modes. Hashin criteria defines four modes which is tensile fiber mode, fiber compressive mode, tensile matrix mode and compressive matrix mode by which the composite could fail and considering the stress

state. Hashin criteria produces a hollowing effect in propagation direction and damage shape [58]. Hashin's matrix compression criteria could be a great choice for engineering applications due to its moderate prediction and simple expression [58].

The Puck failure criteria was developed in 1998 and chosen because of its achievement in the World-Wide Failure Exercise, whereby 12 of the leading theories for predicting failure in composite laminates have been investigated against experimental evidence [60]. The Puck' s criteria has shown particularly well in determined the ultimate strengths of multi- directional composite laminates. Puck's approach was categorized into two main failure types which is Fibre Failure (FF) and Interfibre Fracture (IFF) [57]. Puck's criteria are the criterion that considered a degradation model, characterize laminate behaviour after crack initiation and allowing a variance between initial and final failure. Koh and Madsen (2018) stated that the Puck criteria shares several of the Hashin criteria's advantages. Puck criteria displayed the lowest mean error of 6% among the other four criteria [57]. Other than that, Puck criteria is the best criteria for interfibre failures because it allows three different modes of matrix failure.

Evaluation of the accuracy of failure criteria comparing with experimental data, using tension and compression testing of multiaxial composite laminates, was presented by Koh and Madsen (2018). The Tsai–Hill, Tsai–Wu, Hashin, and Puck failure criteria was compared with experimental data by using tension and compression tests of five layups flax composite laminates with varying fibre orientations [57]. The Hashin and Puck criteria have the lowest error compared with experimental data. Hashin's criteria being simpler to implement, while Puck's criteria have the advantages of considering a plastic failure regime after yielding. Lopez et al. (2009) studied the choice of the failure criterion as well as the load conditions give an impact on the optimal weight of a laminated composite [61]. The chosen criteria will closely reflect the actual behaviour of the laminated composites. This study concluded that the correct choice of failure criterion is essential to determine the optimization of laminated composites.

2.9 Research Gap

The GFRP crossarm has been used successfully to replace the function of steel and wood as the crossarm in transmission tower. Based on previous studies, GFRP has shown great properties and behaviour against environmental condition with many advantages to be used as a composite material. However, many GFRP crossarm was failed during six months of installation which is well before its lifespan. These issues will affect the production of electricity and will increase the maintenance cost as electricity demand increases every day.

Past studies published on this subject was limited to the numerical studies on the GFRP properties and behaviour as well as electrical properties along the crossarm surface during lightning strikes. GFRP crossarm functions as a support to the transmission conductor that holds the transmission wire, hence the GFRP crossarm must endure the load from the wire as well as the conductor. GFRP crossarm must consider both conditions which is normal condition (all wires intact), and broken wire condition. Hence, the mechanical properties of GFRP crossarm by considering these both conditions needs to be determined.

Generally, there are no proper standard and specification published by manufacturers or standard association on the design, material composition and even in manufacturing process in determining the properties and the behaviour of GFRP crossarm. Designing with a better performance of GFRP crossarm will become challenging since crossarm functions to withstand all kinds of loads and internal stresses. Therefore, the physical and mechanical properties as well as behaviour on 275 kV full assembly of GFRP crossarm by using finite element method still needs to be studied since this research area is still limited.

CHAPTER 3

MATERIALS AND METHODOLOGY

3.1 Introduction

This study is based on comparison data from experimental works and data from numerical modelling. Forensic analysis was performed on 275kV 24L type fiberglass crossarm. Forensic testing includes the determination on the physical and mechanical properties of the fiberglass crossarm.

The experimental program was divided into two parts. The first part is the material characterization of GFRP crossarm. The second part is a full-scale testing on the full crossarm members subjected to maximum working loads. The engineering data and materials properties were required to be used as an input parameter to analyse the GFRP crossarm. An experimental work was conducted to investigate the structural performance and integrity of GFRP crossarm under working loads.

The numerical modelling on complete set of composite crossarm was simulate by using ANSYS 18.2 software. Simulation on crossarm consists of modelling and analysis on the complete set of crossarm subjected to working loads. The results obtained from numerical modelling were compared with the experimental data for validation purposes. The work program are illustrated in Figure 3.1.

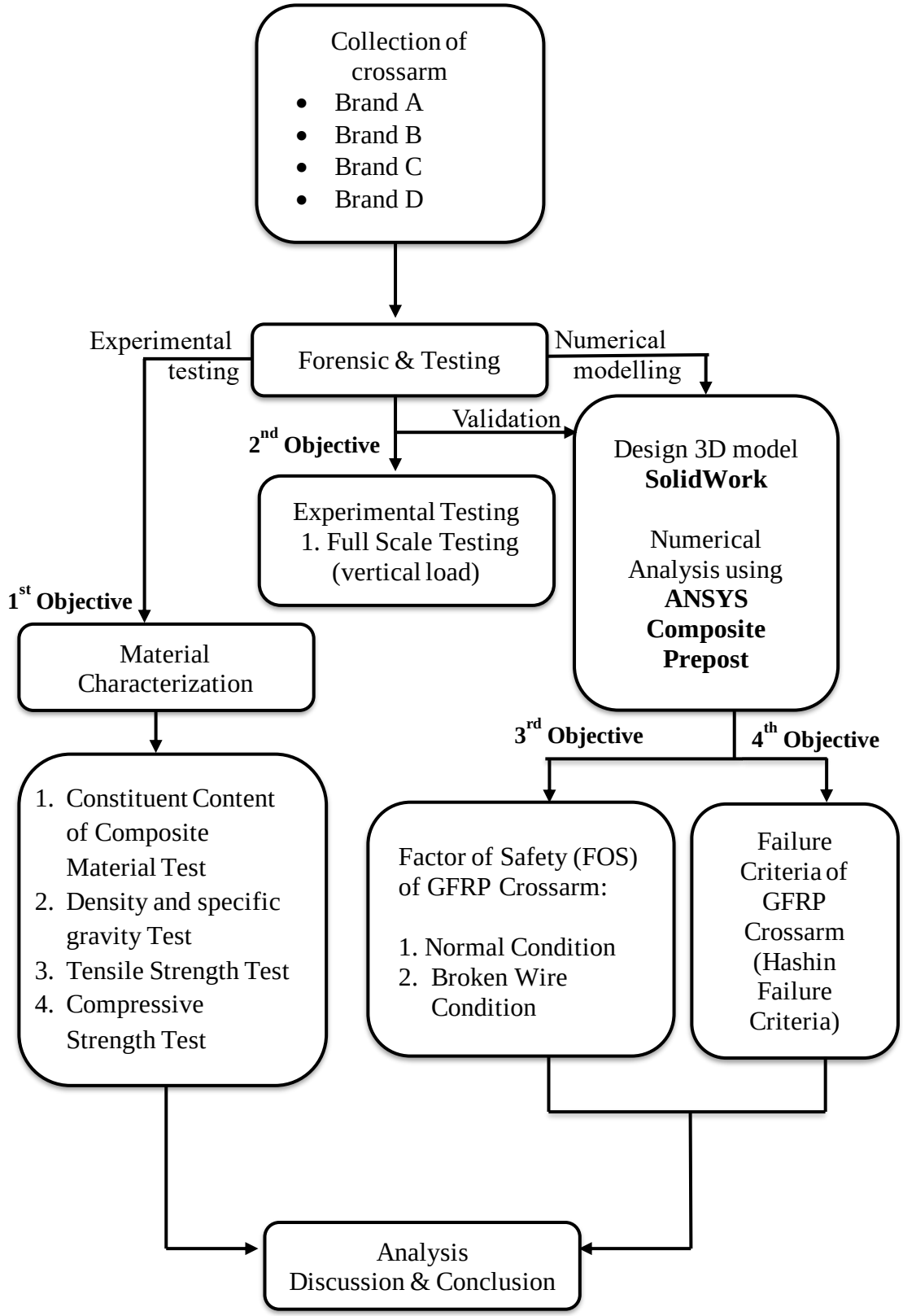

Figure 3.1 Work Program

3.2 Sample Preparation

3.2.1 Glass Fiber Reinforced Polymer (GFRP) crossarm

Glass fiber reinforced polymer (GFRP) crossarm that were tested in this research are Brand A, Brand B, Brand C, and Brand D crossarms. These four brands were compared and the results is discussed in Chapter 4. The composite crossarm type 275 kV 24L was used in this research, since this type was discovered to have failed and broken during its services. The standard specifications of GFRP crossarm are illustrated in Figure 3.2 and Figure 3.3.

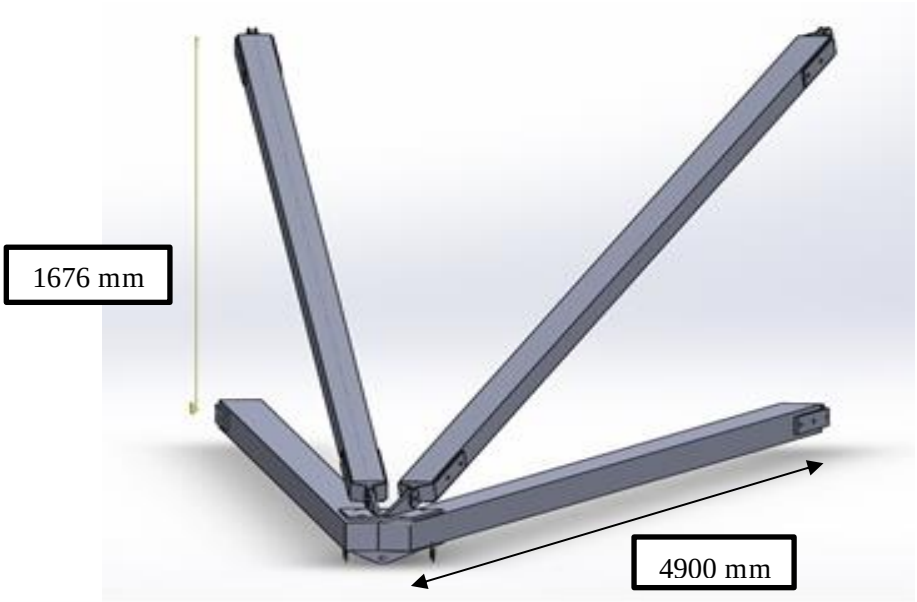

Figure 3.2 Standard specifications of fiberglass crossarm

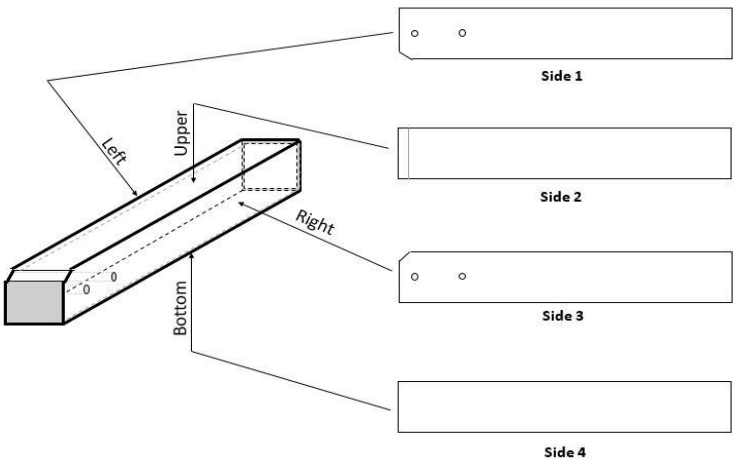

Figure 3.3 Schematic of crossarm.

3.3 Material Characterization

The engineering data and materials properties were required to use as an input parameter to analyse the GFRP crossarm. Four experimental testing which is Constituent Content of Composite Materials, Density and Specific Gravity of Plastics by Displacement, Tensile Properties of Polymer Matrix Composite Material, and Compressive Properties of Rigid Plastics were conducted in order to obtain the material properties of GFRP crossarm.

3.3.1 Standard Test Method for Constituent Content of Composite Materials

Standard Test Method for Constituent Content of Composite Materials (ASTM D3171-99) or resin burn-off test was conducted to determine the constituent content of GFRP composite. This standard has two approaches to determine the constituent of composite which is Test Method I, and Test Method II. Test Method I have been chosen because this method is physically removes the matrix or resin by ignition by one of seven procedures, which leaves the reinforcement unaffected. The matrix was burnt to 500°C to 600°C or more in a muffle furnace for a maximum of 6 hours depending on the sample size. The muffle furnace will burn off the matrix and leave the reinforcement or fiber. The sample was placed in a desiccator and allow to cool in room temperature. The reinforcement or fiber was placed then under confocal microscope as in Figure 3.4 to obtain clear picture of fiber composition as well as fiber orientation.

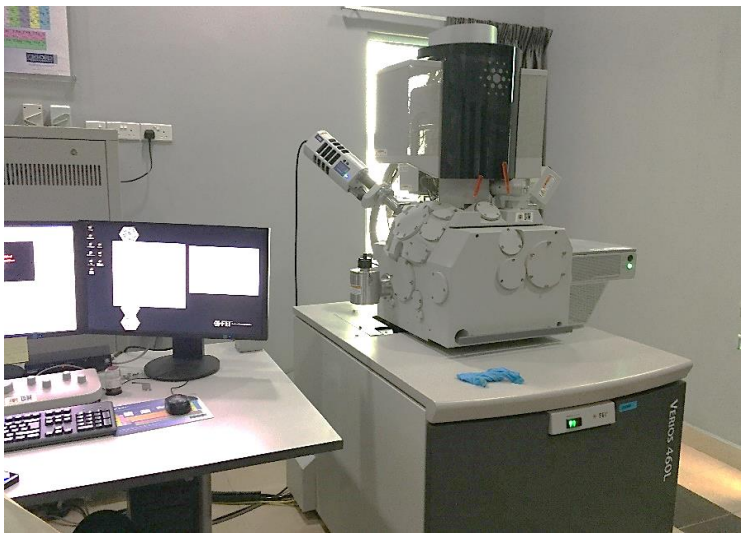

Figure 3.4 Confocal Microscope

3.3.2 Standard Test Method for Density and Specific Gravity

Standard Test Method for Density and Specific Gravity (Relative Density) of Plastics by Displacement (ASTM D792-00) was conducted to determine the mass of a specimen of the solid plastic in air. It is then immersed in water, its apparent mass upon immersion is determined, and its specific gravity (relative density) was calculated. Densometer was used to measure air permeability of the glass fiber reinforced polymer (GFRP). The total of five specimen were prepared for this experiment. The dimension of the test specimen was illustrated in Figure 3.6.

Figure 3.5 Densometer

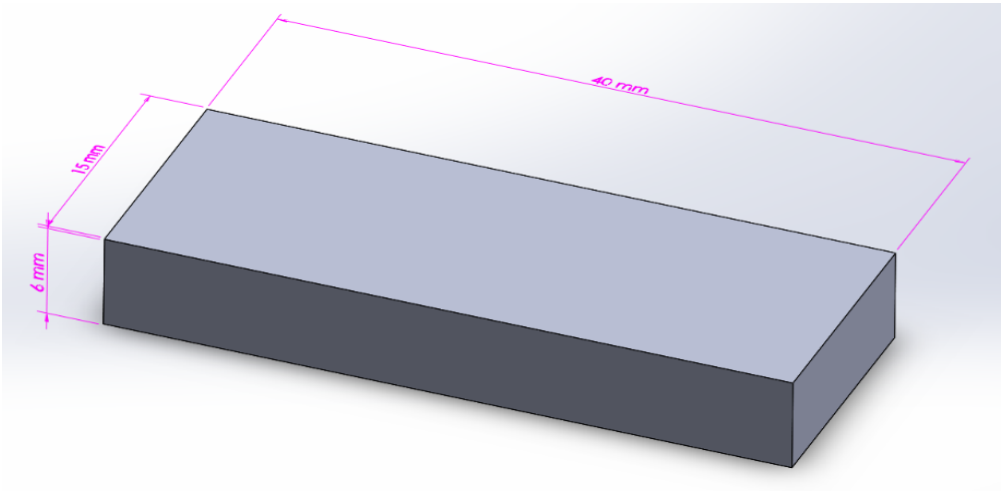

Figure 3.6 Dimension of test specimen

3.3.3 Standard Test Method for Tensile Properties

Standard Test Method for Tensile Properties of Polymer Matrix Composite Materials (ASTM D3039/D 3039M-00) was conducted to determine the tensile strength, ultimate tensile strain and tensile chord modulus of elasticity of a specimen. A thin flat strip of material having a constant rectangular cross section is mounted in the grips of a universal testing machine (INSTRON) and monotonically loaded in tension while recording load. The ultimate strength of the material can be determined from the maximum load carried before failure. The crosshead speed is 1mm/min and the direction of the specimen is unidirection and y-direction. The total of five specimen were prepared for this experiment. The dimension of the test specimen was illustrated in Figure 3.7.

Tensile Modulus or Young Modulus is a measure of stiffness of an elastic material. Tensile Modulus is defined as the ratio of stress (force per unit area) along an axis to strain (ratio of deformation over initial length). Tensile Modulus can be calculated in Equation 3.1.

$$E = \frac{\text{Stress } (\sigma)}{\text{Strain } (\varepsilon)} = \frac{(F/A)}{(dL/L)} \qquad (3.1)$$

where

F = Force

A = Area

dL = Deformation

L = Original length

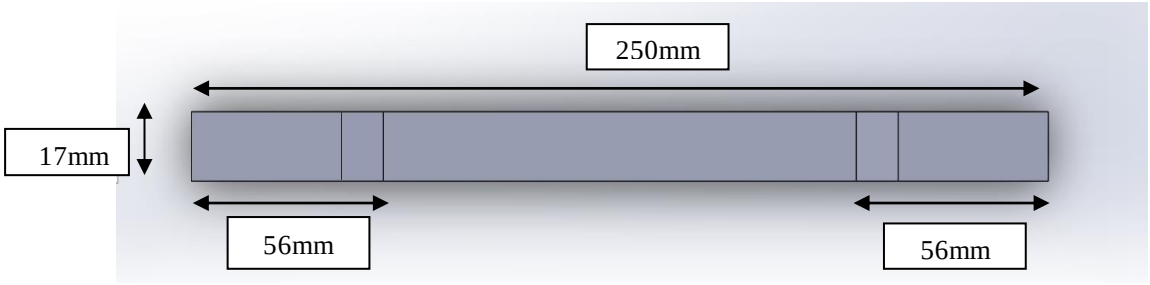

(a) Top view

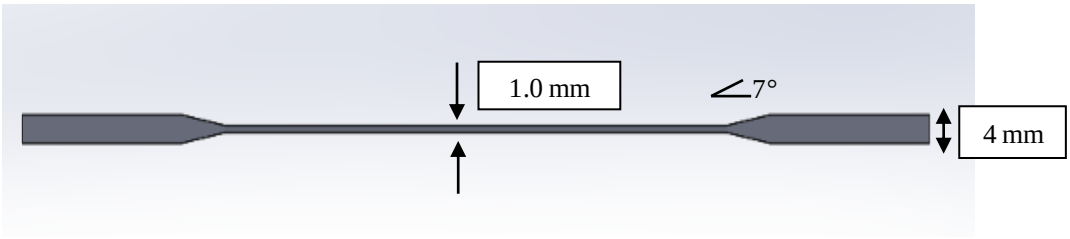

(b) Side view

Figure 3.7 (a) Top view of test specimen , (b) Side view of test specimen

Figure 3.8 Universal Testing Machine (INSTRON)

3.3.4 Standard Test Method for Compressive Properties of Rigid Plastics

Standard Test Method for Compressive Properties of Rigid Plastics (ASTM D695-15) was conducted to determine the compressive properties of a specimen when employed under conditions approximating those under which tests are made. A rectangular cross section thin flat strip is mounted in the grips of a universal testing machine (INSTRON) and monotonically loaded in compression while recording load. The crosshead speed is 1mm/min. The total of five specimen were prepared for this experiment. The dimension of the test specimen was illustrated in Figure 3.9.

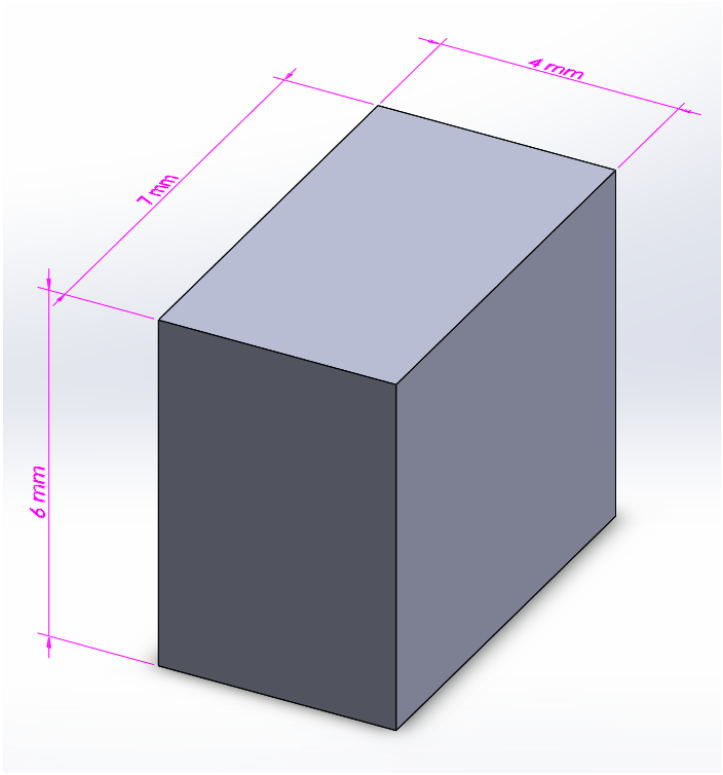

Figure 3.9 Dimension of test specimen

3.4 Forensic and Experimental Testing

The forensic part in this study is a full-scale testing on the full crossarm members subjected to maximum working loads. A laboratory work was conducted to investigate the structural performance and integrity of GFRP crossarm under different working loads. The working load was continuously applied until the GFRP crossarm fail to withstand its structure.

Numerical modelling on complete set of composite crossarm was performed by using ANSYS 18.2 software. The engineering data and material properties of GFRP crossarm obtained was used as input on this simulation. Simulation on crossarm consists of modelling and analysis on the complete set of crossarm subjected to working loads. The results obtained from numerical modelling were compared with the experimental data for validation purposes.

3.4.1 Full Scale Testing

Full scale testing of GFRP crossarm was conducted on a different brands of glass fiber reinforced polymer (GFRP) crossarm which is Brand A, Brand B, Brand C and Brand D. The objective of full scale testing is to determine the flexural properties of GFRP crossarm under different working loads. The setup of the full scale testing was shown in Figure 3.10. Hydraulic pump carrying a vertical working load as stated in Table 3.1 was applied at the tip of the crossarm until the crossarm fail to withstand its structure. Full assembly of composite GFRP crossarm was conducted for normal condition and only vertical loading was applied. The full scale testing takes up to 30 minutes or until the crossarm fail to withstand its structure to completely recorded the results. Deformation of the GFRP crossarm was measured by using ruler that was tied to the tripod and placed in the middle of the crossarm. The deformation was recorded and compared with numerical modelling result. The standard passing criteria for a GFRP crossarm to maintain its structural integrity is at least 2.0 x working load. The details of the load applied was tabulated in Table 3.1.

Table 3.1 Details of working load

Type of load	Load (N)
Vertical	21248 (1WL) 42496 (2WL)

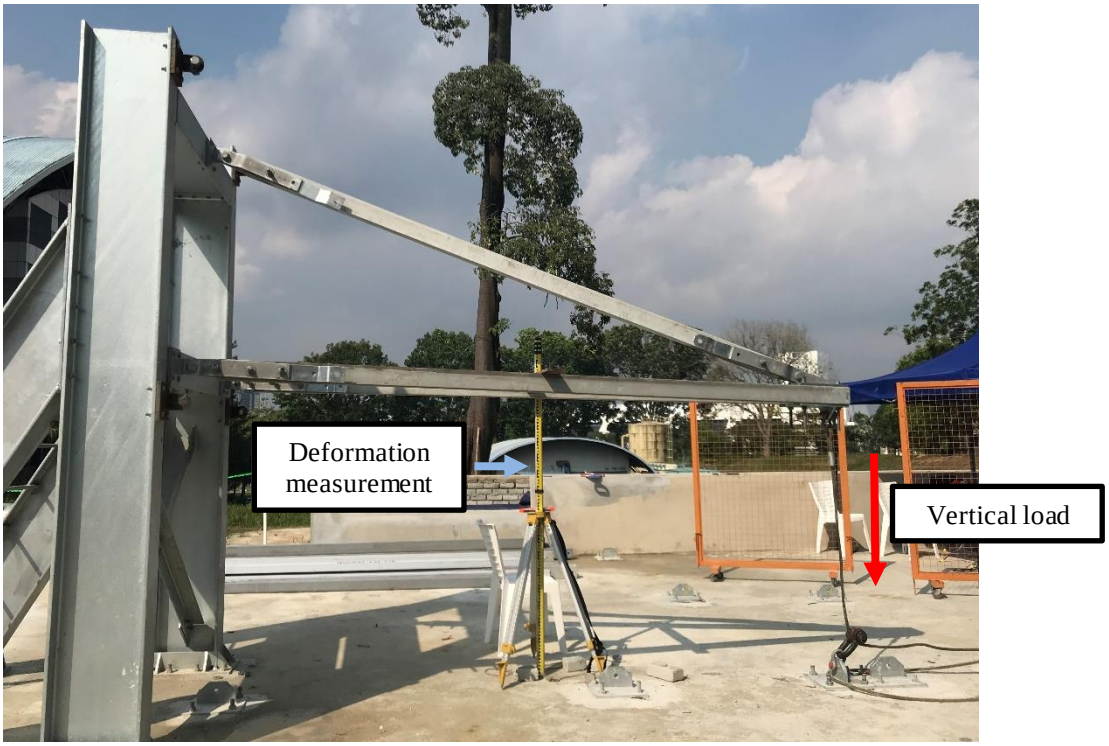

Figure 3.10 Experimental set up of full scale testing

3.5 Numerical Modelling

Numerical model on complete set of composite crossarm was simulated by using ANSYS 18.2 software. The component system used in ANSYS was ANSYS Composite Prepost (ACP) to analyse layered composites. The workbench in ANSYS was illustrated in Figure 3.11. Simulations were performed to those four brands of crossarm which was from Brand A, Brand B, Brand C and Brand D manufacturer. Simulation on crossarm consists of modelling and analysis on the complete set of crossarm subjected to different working loads. There are four different laminate

properties were analyzed in this study, naming as laminate Brand A, laminate Brand B, laminate Brand C and laminate Brand D.

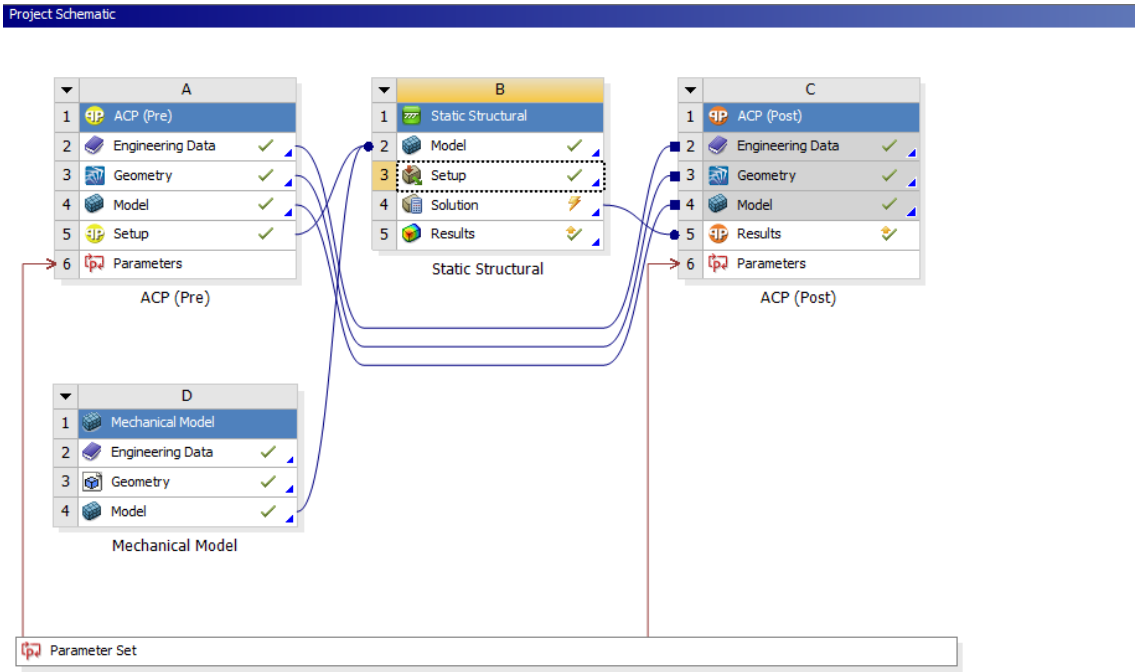

Figure 3.11 The Workbench in ANSYS 18.2

3.5.1 Mesh and Boundary Conditions

As shown in Figure 3.12, the crossarm model consists of four square (0.12 x 0.12 mm^2) composite beam with a length of 4.9 m. The square beam composed stacked plies of glass laminate, each ply having different thickness and orientation. The GFRP crossarm was meshed with SOLID46 elements. SOLID46 is used to model the GFRP composite laminates. The element was defined by the eight nodes having three degrees of freedom at each nodes, x, y and z directions. The element was illustrated by eight nodes, layer thickness, direction angles and orthotropic material properties. The details of the meshing were tabulated in Table 3.2. The other ends of the cross arm were constrained to be pinned supported in all directions.

Table 3.2 Details meshing of GFRP Crossarm

Nodes	65496
Elements	51448

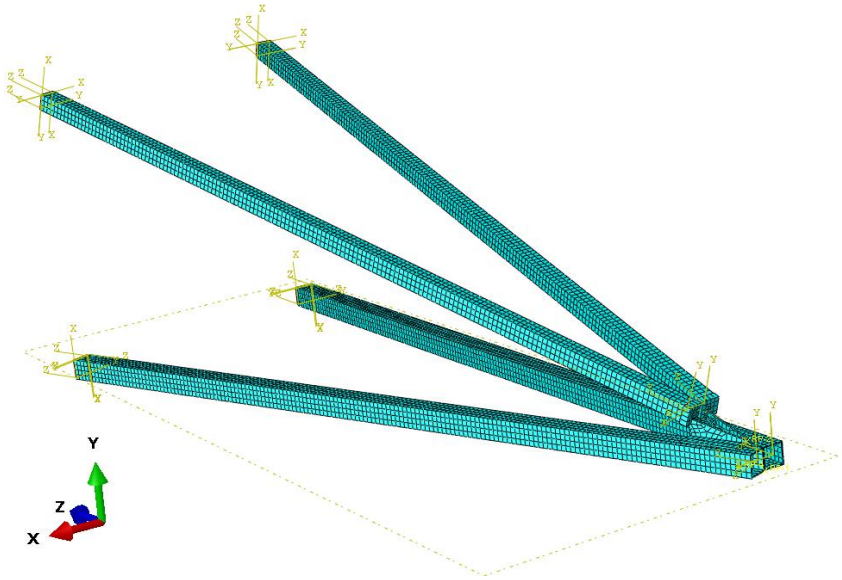

Figure 3.12 Geometry and mesh of the finite element of composite crossarm

3.5.2 Composite Orientations

Different brands have a different orientations and different thickness of lamina. Resin burn-off was carried out on a sample to identify the thickness and the orientations of each lamina. Four laminate orientation were tabulated in Table 3.3, 3.4, 3.5 and 3.6. These laminate orientations were required as an input parameter in order to perform analysis in ANSYS software.

Table 3.3 Orientation of each layer for Brand A laminate

Layer	Fiber orientation	Thickness (mm)
1	0	0.7
2	45	0.7
3	0	0.7
4	-45	0.7
5	0	0.7
6	-45	0.7
7	0	0.7
8	45	0.7
9	0	0.7

Table 3.4 Orientation of each layer for Brand B laminate

Layer	Fiber orientation	Thickness (mm)
1	45	0.5
2	-45	0.5
3	90	0.7
4	0	3.6
5	45	0.7

Table 3.5 Orientation of each layer for Brand C laminate

Layer	Fiber orientation	Thickness (mm)
1	45	1.04
2	0	3.12
3	45	1.04

Table 3.6 Orientation of each layer for Brand D laminate

Layer	Fiber orientation	Thickness (mm)
1	45	0.72
2	-45	0.72
3	0	0.72
4	0	0.72
5	0	0.72
6	0	0.72
7	0	0.72
8	0	0.72
9	-45	0.72
10	45	0.72

3.5.3 Laminate Properties

The material that constitutes each ply of the crossarm called laminate. The mechanical properties of each laminate are presented in Table 3.9. Four laminate properties as shown in Table 3.7, which is laminate Brand A, Brand B, Brand C and Brand D were considered to evaluate the structural deformation of the cross arm. These laminate properties were required as an input parameter in order to perform analysis in ANSYS software.

Table 3.7 Parameter required to perform analysis in ANSYS

Parameter
Density
Young's modulus, E_1
Young's modulus, E_2
Young's modulus, E_3
Poisson's ratio (V_{12}=V_{13}=V_{23})
Shear modulus (G_{12}=G_{13}=G_{23})
Ultimate tensile stress, X_{1T}
Ultimate compressive stress, X_{1C}
Ultimate tensile stress, X_{2T}
Ultimate compressive stress, X_{2C}
Ultimate shear stress, S_{12}
Ultimate shear stress, (S_{13} = S_{23})

3.5.4 Working Loads

Simulation on crossarm consists of modelling and analysis on the complete set of crossarm subjected to working loads as per TNB specification as shown in Table 3.8. The working load as shown in Figure 3.12 was applied on the crossarm using ANSYS software to estimate the maximum deformation, stress, strain and failure load. The load was applied at the tip of crossarm as shown in Figure 3.13. Simulation input for type of working load was limited to vertical loading only which follows the type of working load used in flexural testing of full assembly of GFRP crossarm. This limitation purposes were to validate the simulation results with experimental results in order to find the correlation percentage of simulation results.

Table 3.8 Working Load (WL) as per TNB specification for 275kV 24 L

Type of Working Loads (N)					
Normal condition (All wires intact)			**Brokenwire condition**		
Vertical	Transverse	Longitudinal	Vertical	Transverse	Longitudinal
21248	11718	0	16,436	8,667	25,779

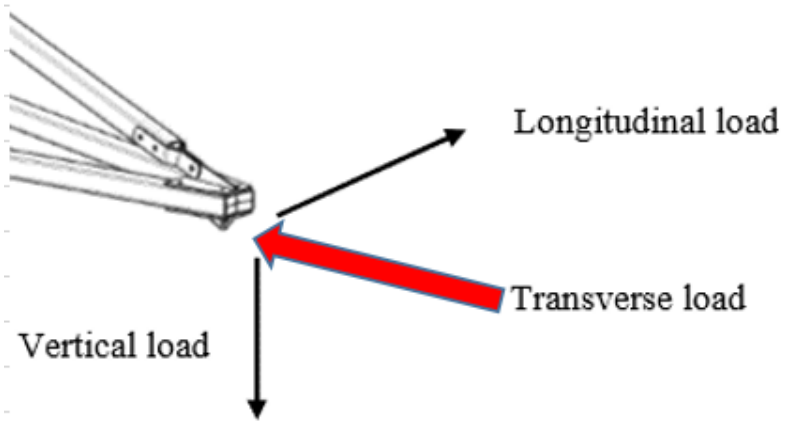

Figure 3.13 Working load in Numerical Model

3.6 Parametric Study

Parametric study is one of the main objectives in this research that allow nominations parameters for evaluation purposes. Besides, parametric study is important in order to define the parameter range and find the best design constraints in designing the GFRP crossarm. The flow of parametric study is shown in Figure 3.14. The variable parameters of these parametric study are load and deformation.

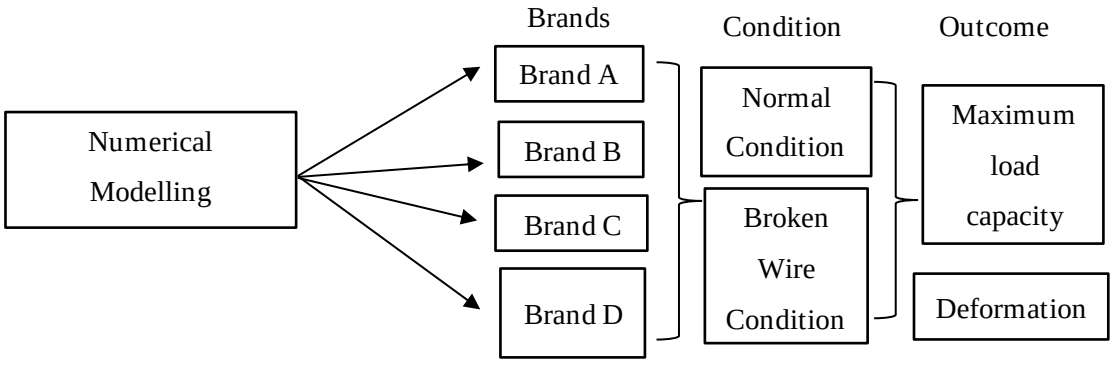

Figure 3.14 Parametric study flow

3.6.1 Working Loads

Simulation on crossarm consists of modelling and analysis on the complete set of crossarm subjected to different type of working loads was tabulated in Table 3.9 and 3.10. All of the three types of working load (vertical load, transverse load and longitudinal load) were used in this parametric study. Finalized maximum capacity load of different brands of GFRP crossarm are discussed in details on Chapter 4.

Table 3.9 Working Loads (WL) for normal condition

Working Load	Type of Working Loads (N)	
	Vertical	Transverse
1 WL	21248	11718
2 WL	42496	23436
3 WL	63744	35154
4 WL	84992	46872
5 WL	106240	58590
6 WL	127488	70308

Table 3.10 Working Loads (WL) for broken wire condition

Working Load	Working Loads (N)		
	Vertical	Transverse	Longitudinal
1 WL	16436	8667	25779
2 WL	32872	17334	51558
3 WL	49308	26001	77337
4 WL	65744	34668	103116

3.6.2 Deformation

All of the three types of working load which is longitudinal load (x), vertical load (y), and transverse load (z) were used to measure deformation. Due to limitation to measure x and z deformation, only the vertical loading (y) was applied until the crossarm fail to withstand its structure in full scale testing. The deformation was measured at 30 minutes by using a ruler that was tied to the tripod and was placed at the middle of the crossarm as shown in Figure 3.10. Deformation of GFRP composite due to the compressive stress can cause failure.

3.7 Hashin Failure Criteria

GFRP composite has a different failure mode which are fiber failure, matrix failure and delamination changes. The composite part is very susceptible to compressive force or deformation that can cause delaminating or de-bonding of the lamina (GFRP layers) in the member of GFRP crossarm. Initial de-bonding will appear when the stress at certain layer of lamina is greater than the strength of the resin or glass fibers. Due to the continuous applied load, the de-bonding will continue to the other layers or lamina up to failure occur to the GFRP composite crossarm.

Hashin (1973) come up with theory that consider two failure mechanisms which is based on the failure of the fiber and the other was based on the failure of matrix analyse between both tension and compression. Failure of fiber was causes by the longitudinal stress, with reference to the fiber orientation, transversal and tangential stress to the fiber. Hashin's theory criteria is based on failure modes as fiber failure and matrix failure. Fiber tension and compression are calculated in Equation 3.8 and 3.9. Fiber matrix tension and compression are calculated in Equation 4.0 and 4.1.

Fiber Tension

$$\left(\frac{\sigma_{11}}{X_T}\right)^2 + \frac{\sigma_{12}^2 + \sigma_{13}^2}{S_{12}^2} = \begin{cases} \geq 1 & \text{failure} \\ < 1 & \text{no failure} \end{cases} \tag{3.8}$$

Fiber Compression

$$\left(\frac{\sigma_{11}}{X_C}\right)^2 = \begin{cases} \geq 1 & \text{failure} \\ < 1 & \text{no failure} \end{cases} \tag{3.9}$$

Matrix Tension

$$\frac{\left(\sigma_{22} + \sigma_{33}\right)^2}{Y_T^2} + \frac{\sigma_{23}^2 - \sigma_{22}\sigma_{33}}{S_{23}^2} + \frac{\sigma_{12}^2 + \sigma_{13}^2}{S_{12}^2} = \begin{cases} \geq 1 & \text{failure} \\ < 1 & \text{no failure} \end{cases} \tag{3.10}$$

Matrix Compression

$$\left[\left(\frac{Y_C}{2S_{23}}\right)^2 - 1\right]\left(\frac{\sigma_{22} + \sigma_{33}}{Y_C}\right) + \frac{(\sigma_{22} + \sigma_{33})^2}{4S_{23}^2} + \frac{\sigma_{23}^2 - \sigma_{22}\sigma_{33}}{S_{23}^2} + \frac{\sigma_{12}^2 + \sigma_{13}^2}{S_{12}^2} = \begin{cases} \geq 1 & \text{failure} \\ < 1 & \text{no failure} \end{cases} \tag{3.11}$$

where

σ = Stress in plane

X_t = Longitudinal tensile strength

X_c = Longitudinal compressive strength

Y_t = Tensile strength in transverse direction

Y_c = Compression strength in transverse direction

S_{12} = Longitudinal shear strength

S_{23} = Transverse shear strength

3.8 Important Assumptions

There were a few assumptions made in this research. It was assumed that the material characteristic of the GFRP crossarm was different since the GFRP came from a different source of manufacturer that uses a different fabrication method. Therefore, the material and physical characterization testing were conducted in order to figure out the characteristics of GFRP crossarm from different manufacturers. The testings that were conducted are density and specific gravity of plastics by displacement, tensile properties of polymer matrix composite material and compressive properties of rigid plastics. Other than that, it was assumed that the flexural properties will be different since different brand of crossarms have different strength. Full assembly tests were conducted to determine the flexural properties of GFRP crossarm under different working loads. In addition, a simulation has been done in order to validate the experimental testing.

3.9 Chapter Summary

This chapter presents the materials and methodology used in this research. The explanation starts with the simple work flow taken throughout this research. Materials used in experimental testing which is GFRP crossarm with different brands, Brand A, Brand B, Brand C and Brand D were briefly discussed in this chapter. All conducted test and equipment used to analyse the experimental data were also discussed in this chapter. In addition, numerical modelling on full assembly of GFRP crossarm using ANSYS 18.2 software were also briefly discussed. In the next chapter, the result obtained from the experimental testing and numerical modelling in this research are briefly discussed.

CHAPTER 4

RESULT AND DISCUSSION

4.1 Introduction

This chapter discusses on the result of experimental testing and numerical modelling in order to achieve the objective of this study. The material characterization using four experimental testing which are density and test method for constituent content of composite materials, specific gravity of plastics by displacement, tensile properties of polymer matrix composite material and compressive properties of rigid plastics were conducted to obtain the material properties of the glass fiber reinforced polymer (GFRP). This material properties which is density, tensile properties and compression strength were required to use an input parameter in numerical modelling analysis. Different brands will shows a different material properties and the comparison of material properties are discussed in this chapter. Results for flexural testing for full assembly of GFRP crossarm under normal condition (all wires intact) are explained further.

Results of numerical simulation for full assembly of GFRP crossarm were compared with experimental results of flexural testing for validation purposes. The parametric study which aimed to find out the maximum load capacity and maximum deformation for every brand of GFRP crossarm were evaluated in this chapter.

4.2 Material Characterization

Characterization of GFRP crossarm was determined by using Standard Test Method for Constituent Content of Composite Materials (ASTM D3171-99), Standard Test Method for Density and Specific Gravity (Relative Density) of Plastics by Displacement (ASTM D792-00), Standard Test Method for Tensile Properties of Polymer Matrix Composite Materials (ASTM D3039/D 3039M-00), and Standard Test Method for Compressive Properties of Rigid Plastics (ASTM D695-15).

4.2.1 Density, fiber content, void content and fiber arrangement

Table 4.1 summarize the average fibre content, densities and void contents of samples produced by Brand A, Brand B, Brand C and Brand D manufacturer.

Table 4.1 Density, fibre mass fraction, and fibre volume

Sample	Fibre mass fraction (%)	Fibre volume fraction (%)	Density (kg/m^3)	Void content (%)
Brand A	78.04	70.45	2030	13.97
Brand B	64.67	61.95	1800	19.43
Brand C	64.11	60.85	1890	13.87
Brand D	74.17	67.40	1900	17.31

The densities of samples taken from different manufacturers fall in the range of 1800 – 2030 kg/m^3 and the highest density was recorded in samples produced by Brand A. This is due to the higher glass fibre content in the Brand A sample. It is expected Brand A sample to be denser due to the presence of more glass fibre in the sample.

The void content in samples manufactured by Brand B and Brand D are relatively higher than samples produced by established manufacturers, Brand A and Brand C. The higher fibre content coupled with the lower void content of Brand A samples could be one of the possible reasons for the superior mechanical performance of Brand A samples as compared to samples produced by other manufacturers.

Further analysis was also conducted by examining the cross-section of the crossarm at different locations to check if any variation in density, fibre content and thickness from different side of GFRP crossarm as illustrated in Figure 3.3. Furthermore, this analysis also to analyse the different fibre arrangement at different side of GFRP crossarm across the thickness of the sample.

4.2.1.1 Brand A Crossarm

This section explained the details of the fiber arrangement of Brand A's sample. Figure 4.1 shows the variation in density, fibre content and thickness of Brand A's sample at different side of GFRP crossarm. The thickness of the cross-section is fairly constant which is between 6.3 to 6.5mm. The fiber content and densities are not only fairly constant at all sides 1,2,3 and 4 but even at the corner.

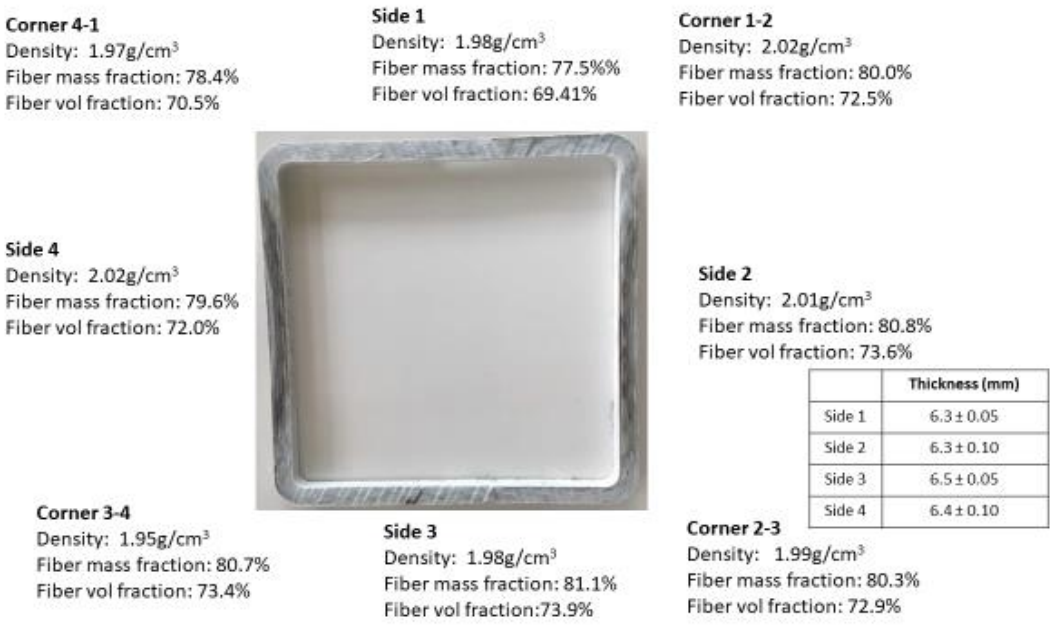

Figure 4.1 Density, fiber mass fraction and fiber volume fraction of Brand A's sample

Apparently, only two types of glass fiber form were used for the fabrication of the GFRP crossarms. Resin burn-off was carried out on sample taken from side 2 and it was found that the fabrication of the pultruded crossarms comprised of fibre glass roving and fibre glass mat. There was 5 layers of continuous fibre rovings are interspaced with 4 layers of stitched glass fibre mat as shown in Figure 4.2. This finding resemblance with finding reported by Muttashar et al. (2017) on Brand A's pultruded sample [62]. The fiber layering appears to be well consolidated even at the corner. This explain for the consistent fibre content even at the corner of the profile. The radius of curvature at the corner appear to be more rounded. Thus, it helps to reduce the stress concentration point at the corner.

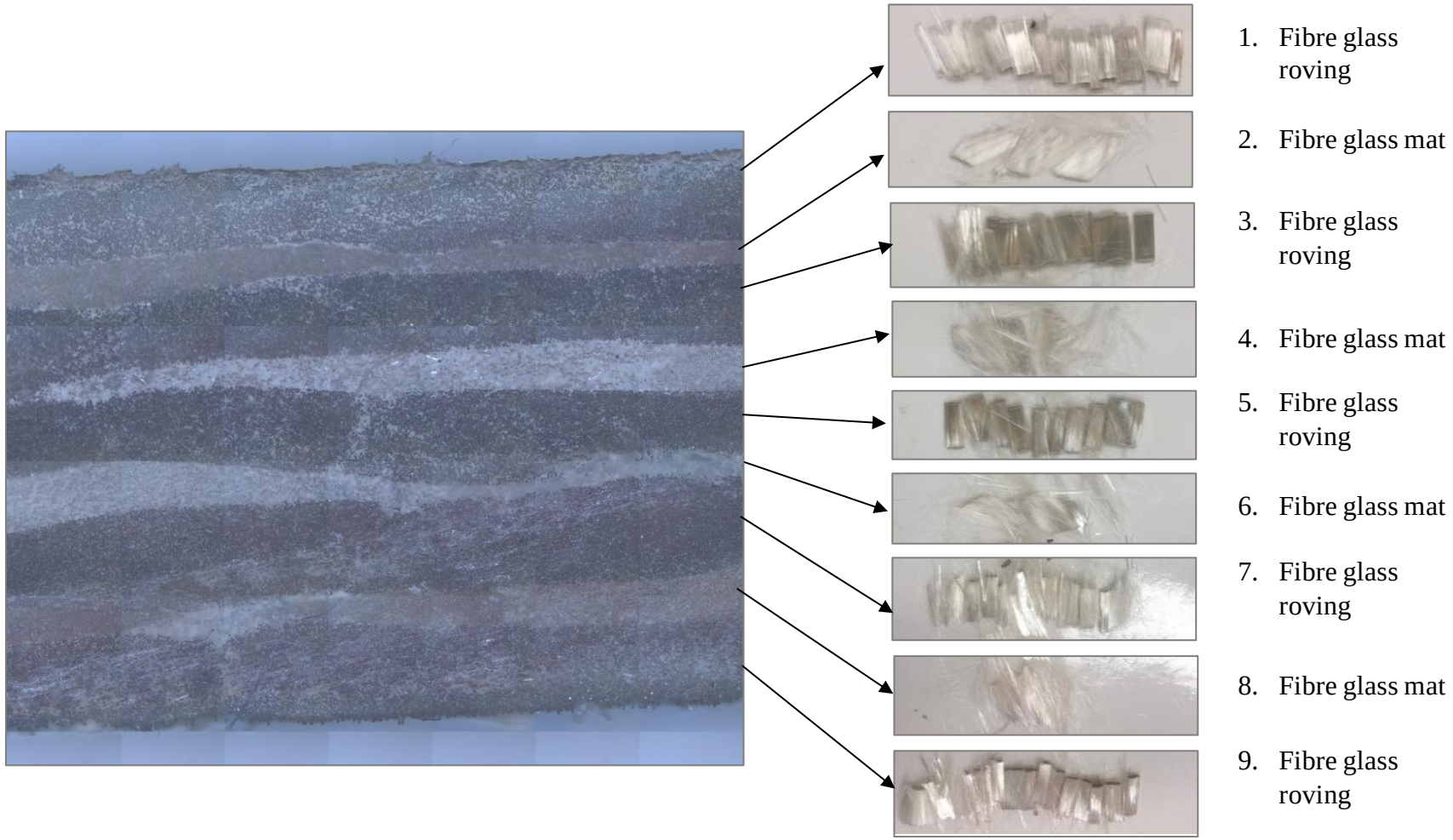

Figure 4.2 Fiberglass layering of Brand A's sample obtained from confocal microscope

Table 4.2 Fiber arrangement of Brand A crossarm

No. of Layer	Fiber direction (°)	Thickness (mm)
Layer 1	0	0.7
Layer 2	45	0.7
Layer 1	0	0.7
Layer 3	-45	0.7
Layer 4	0	0.7
Layer 5	-45	0.7
Layer 6	0	0.7
Layer 7	45	0.7
Layer 8	0	0.7
Layer 9	0	0.7

4.2.1.2 Brand B Crossarm

Figure 4.3 shows the variation in density, fibre content and thickness of Brand B's sample at different side of GFRP crossarm. There are some irregularities in the thickness of the cross-section. The thickness of the cross-section varies from 5.7 to 6.8mm. Difference on value of cross-section up to 1mm for a load bearing structural component need to be looked into seriously since it will affect the overall performance of the structure. The fibre content and densities of Brand B's sample are discovered fairly constant at sides 1,2,3 and 4. However, there was a slight drop in fibre content and densities observed at the corners that could be a potential weak point in the crossarms.

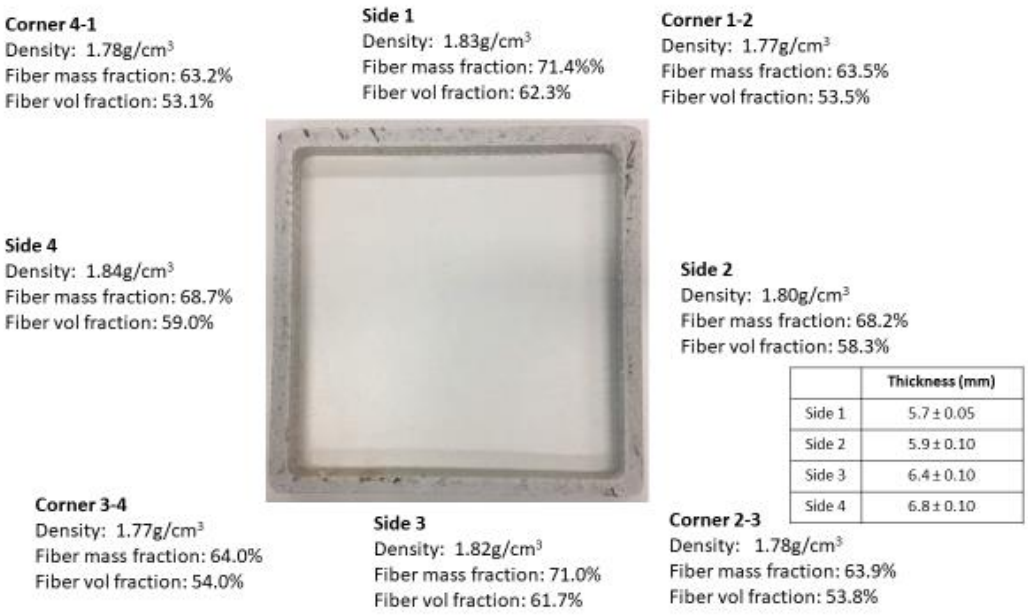

Figure 4.3 Density, fiber mass fraction and fiber volume fraction of Brand B's sample

There was 5 layers of different fiberglass observed on the Brand B's sample. Resin burn-off was carried out on sample taken from side 2 and it was found that the fabrication of the pultruded crossarms comprised of several layers of fiberglass and those are fiberglass cloth, fiberglass chopped strand mat, continuous fiberglass roving and fiberglass stitch mat as shown in Figure 4.4. From Figure 4.4, it can be seen that the major portion of the layers was contributed by the continuous fiberglass roving which providing the stiffness and strength to the pultruded crossarms.

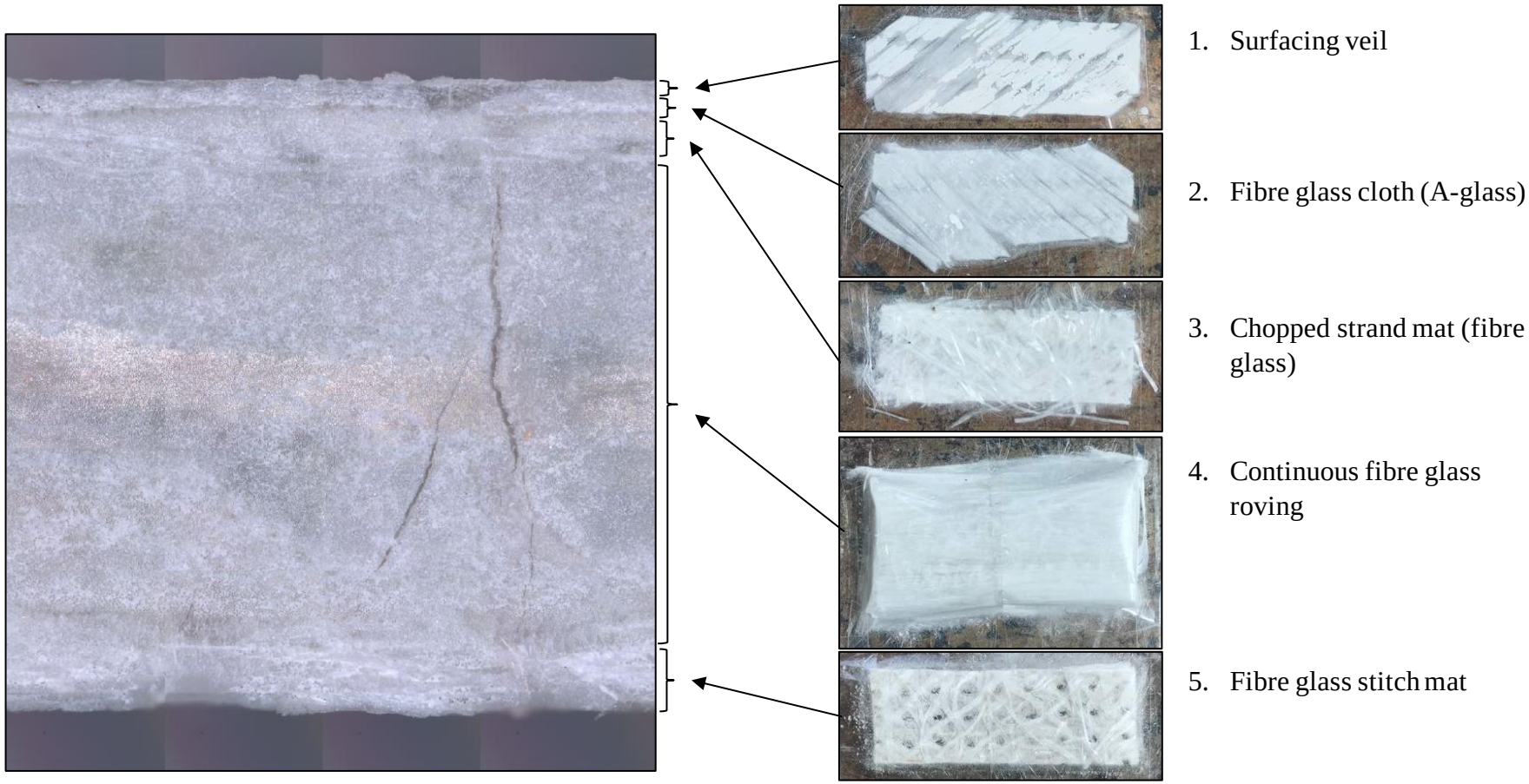

Figure 4.4 Fiberglass layering of Brand B's sample obtained from confocal microscope

Table 4.3 Fiber arrangement of Brand B crossarm

No. of Layer	Fiber direction (°)	Thickness (mm)
Layer 1	45	0.5
Layer 2	-45	0.5
Layer 1	90	0.7
Layer 3	0	3.6
Layer 4	45	0.7
Layer 5	45	0.5

4.2.1.3 Brand C Crossarm

The variation in density, fibre content and thickness of Brand C's sample at different side of GFRP crossarm was shown in Figure 4.5. The thickness of the sample cross-section produced by Brand C falls in the range of 5mm which is relatively thin. The fibre content and densities are fairly constant at all sides 1,2,3 and 4. There was only two types of fiberglass form were used for the fabrication of the GFRP crossarms which is Fiberglass Chopped Strand Mat and Fiberglass Roving. Besides, there was only 3 layers of different fiberglass observed on the Brand C's sample as shown in Figure 4.6. The Fiberglass Roving was sandwiched with the Chopped Strand Mat (CSM).

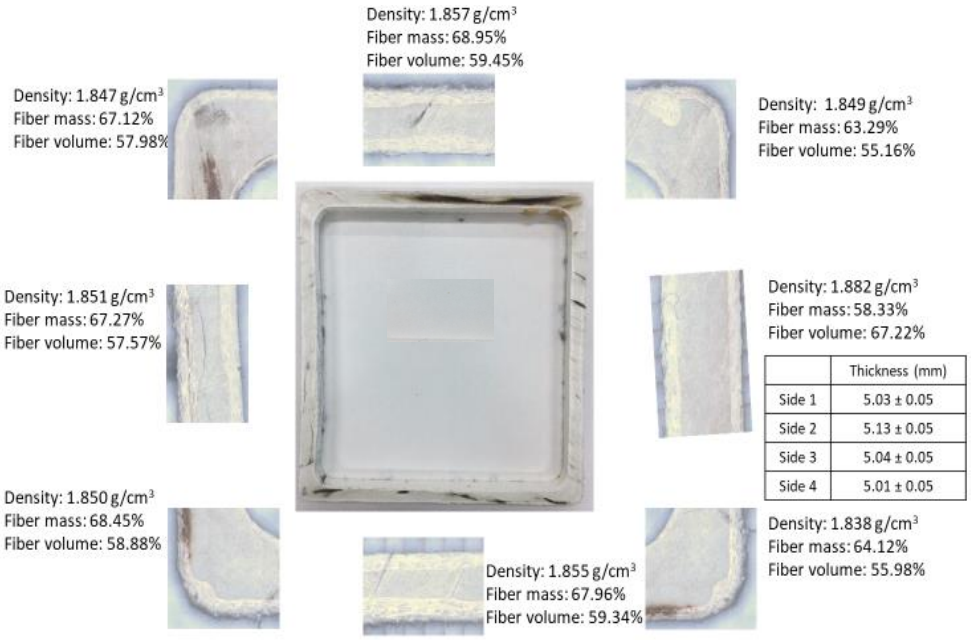

Figure 4.5 Density, fiber mass fraction and fiber volume fraction of Brand C's sample

Based on cross-section of sample shown in Figure 4.5, it can be seen that the thickness of the CSM which formed the skin layer varies at different locations. The fiber layering is not well consolidated as samples produced by Brand A especially at the corner. This explain for the variation in fibre content at different location of the profile.

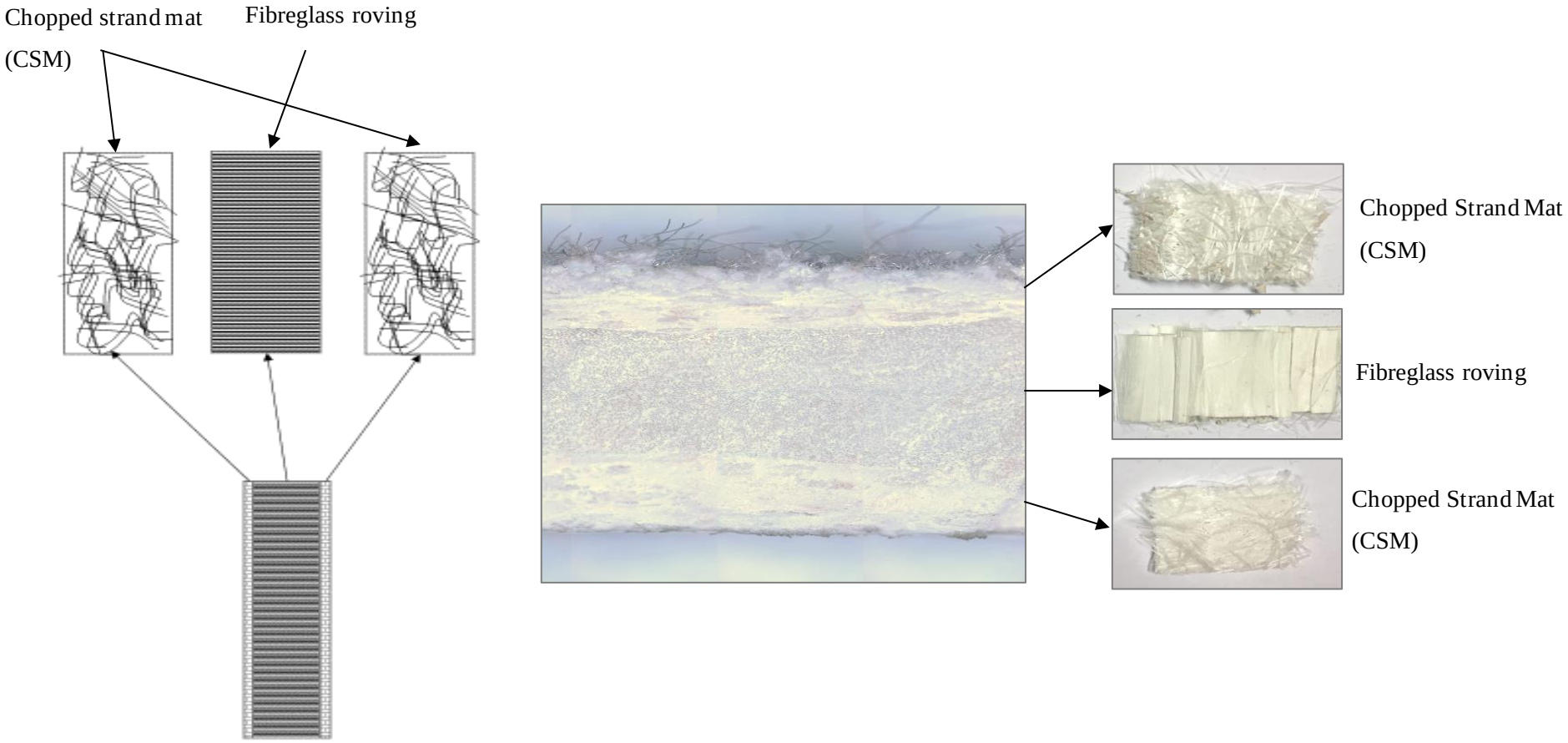

Figure 4.6 Fiberglass layering of Brand C's sample obtained from confocal microscope

Table 4.4 Fiber arrangement of Brand C crossarm

No of Layer	Fiber direction (°)	Thickness (mm)
Layer 1	45	1.04
Layer 2	0	3.12
Layer 3	45	1.04

4.2.1.4 Brand D Crossarm

Figure 4.7 shows the variation in density, fibre content and thickness of Brand D's sample at different side of GFRP crossarm. The thickness of the cross-section is between 7.2 to 7.4mm which is relatively high compared to samples produced by other manufacturers which ranged between 5 to 6mm. The fiber content and densities are fairly constant at all sides 1,2,3 and 4. Same as Brand B's sample, Brand D's sample also experience a slight drop in fibre content at the corners of the sample.

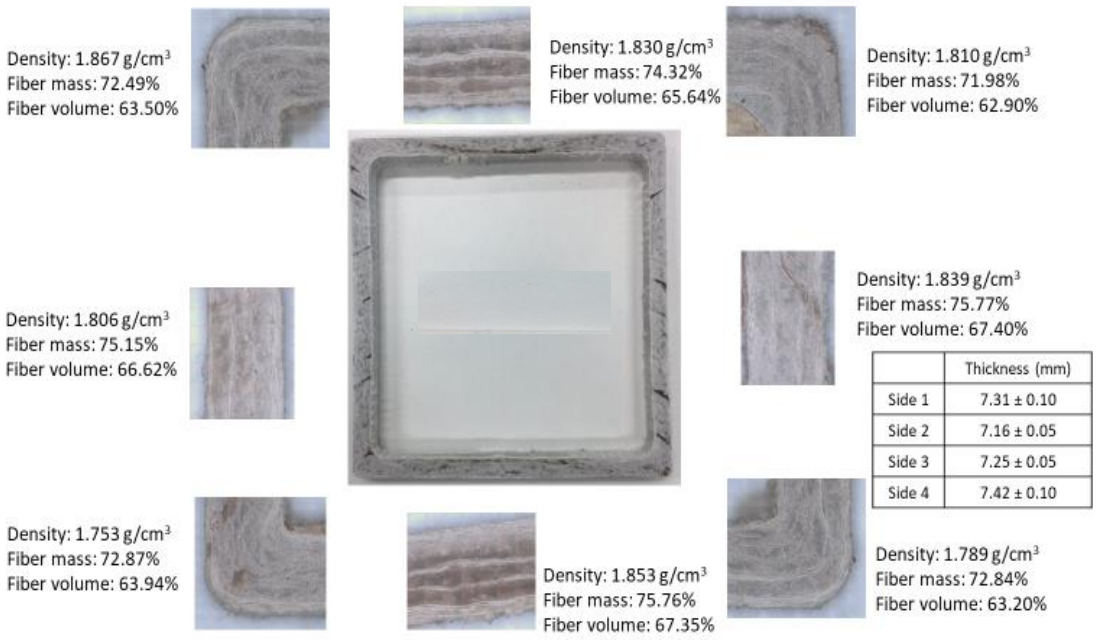

Figure 4.7 Density, fiber mass fraction and fiber volume fraction of Brand D's sample

From the resin burn-off that was carried out on Brand D's sample, it was found that the fabrication of the pultruded crossarms comprised of 10 layers fiberglass which comprised 4 layers of Fiberglass Cloth, 3 layers of Fiberglass Roving and and 3 layers Fiberglass Chopped Strand Mat (CSM) as shown in Figure 4.8.

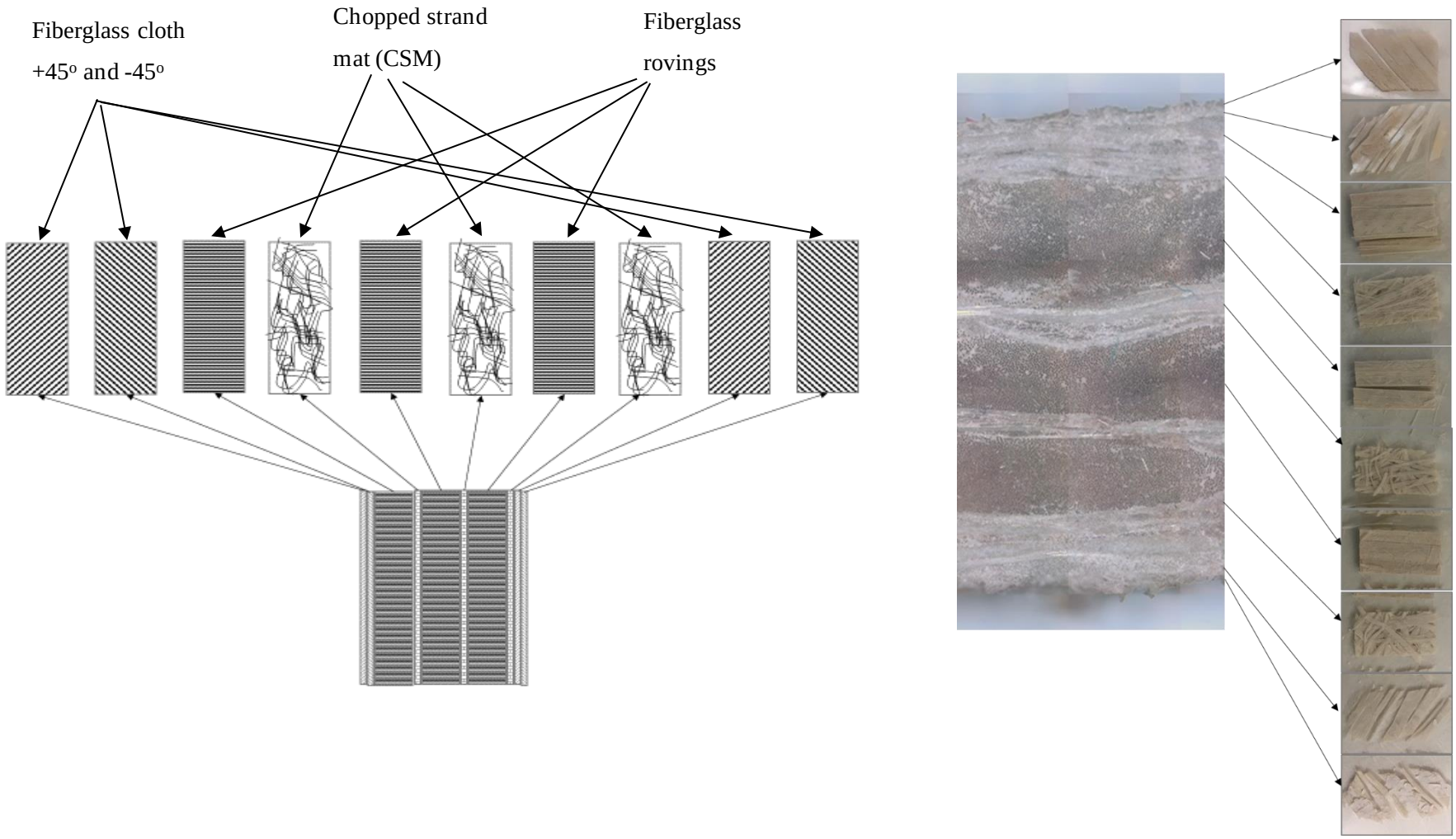

Figure 4.8 Fiberglass layering of Brand D's sample obtained from confocal microscope

Table 4.5 Fiber arrangement of Brand D crossarm

No. of Layer	Fiber direction (°)	Thickness (mm)
Layer 1	45	0.72
Layer 2	-45	0.72
Layer 1	0	0.72
Layer 3	0	0.72
Layer 4	0	0.72
Layer 5	0	0.72
Layer 6	0	0.72
Layer 7	0	0.72
Layer 8	-45	0.72
Layer 9	45	0.72
Layer 10	45	0.72

4.2.1.5 Summary

Comparing all the cross section of manufacturer sample, Brand A's sample has such a high precision profiles because of the fairly constant thickness and even at the corners. There was a tiny crack line observed in the cross section of Brand B's sample and this provide supportive evidence for the presence of highest percent of void content as shown in Table 4.1 compared to other manufacturer samples. Cracks is one of the main causes that will contribute to the damaging of mechanical performance of composites since it could act as a stress concentration point which could lead to a premature failure of the composites. Based on Table 4.6, the thickness of Brand A's sample is about 1 mm less than the thickness of Brand D's sample. This indicates better fibre consolidation is achieved in the case of samples produced by Brand A. The choice of fiber form used in Brand A also facilitates better consolidation of fibers during the fabrication of crossarms products pultrusion process.

Table 4.6 Comparison of the thickness sample for all brands of GFRP crossarms

Side/Corner	Brand A	Brand B	Brand C	Brand D
Side 1 (mm)	6.3± 0.05	5.7± 0.05	5.03± 0.05	7.31± 0.10
Side 2 (mm)	6.3± 0.10	5.9± 0.10	5.13± 0.05	7.16± 0.05
Side 3 (mm)	6.3± 0.05	6.4± 0.10	5.04± 0.05	7.25± 0.05
Side 4 (mm)	6.3± 0.10	6.8± 0.10	5.01± 0.05	7.42± 0.10

Table 4.7 Comparison of the parameter for all brands of GFRP crossarms

Parameter	Brand A	Brand B	Brand C	Brand D
Density	2.03 g/cm^3	1.8 g/cm^3	1.89 g/cm^3	1.9 g/cm^3
Young's modulus, E_1	34000 MPa	21000 MPa	16900 MPa	20000 MPa
Young's modulus, E_2	10200 MPa	5000 MPa	4500 MPa	8820 MPa
Young's modulus, E_3	3100 MPa	1800 MPa	1100 MPa	2646 MPa
Poisson's ratio (V_{12}=V_{13}=V_{23})	0.28	0.28	0.28	0.28
Shear modulus (G_{12}=G_{13}=G_{23})	4280 MPa	5000 MPa	2000 MPa	4280 MPa
Ultimate tensile stress, X_{1T}	429 MPa	321 MPa	485 MPa	323 MPa
Ultimate compressive stress, X_{1C}	320 MPa	150 MPa	165 MPa	151 MPa
Ultimate tensile stress, X_{2T}	100 MPa	80 MPa	85 MPa	81 MPa
Ultimate compressive stress, X_{2C}	76 MPa	65 MPa	70 MPa	66 MPa
Ultimate shear stress, S_{12}	95 MPa	90 MPa	89 MPa	90 MPa
Ultimate shear stress, (S_{13} = S_{23})	70 MPa	60 MPa	52.45 MPa	35 MPa

4.2.2 Tensile Properties

Experimental tensile testing was conducted to find the ultimate tensile strength, ultimate tensile strain and tensile chord modulus of elasticity of polymer matrix composite material. The tensile properties were required to use an input in the numerical modelling analysis. The results of tensile test for different brands of GFRP crossarm is tabulated in Table 4.8 while Figure 4.9 and Figure 4.10 shows the tensile properties of various samples produced by different manufacturers.

Table 4.8 Results of tensile test for different brands of GFRP crossarm

Sample	Maximum Load (N)	Extension at break (mm)	Tensile strength (MPa)	Tensile Modulus (GPa)
Brand A	46003	8.32	535.63	26.54
Brand B	34919	9.27	369.08	19.2
Brand C	37695	9.34	503.29	23.92
Brand D	28550	9.55	348.65	15.99

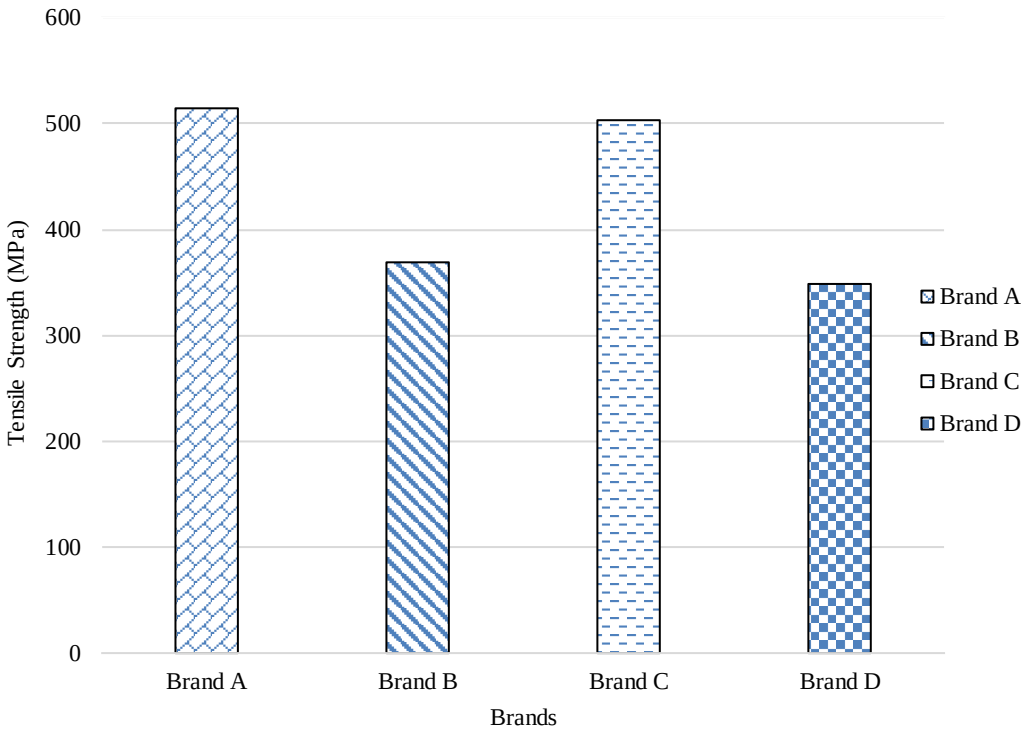

Figure 4.9 Comparison of tensile strength of various samples produced by different manufacturer

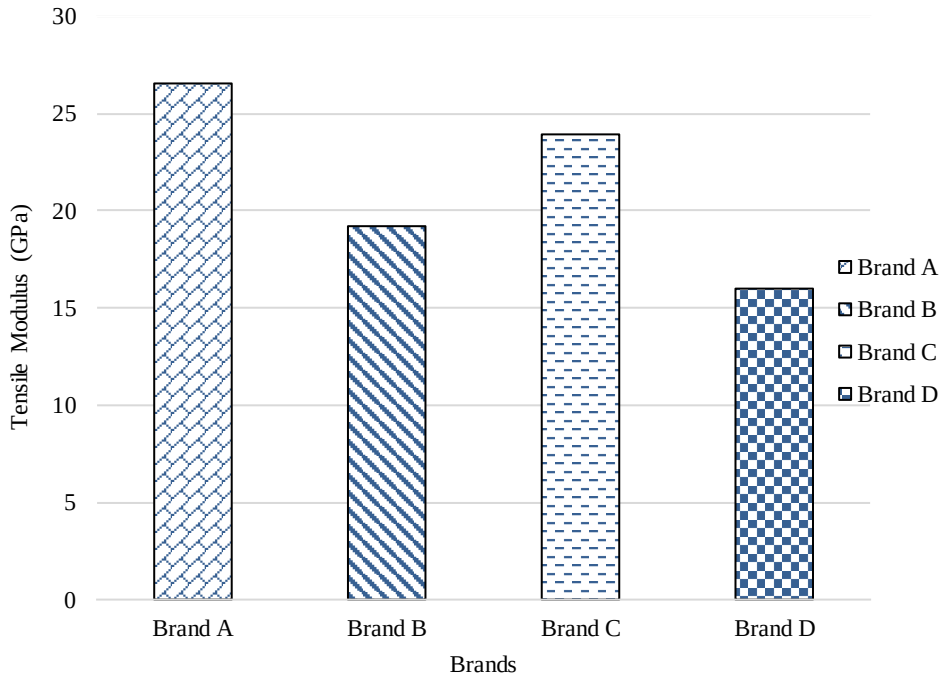

Figure 4.10 Comparison of tensile modulus of various samples produced by different manufacturer

Referring Figure 4.9, it was found that the tensile strength of Brand A's sample is the highest which is 535.63 MPa compared to other samples produced by other manufacturers which falls between 500 MPa to 300 MPa. Brand C's sample recorded value of 503.29 MPa tensile strength which is 6% lower than Brand A's sample. Refer from Figure 4.9 and Table 4.8, the tensile properties for Brand B's sample is 369.08 MPa while the tensile properties for Brand D's sample recorded the lowest value which is 348.65 MPa. The higher tensile strength and modulus of Brand A's samples could again is due to the higher content of continuous roving used in fabricating the profiles.

From Figure 4.10, it was found that the tensile modulus of Brand A's sample is the highest which is 26.54 GPa compared to other samples produced by other manufacturers. Brand C sample recorded value of 23.92 GPa tensile modulus which is 10% lower than Brand A sample. Figure 4.10 and Table 4.8 shows the tensile modulus for Brand B's sample is 19.2 GPa while the tensile modulus for Brand D's sample recorded the lowest value which is 15.99 GPa.

4.2.3 Compressive Strength

Compression tests was conducted to provide information about the compressive properties of glass fibre when employed under different loads. Other than tensile properties, the compressive properties were also required as an input in the numerical modelling analysis. The results of compression test for different brands of GFRP crossarm is tabulated in Table 4.9 while Figure 4.11 and Figure 4.12 shows the compressive properties of various samples produced by different manufacturers.

Table 4.9 Results of compression test for different brands of GFRP crossarm

Sample	**Compressive**	
	Stress (MPa)	**Modulus (GPa)**
Brand A	320.2	36.24
Brand B	151.03	5.45
Brand C	165.21	6.15
Brand D	151.03	5.78

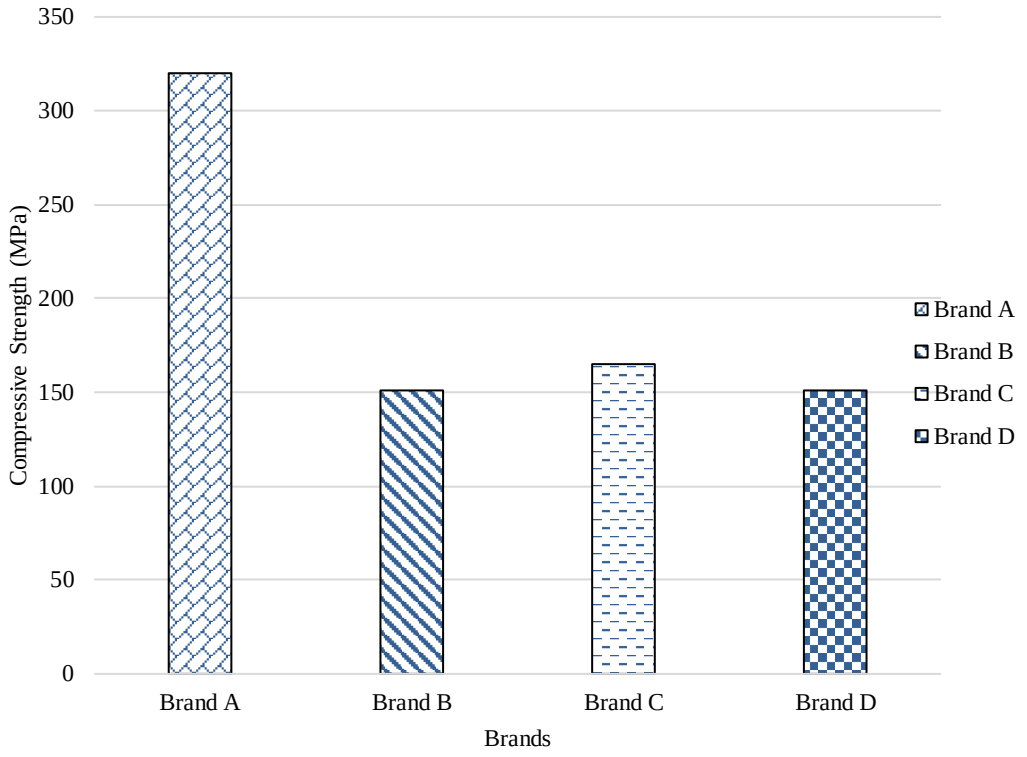

Figure 4.11 Comparison of compressive stress between samples produced by different manufacturers.

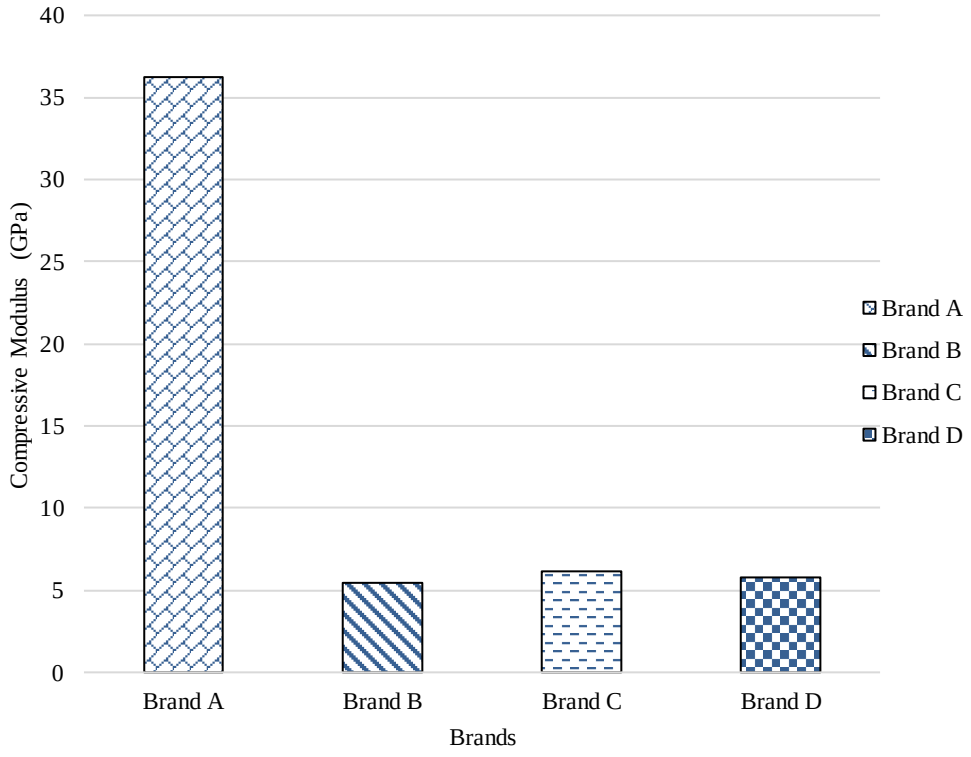

Figure 4.12 Comparison of compressive modulus between samples produced by different manufacturers.

From Figure 4.11, it was discovered that the value of compressive stress of Brand A's sample is two times higher compared to other samples produced by other manufacturers which is 320.2 MPa. The other manufacturer sample recorded slightly the same value of compressive stress which is 151.03 MPa for both Brand B and Brand D sample and 165.21 MPa for Brand C's sample. Refer from Figure 4.12 and Table 4.9, the compressive modulus value for Brand A's sample also recorded seven times higher than the other manufacturer compressive modulus values. The value of compressive modulus for Brand A's sample is 36.24 GPa while the compressive modulus for the Brand B's sample is 5.45 GPa and 5.78 GPa for Brand D's sample. The value of compressive modulus for Brand C's sample recorded slightly higher than both Brand B and Brand D sample which is 6.15 GPa.

The samples produced by Brand A has shown better compressive properties as compared to those produced by other manufacturer. This could be attributed to a good combination of both continuous roving and stitched glass fabric used by Brand A in manufacturing the crossarms. The strategy of using several layers of Chopped Strand Mat (CSM) and glass cloth as used by other manufacturers did not provide much contribution towards enhancing the compressive properties of the composites especially when the interfacial bonding between resin and glass fibre reinforcement is not that good.

4.3 Full Assembly Testing of GFRP Crossarm (Vertical load)

4.3.1 Experimental Testing

The flexural properties of GFRP crossarm under different working loads is shown in Table 4.10. Full assembly of composite GFRP crossarm was conducted for normal condition and only vertical loading was applied. Deformation at 30 minutes and breaking load was recorded and compared with numerical modelling result. It was found that the deformation of Brand A's sample recorded the minimal deformation compared to other manufacturer. The deformation of Brand A's sample is 7.7 cm while the deformation of Brand B's sample was observed is slightly higher which is 11.3 cm.

It was discovered that during the experimental testing, the Brand A's sample was not failed even the load has been exceed until 80 kN. This proves that Brand A's sample has the ability to withstand highest working load. Meanwhile, the buckling failure or called as compressive rupture has been seen at the center of the main member of Brand B's sample.

Table 4.10 Results of flexural testing of full assembly of GFRP crossarm

Manufacturer	Deformation at 30 minutes (cm)	Breaking load (kN)	Breaking load ratio
Brand A	7.7	>80	3.77
Brand B	11.3	60.25	2.84
Brand C	12.0	60	2.82
Brand D	13.9	72.33	3.41

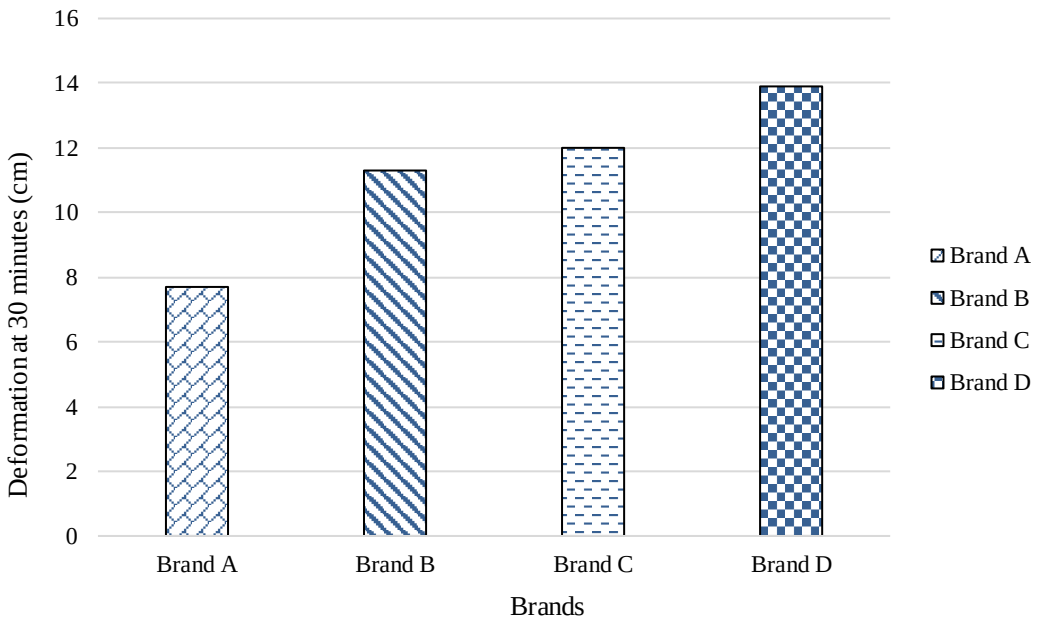

Figure 4.13 Deformation at 30 minutes for different brand of GFRP crossarm

The deformation of Brand C's sample is 12.0 cm while the deformation of Brand D's sample was observed have the highest deformation which is 13.9 cm. During the experimental testing, the Brand C's sample was observed have a bolt hole shear at tie member joint at the nose plate of the GFRP crossarm. Meanwhile, the Brand D's

sample has the same failure as Brand B's sample which failed due to buckling at the center of the main member.

4.3.2 Numerical Modelling

The objective of this analysis on full assembly of GFRP crossarm is to validate the experimental result obtained from the full assembly testing mentioned in Section 4.3.1. Follows the experimental testing procedure, the GFRP was analyse for normal condition and only vertical loading was applied. Results from material characterization in Section 4.2 were used as an input parameter in engineering data of GFRP crossarm. Table 4.11 shows the result and comparison between experimental results and numerical analysis results.

Table 4.11 Comparison between experimental and numerical analysis

Brands	**Deformation (cm)**		**Percentage Difference (%) < 5 %**
	Experimental	**Numerical**	
Brand A	7.7	7.68	0.23
Brand B	11.3	11.5	1.75
Brand C	12.0	11.85	1.25
Brand D	13.90	13.70	1.47

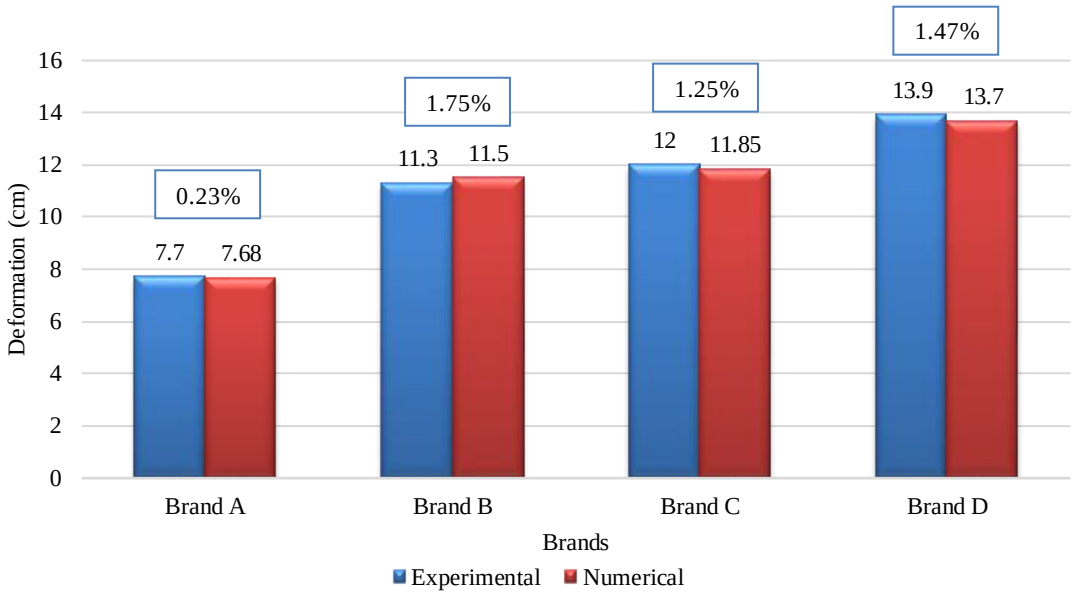

Figure 4.14 Percentage difference between experimental and numerical results

Referring Table 4.11, it was discovered that percentage difference between experimental and numerical analysis results for all the GFRP crossarm falls below 5% which is considered acceptable [63]. In any experiment, there is always the possibility that an observed effect would have occurred due to sampling error alone or other external causes. Numerical analysis results show lesser in values of deformation compared with experimental results.

From Table 4.11, it can be observed that Brand D's sample has the highest deformation which is 13.70 cm while Brand A's sample has the minimum deformation when compared with the other manufacturer's sample. Other than that, Brand A's sample also has the lowest percentage of difference which is 0.23% while other manufacturer's sample values of percentage difference are more than 1%.

4.4 Parametric Study for Determining Factor of Safety (FOS)

Parametric study is one of the main objectives in this study that allow nominations parameters for evaluation purposes. Parametric study for this research involves two cases which is normal condition and broken wire condition. Normal condition is when the condition of all the wires are intact at the GFRP crossarm while the broken wire condition is the condition when the simulation conductor or earth wire was discovered broken. The variable parameters of these parametric study are load and deformation.

4.4.1 Case 1: Normal Condition

Simulation on crossarm consists of modelling and analysis on the complete set of crossarm subjected to different type of working loads is tabulated in Table 3.8. For normal condition, only two types of working load which is vertical load and transverse load were applied in this parametric study.

4.4.1.1 Brand A Sample

The results of parametric study for Brand A's GFRP crossarm is shown in Table 4.12 and 4.13. From Table 4.12, it can be observed that the maximum deformation for 1WL is 49.60 mm which is higher than the latest TNB requirement that is L/400 (12.3 mm). However, based on the minimum strength of materials it is found that the Factor of Safety (FOS) is 5.16 which is higher than 1, which is consider safe. Maximum deformation of Brand A crossarm right before it fails is 226.35 mm at FOS of 1.08. Maximum stress of material is 296.12 N/mm2 which give FOS of 1.08 at 5 times of applied working load that indicate the maximum loads that can be supported by Brand A crossarm.

Table 4.12 Maximum load capacity and deformation of Brand A crossarm

Working load	Vertical load (N)	Transverse Load (N)	Deformation (mm)
1WL	21248	11718	49.60
2WL	42496	23436	93.77
3WL	63744	35154	137.96
4WL	84992	46872	182.15
5WL	106240	58590	226.35
6WL	127488	70308	270.54

Table 4.13 Maximum stress in lamina of Brand A crossarm

Load	Deformation (mm)	Stress ply (N/mm^2) First Layer		Compressive Strength (N/mm^2)	Minimum Factor of Safety (Strength/Stress)
		Main	Tie		
1WL	49.60	61.98	56.89	320	5.16
2WL	93.77	120.52	111.49	320	2.66
3WL	137.96	179.05	166.09	320	1.79
4WL	182.15	237.59	220.69	320	1.35
5WL	226.35	296.12	275.28	320	1.08
6WL	270.54	354.66	329.88	320	0.90

Figure 4.15 Deformation and Factor of Safety (FOS) for Brand A crossarm (Normal Condition)

Figure 4.16, 4.17, and 4.18 shows the maximum deformation, equivalent stress first ply for main member, and tie member of Brand A's GFRP crossarm for 5 x Working Load (WL). Referring to Figure 4.15, it was discovered that the working load is inversely proportional with the FOS of the GFRP crossarm. When the working load increased, the FOS of GFRP crossarm will slowly decreased. Maximum load that can hold by Brand A's sample are 106240 N and 58590 N for vertical and transverse loads, respectively. Referring to Equation 2.1, the FOS of GFRP crossarm must exceed values of 1 in order to be considered as safe.

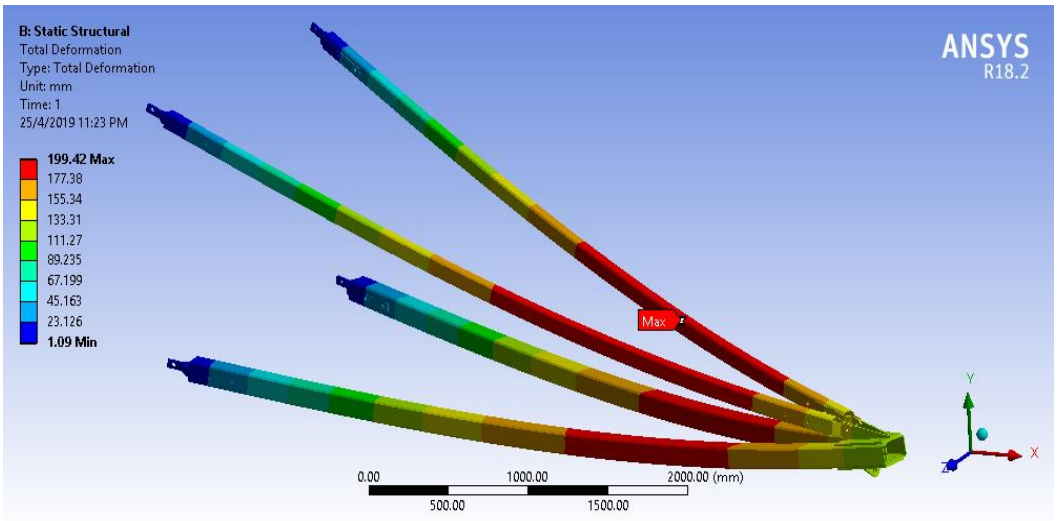

Figure 4.16 Maximum deformation of Brand A's crossarm

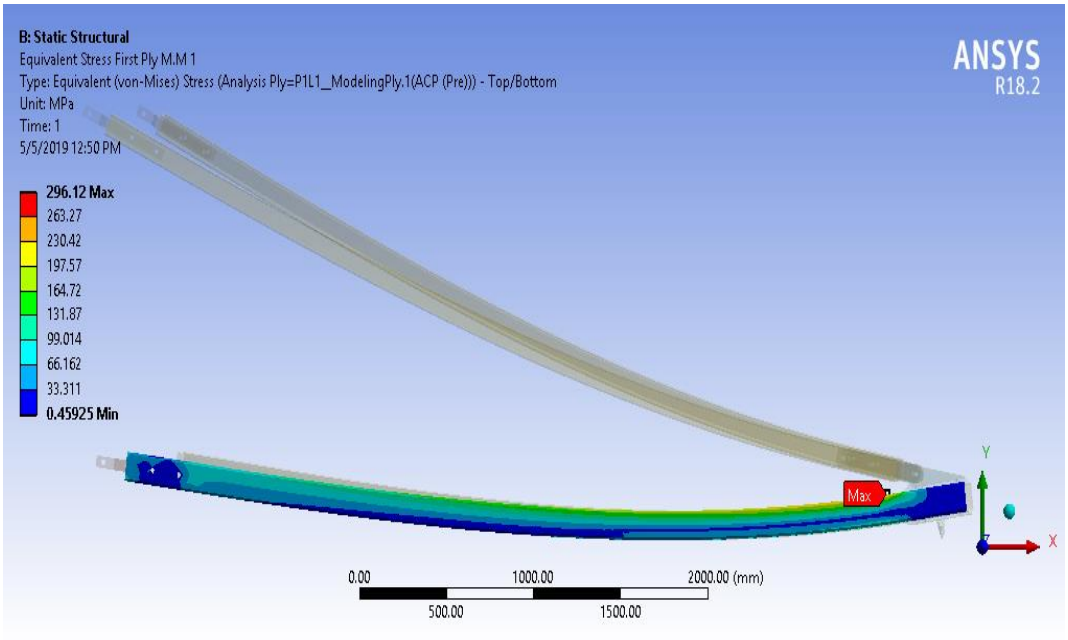

Figure 4.17 Equivalent stress ply first layer of main member

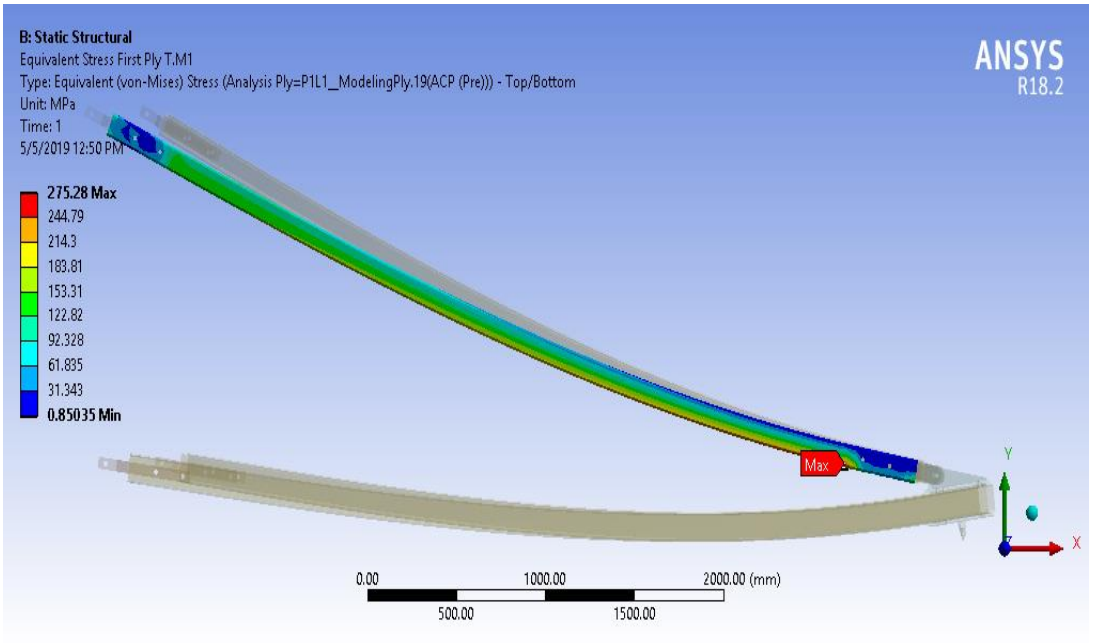

Figure 4.18 Equivalent stress ply first layer of tie member

4.4.1.2 Brand B Sample

The results of parametric study for Brand B's GFRP crossarm is shown in Table 4.14 and 4.15. From Table 4.14, it can be observed that the maximum deformation for 1WL is 64.76 mm which is higher than the latest TNB requirement that is L/400 (12.3 mm). Figure 4.19, 4.20, and 4.21 shows the maximum deformation, equivalent stress first ply for main member, and tie member of Brand A's GFRP crossarm for 1 x Working Load (WL). Based on the minimum strength of materials it is found that the Factor of Safety (FOS) is 0.67 which mean Brand B's sample cannot withstand the working load even 1WL in normal condition.

Table 4.14 Maximum load capacity and deformation of Brand B crossarm

Working load	Vertical load (N)	Transverse Load (N)	Deformation (mm)
1WL	21248	11718	64.76

Table 4.15 Maximum stress in lamina of Brand B crossarm

Load	Deformation (mm)	Stress ply (N/mm^2) First Layer		Compressive Strength (N/mm^2)	Minimum Factor of Safety (Strength/Stress)
		Main	Tie		
1WL	64.76	222.73	37.42	150	0.67

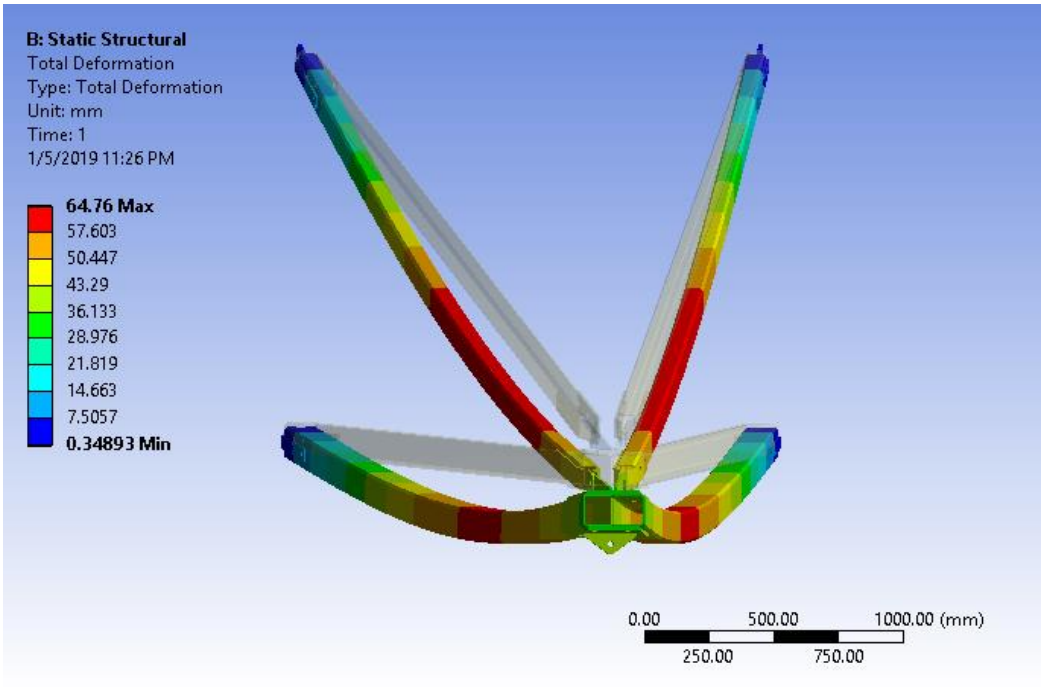

Figure 4.19 Maximum deformation of Brand B's crossarm

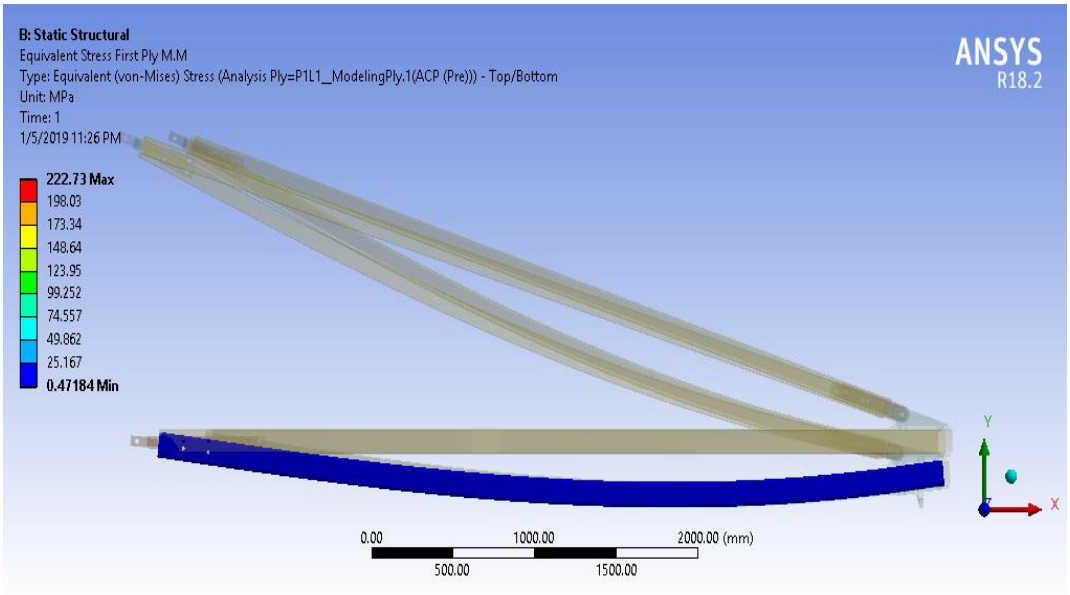

Figure 4.20 Equivalent stress ply first layer of main member

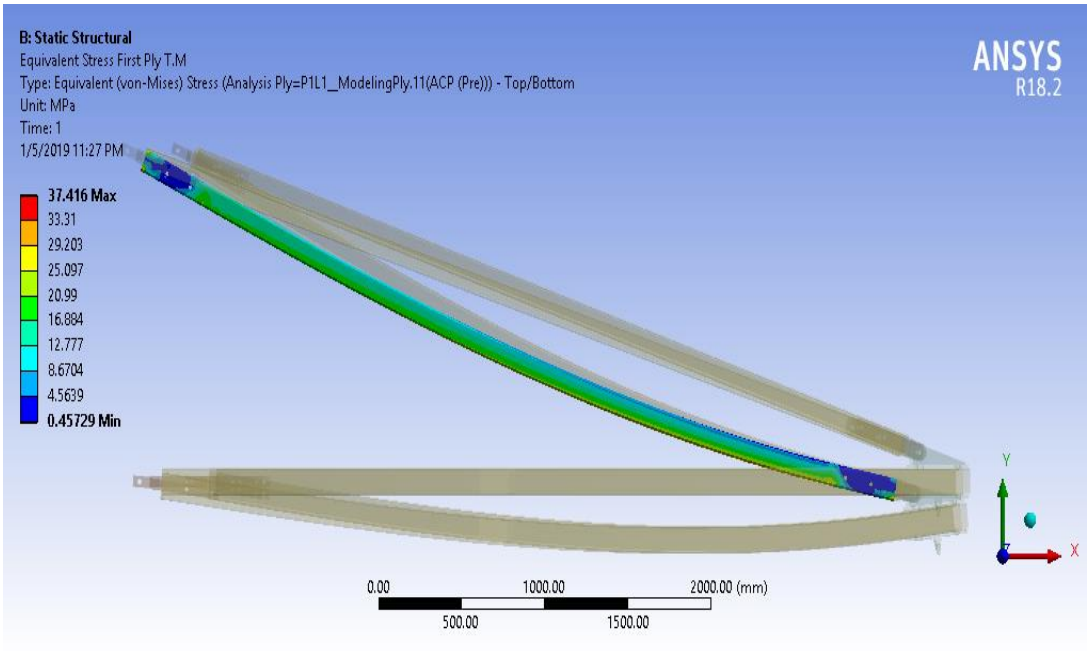

Figure 4.21 Equivalent stress ply first layer of tie member

4.4.1.3 Brand C Sample

The results of parametric study for Brand C's GFRP crossarm was shown in Table 4.16 and 4.17. From Table 4.16, it can be observed that the maximum deformation for 1WL is 148.40 mm which is higher than the latest TNB requirement that is L/400 (12.3 mm). However, based on the minimum strength of materials it is found that the Factor of Safety (FOS) is 4.60 which is higher than 1, which is consider safe. Maximum deformation of Brand C crossarm right before it fails is 554.50 mm at FOS of 1.18. Maximum stress of material is 140.21 N/mm^2 which give FOS of 1.18 at 4 times of applied working load that indicate the maximum loads that can be supported by Brand C crossarm.

Table 4.16 Maximum load capacity and deformation of Brand C crossarm

Working load	Vertical load (N)	Transverse Load (N)	Deformation (mm)
1WL	21248	11718	148.40
2WL	42496	23436	283.76
3WL	63744	35154	419.12

Working load	Vertical load (N)	Transverse Load (N)	Deformation (mm)
4WL	84992	46872	554.50
5WL	106240	58590	689.88

Table 4.17 Maximum stress in lamina of Brand C crossarm

Load	Deformation (mm)	Stress ply (N/mm^2) First Layer		Compressive Strength (N/mm^2)	Minimum Factor of Safety (Strength/Stress)
		Main	Tie		
1WL	148.40	35.88	35.72	165	4.60
2WL	283.76	70.66	69.97	165	2.34
3WL	419.12	105.44	104.22	165	1.56
4WL	554.50	140.21	138.47	165	1.18
5WL	689.88	174.99	172.72	165	0.94

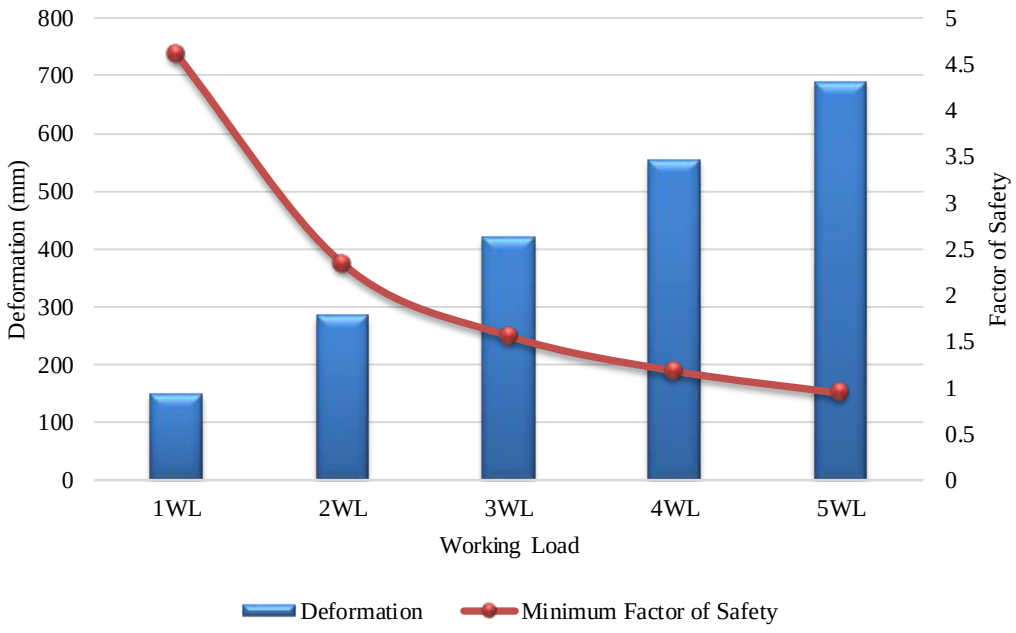

Figure 4.22 Deformation and Factor of Safety (FOS) for Brand C crossarm (Normal Condition)

Figure 4.23, 4.24, and 4.25 shows the maximum deformation, equivalent stress first ply for main member, and tie member of Brand C's GFRP crossarm for 4 x Working Load (WL). Referring Figure 4.22, it was discovered that when the working load increased, the FOS of GFRP crossarm will slowly decreased. Brand C crossarm failed at 5WL with deformation of 174.99 mm and 0.94 FOS. Maximum load that can hold by Brand C's sample are 84992 N and 46872 N for vertical and transverse loads, respectively.

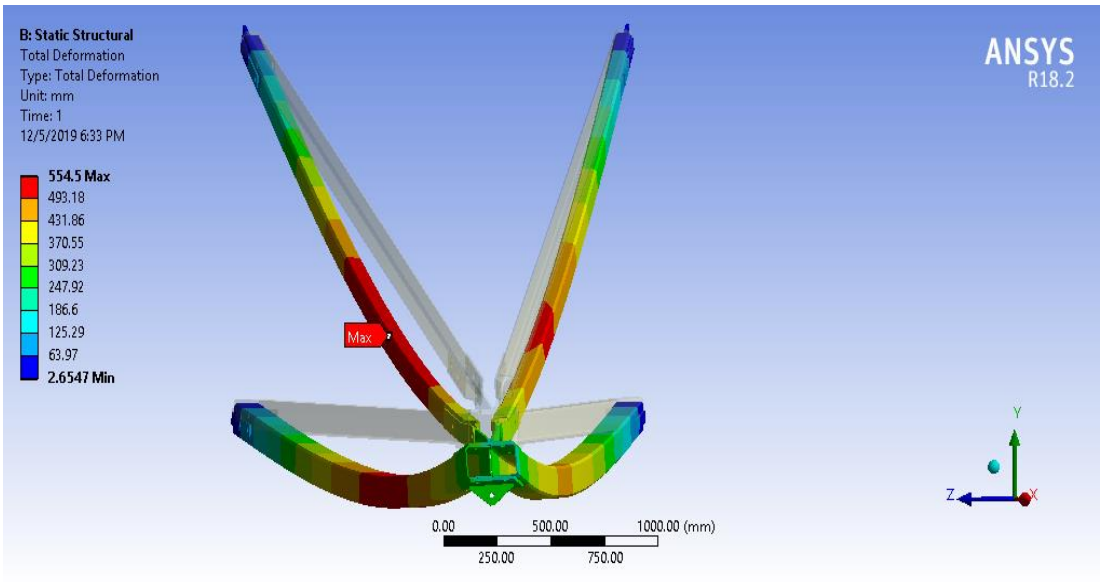

Figure 4.23 Maximum deformation of Brand C's crossarm

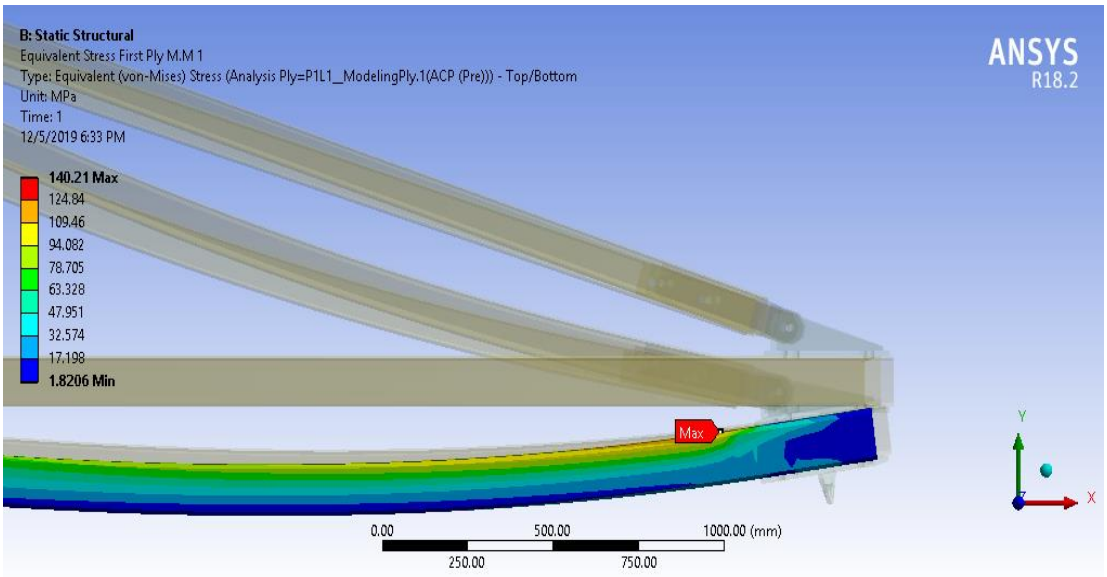

Figure 4.24 Equivalent stress ply first layer of main member

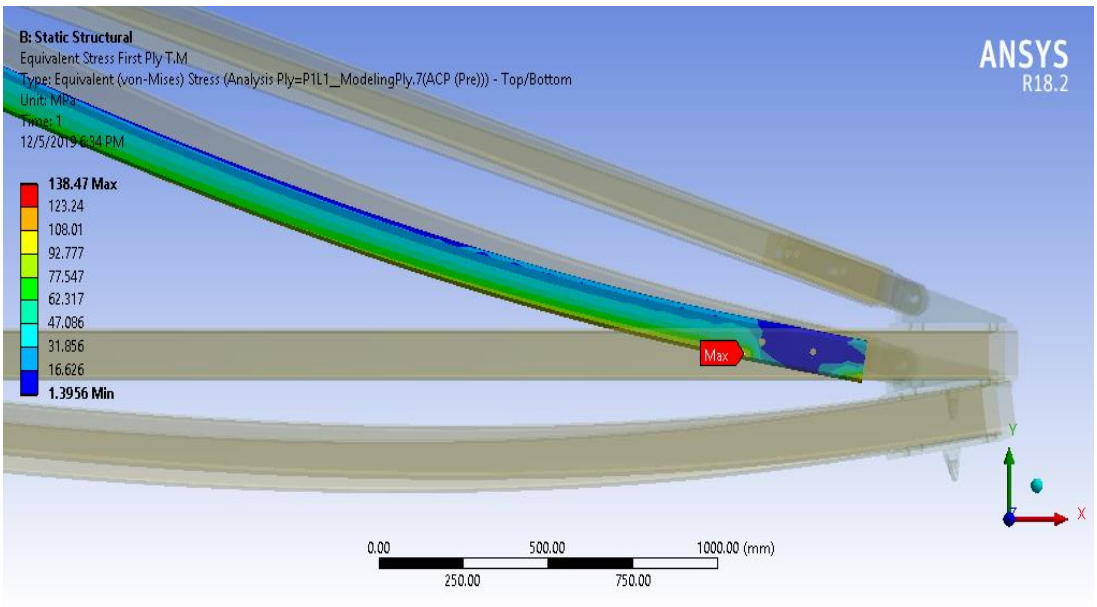

Figure 4.25 Equivalent stress ply first layer of tie member

4.4.1.4 Brand D Sample

From Table 4.18, it can be observed that the maximum deformation for 1WL is 56.29 mm which is higher than the latest TNB requirement that is L/400 (12.3 mm). However, based on the minimum strength of materials it is found that the Factor of Safety (FOS) is 1.36 which is higher than 1, which is consider safe. Maximum deformation of Brand C crossarm right before it fails is 56.29 mm at FOS of 1.36. Maximum stress of material is 209.59 N/mm^2 which give FOS of 1.36 at only 1 time of applied working load that indicate the maximum loads that can be supported by Brand D crossarm.

Table 4.18 Maximum load capacity and deformation of Brand D crossarm

Working load	Vertical load (N)	Transverse Load (N)	Deformation(mm)
1WL	21248	11718	56.29
2WL	42496	23436	106.27

Table 4.19 Maximum stress in lamina of Brand D crossarm

Load	Deformation (mm)	Stress ply (N/mm^2) First Layer		Compressive Strength (N/mm^2)	Minimum Factor of Safety (Strength/Stress)
		Main	Tie		
1WL	56.29	209.59	34.59	284	1.36
2WL	106.27	394.27	67.77	284	0.72

Figure 4.26 Deformation and Factor of Safety (FOS) for Brand D crossarm (Normal Condition)

Figure 4.27, 4.28, and 4.29 shows the maximum deformation, equivalent stress first ply for main member, and tie member of Brand D's GFRP crossarm for 1 x Working Load (WL). Referring to Figure 4.26, Brand D crossarm failed at 2WL with deformation of 106.27 mm and 0.72 FOS. Maximum load that can hold by Brand D's sample are 21248 N and 11718 N for vertical and transverse loads, respectively.

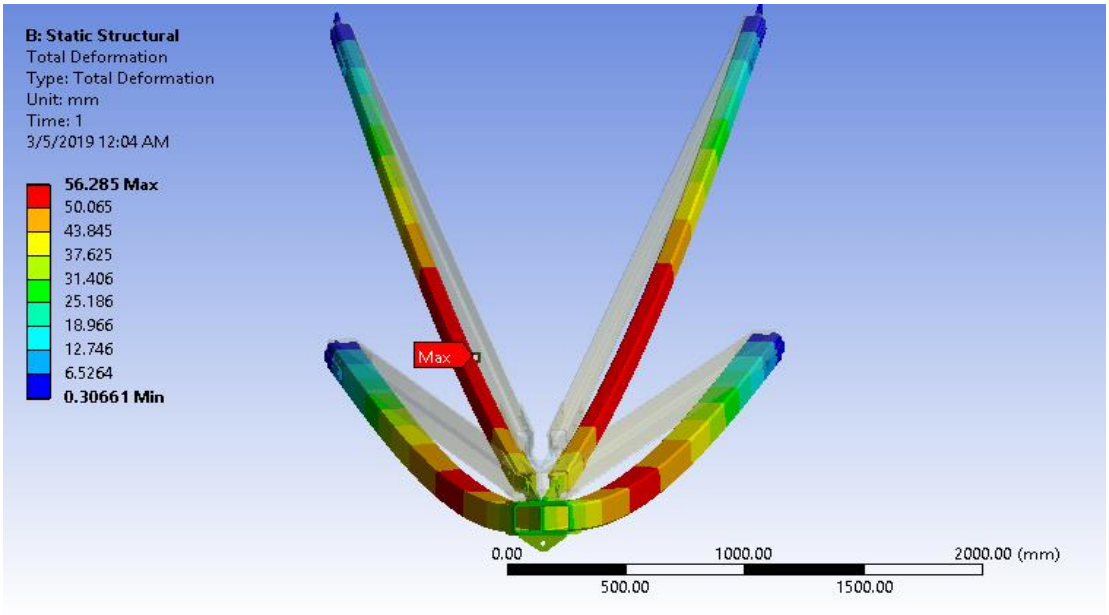

Figure 4.27 Maximum deformation of Brand D's crossarm

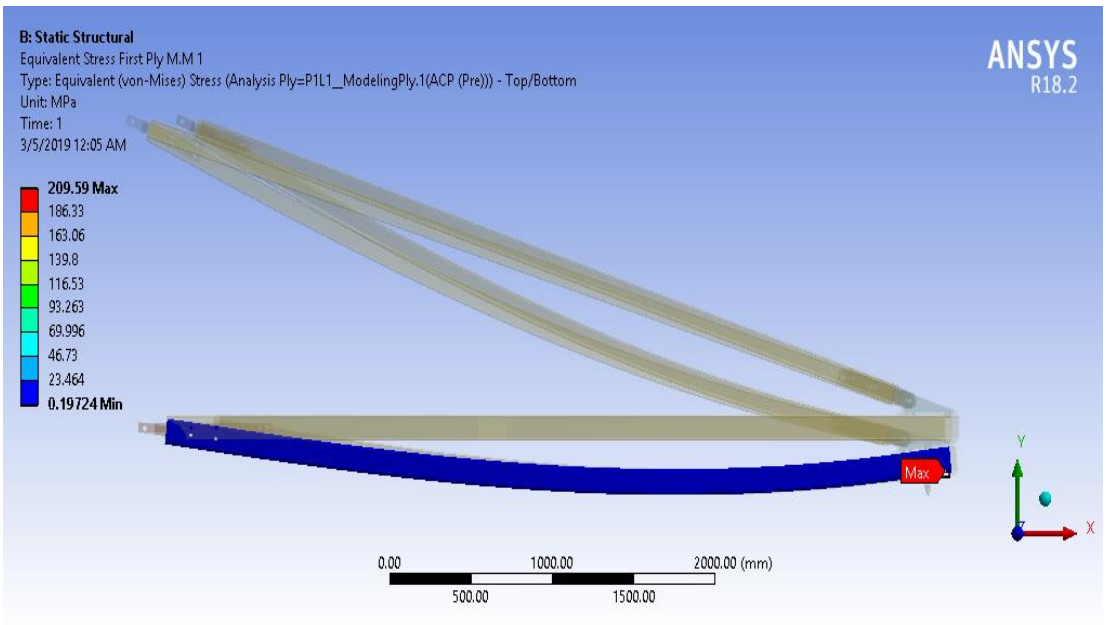

Figure 4.28 Equivalent stress ply first layer of main member

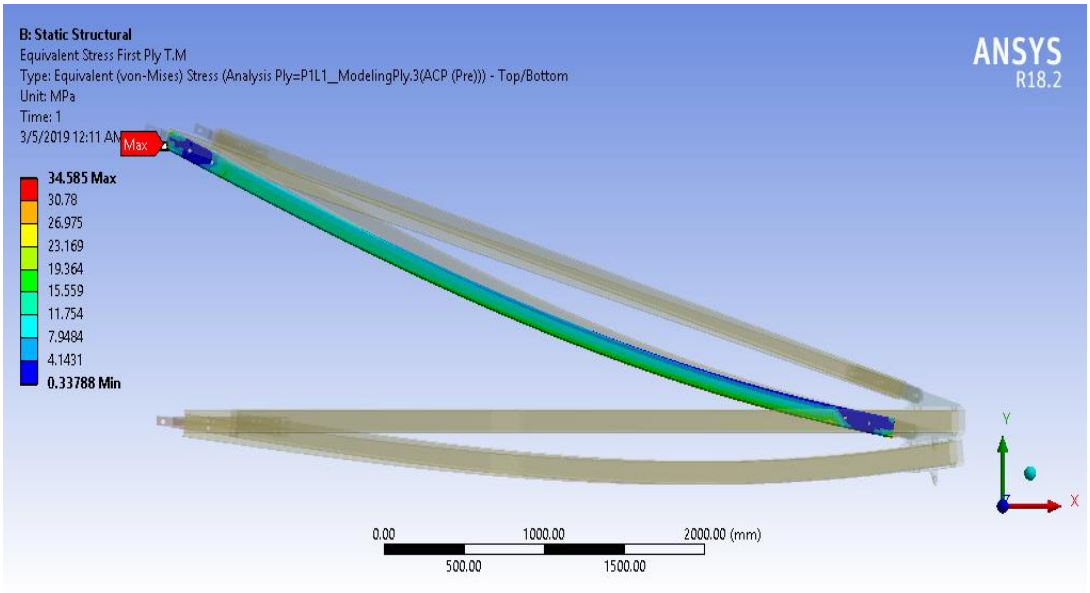

Figure 4.29 Equivalent stress ply first layer of tie member

4.4.2 Case 2: Broken Wire Condition

Simulation on crossarm consists of modelling and analysis on the complete set of crossarm subjected to different type of working loads was tabulated in Table 3.10. For broken wire condition, three types of working load which is vertical load, transverse load and longitudinal load were applied in this parametric study.

4.4.2.1 Brand A Sample

The results of parametric study for Brand A's GFRP crossarm in broken wire condition was shown in Table 4.20 and 4.21. Refer from Table 4.20, it can be observed that the maximum deformation for 1WL is 55.70 mm which is higher than the latest TNB requirement that is L/400 (12.3 mm). However, based on the minimum strength of materials it is found that the Factor of Safety (FOS) is 3.22 which is higher than 1, which is consider safe. Maximum deformation of Brand A crossarm right before it fails is 162.42 mm at FOS of 1.10 for broken wire condition. Maximum stress of material is 291.96 N/mm^2 which give FOS of 1.10 at 3 times of applied working load that indicate the maximum loads that can be supported by Brand A crossarm in broken wire condition.

Table 4.20 Maximum load capacity and deformation of Brand A crossarm

Working load	Vertical load (N)	Transverse Load (N)	Longitudinal load (N)	Deformation (mm)
1WL	16436	8667	25779	55.70
2WL	32872	17334	51558	109.05
3WL	49308	26001	77337	162.42
4WL	65744	34668	103116	215.79

Table 4.21 Maximum stress in lamina of Brand A crossarm

Load	Deformation (mm)	Stress ply (N/mm^2) First Layer		Compressive Strength (N/mm^2)	Minimum Factor of Safety (Strength/Stress)
		Main	Tie		
1WL	55.70	99.24	92.67	320	3.22
2WL	109.05	195.60	183.51	320	1.64
3WL	162.42	291.96	274.35	320	1.10
4WL	215.79	388.32	365.19	320	0.82

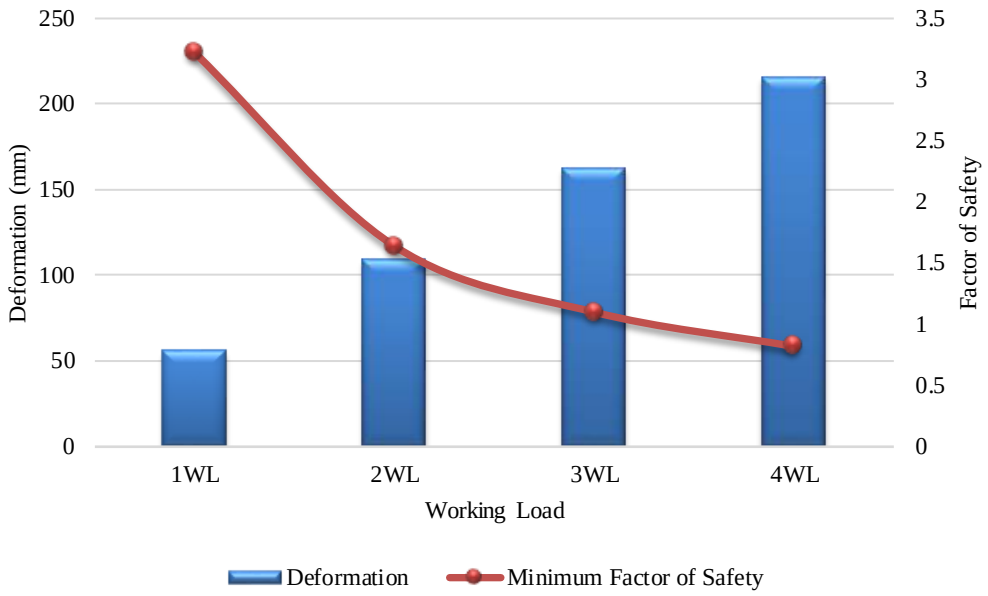

Figure 4.30 Deformation and Factor of Safety (FOS) for Brand A crossarm (Broken Wire Condition)

Figure 4.31, 4.32, and 4.33 shows the maximum deformation, equivalent stress first ply for main member, and tie member of Brand A's GFRP crossarm for 3 x Working Load (WL) for broken wire condition. Refer from Figure 4.30, maximum load that can hold by Brand A's sample for broken wire condition are 49308 N, 26001 N, and 77337 N for vertical, transverse, and longitudinal load respectively.

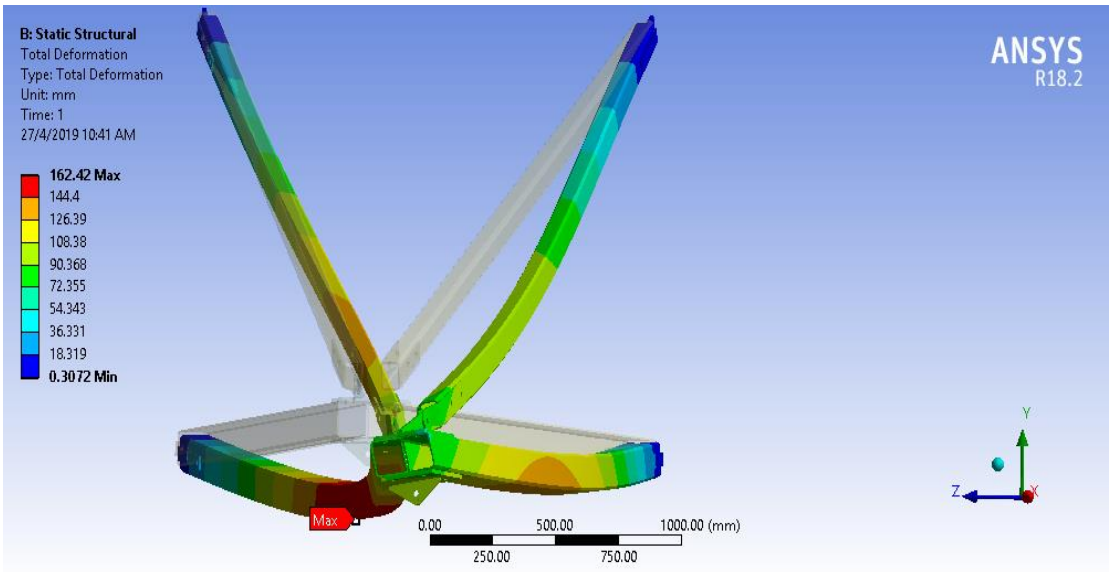

Figure 4.31 Maximum deformation of Brand A's crossarm (Broken Wire Condition)

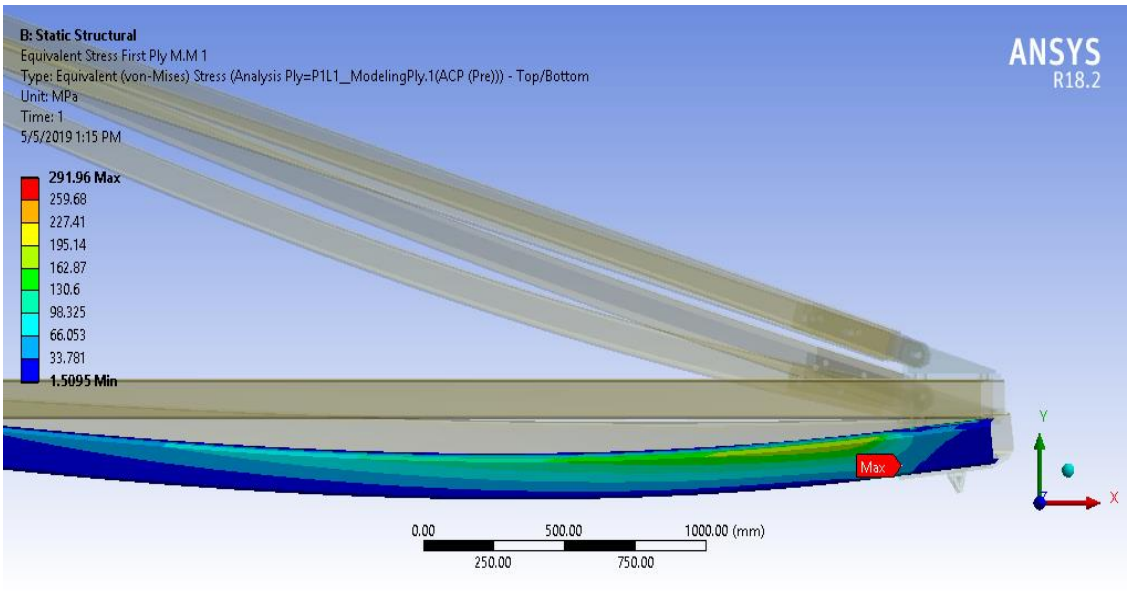

Figure 4.32 Equivalent stress ply first layer of main member

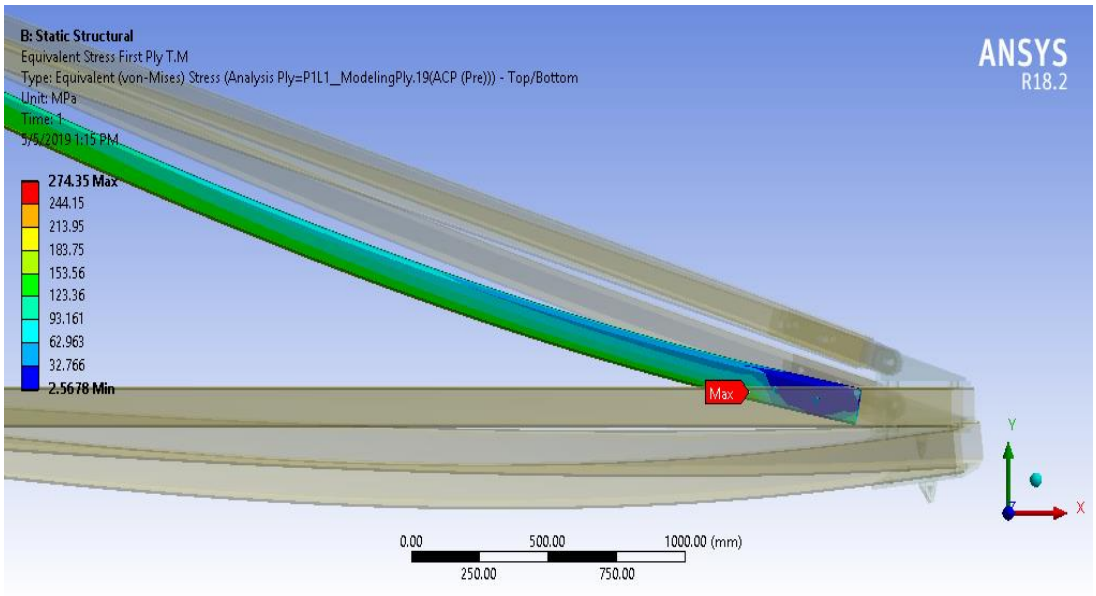

Figure 4.33 Equivalent stress ply first layer of tie member

4.4.2.2 Brand B Sample

The results of parametric study for Brand B's GFRP crossarm is shown in Table 4.22 and 4.23 for broken wire condition. From Table 4.22, it can be observed that the maximum deformation for 1WL is 82.83 mm which is higher than the latest TNB requirement that is L/400 (12.3 mm). Figure 4.34, 4.35, and 4.36 shows the maximum deformation, equivalent stress first ply for main member, and tie member of Brand A's GFRP crossarm for 1 x Working Load (WL). Based on the minimum strength of materials, it is found that the Factor of Safety (FOS) is 0.40 which mean Brand B's sample cannot withstand the working load even 1WL in broken wire condition same as normal condition.

Table 4.22 Maximum load capacity and deformation of Brand B crossarm

Working load	Vertical load (N)	Transverse Load (N)	Longitudinal Load (N)	Deformation (mm)
1WL	16436	8667	25779	82.825

Table 4.23 Maximum stress in lamina of Brand B crossarm

Load	Deformation (mm)	Stress ply (N/mm^2) First Layer		Compressive Strength (N/mm^2)	Minimum Factor of Safety (Strength/Stress)
		Main	Tie		
1WL	82.825	371.51	61.496	150	0.40

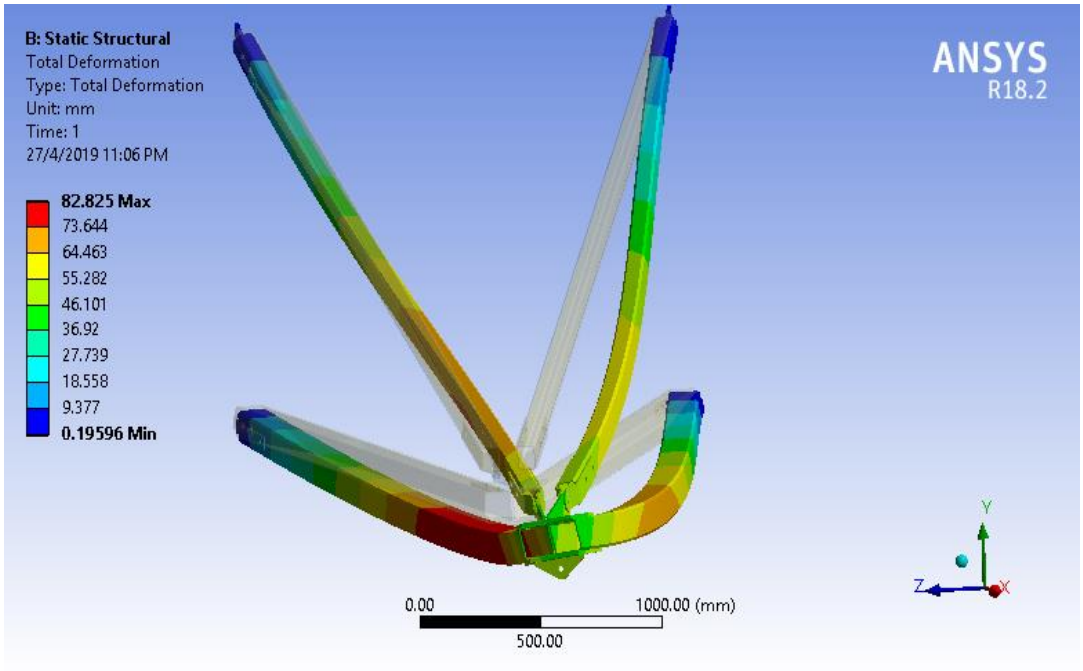

Figure 4.34 Maximum deformation of Brand B's crossarm (Broken Wire Condition)

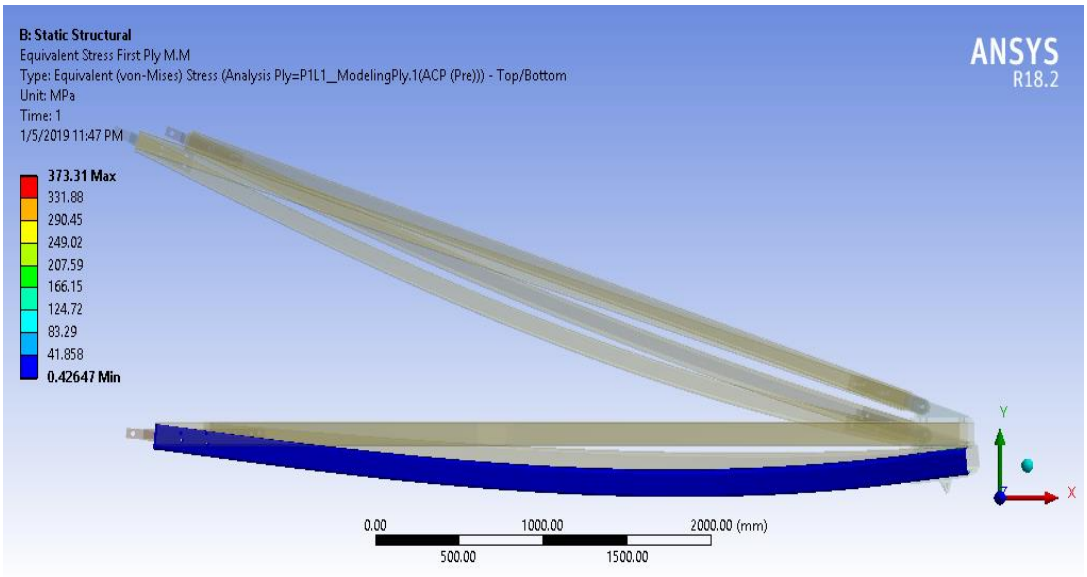

Figure 4.35 Equivalent stress ply first layer of main member

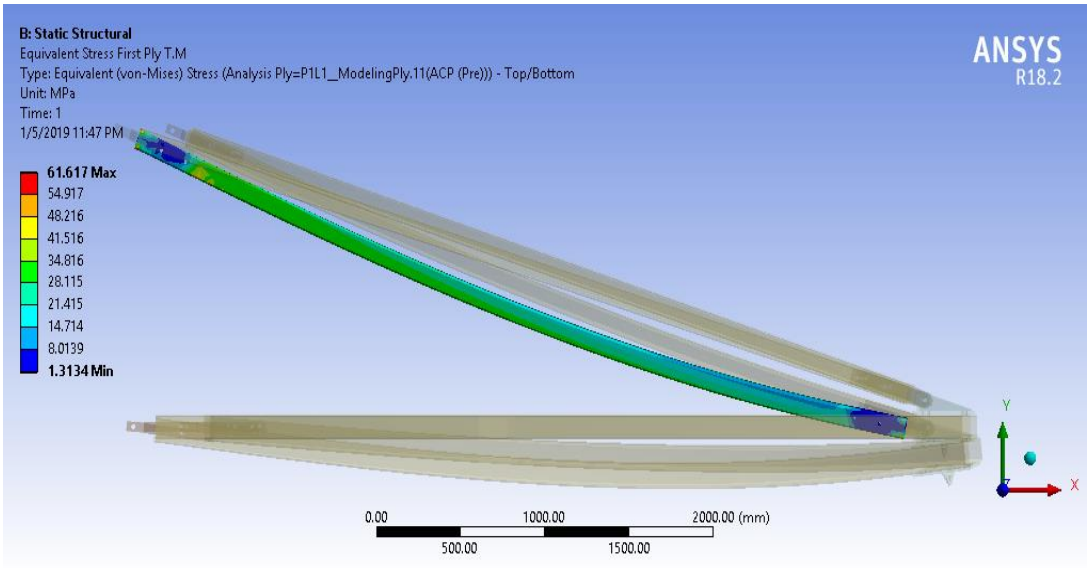

Figure 4.36 Equivalent stress ply first layer of tie member

4.4.2.3 Brand C Sample

Table 4.24 and 4.25 shows the results of parametric study for Brand C's GFRP crossarm in broken wire condition. From Table 4.24, it can be observed that the maximum deformation for 1WL is 201.76 mm which is higher than the latest TNB requirement that is L/400 (12.3 mm). However, based on the minimum strength of materials it is found that the Factor of Safety (FOS) is 2.75 which is higher than 1, which is consider safe. Maximum deformation of Brand C crossarm right before it fails is 393.79 mm at FOS of 1.37. Maximum stress of material is 120.24 N/mm^2 which give FOS of 1.37 at 2 times of applied working load that indicate the maximum loads that can be supported by Brand C crossarm in broken wire condition.

Table 4.24 Maximum load capacity and deformation of Brand C crossarm

Working load	Vertical load (N)	Transverse Load (N)	Longitudinal Load (N)	Deformation (mm)
1WL	16436	8667	25779	201.76
2WL	32872	17334	51558	393.79
3WL	49308	26001	77337	585.86

Table 4.25 Maximum stress in lamina of Brand C crossarm

Load	Deformation (mm)	Stress ply (N/mm^2) First Layer		Compressive Strength (N/mm^2)	Minimum Factor of Safety (Strength/Stress)
		Main	Tie		
1WL	201.76	60.10	65.55	165	2.75
2WL	393.79	120.24	129.63	165	1.37
3WL	585.86	180.37	193.72	165	0.91

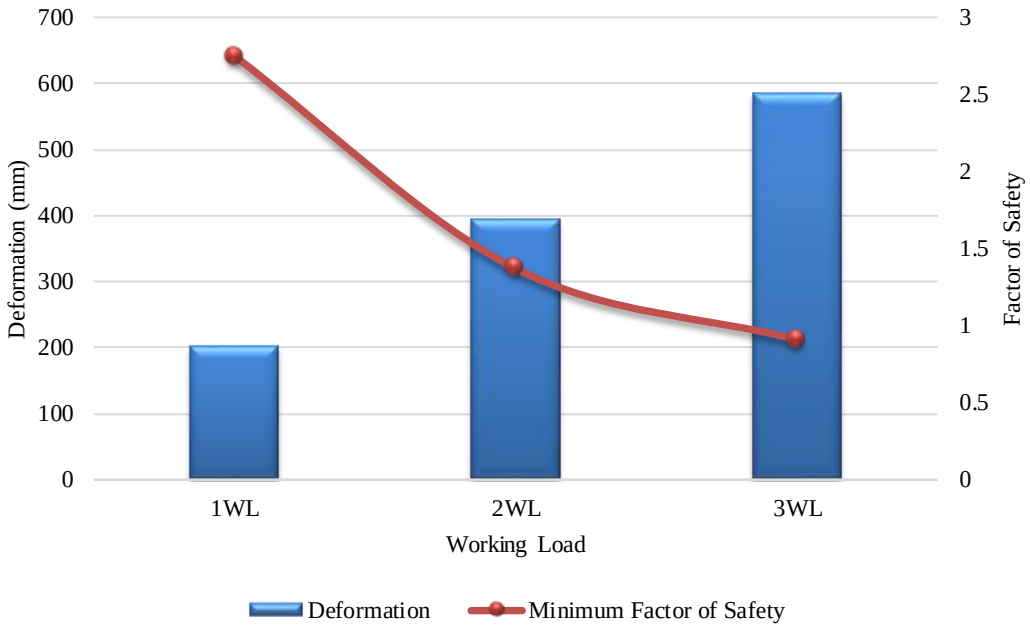

Figure 4.37 Deformation and Factor of Safety (FOS) for Brand C crossarm (Broken Wire Condition)

Figure 4.38, 4.39, and 4.40 shows the maximum deformation, equivalent stress first ply for main member, and tie member of Brand C's GFRP crossarm for 2 x Working Load (WL). Referring to Figure 4.37, Brand C crossarm failed at 3 WL with deformation of 585.86 mm and 0.91 FOS. Maximum load that can hold by Brand C's sample for broken wire condition are 32872 N, 17334 N, and 51558 N for vertical, transverse, and longitudinal load respectively.

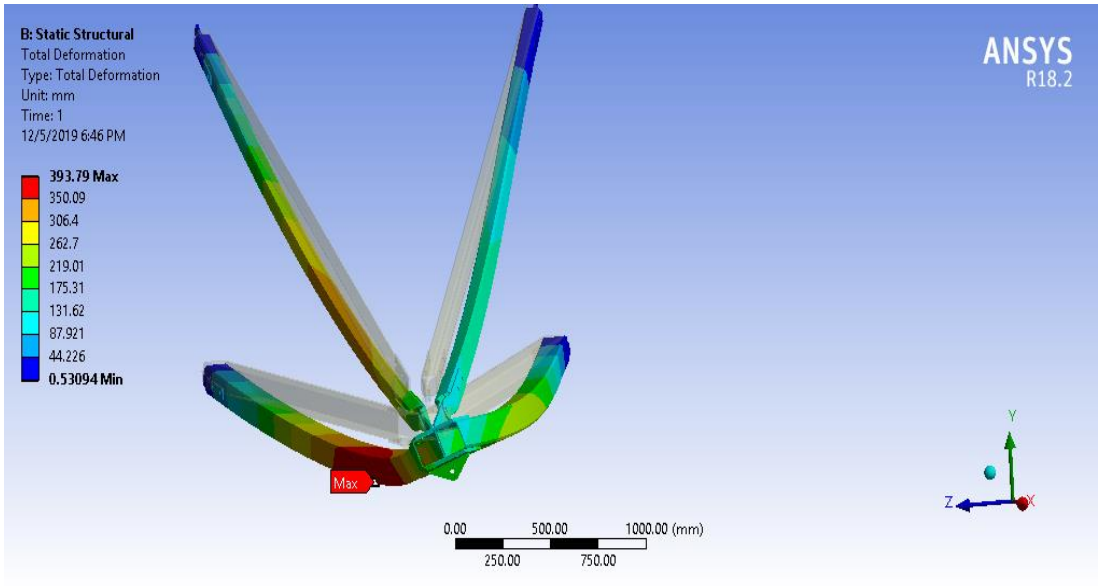

Figure 4.38 Maximum deformation of Brand C crossarm (Broken Wire Condition)

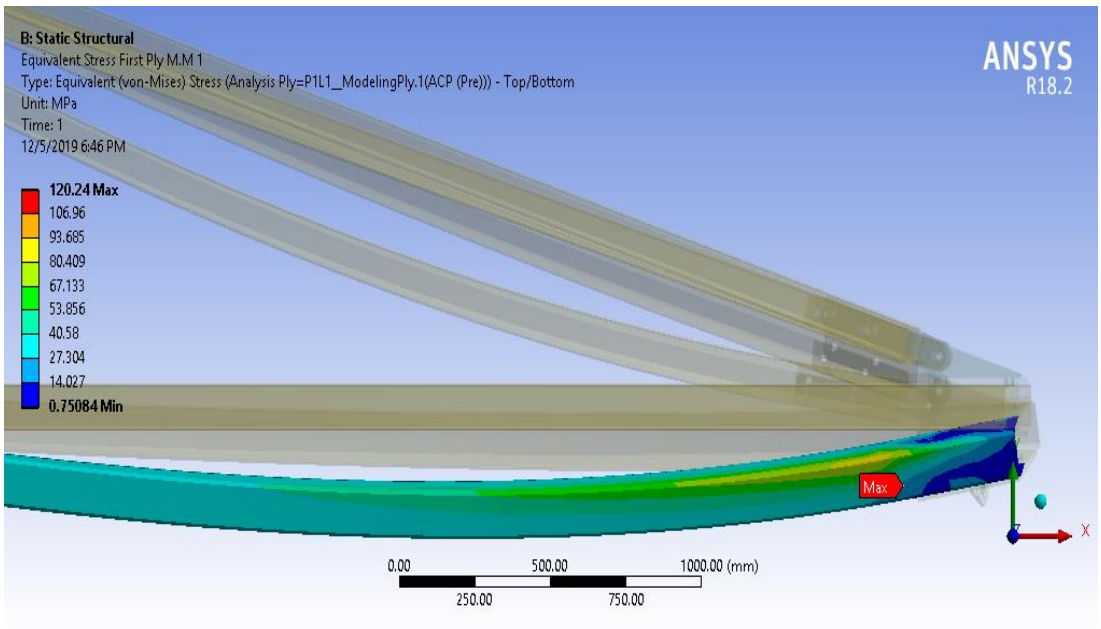

Figure 4.39 Equivalent stress ply first layer of main member

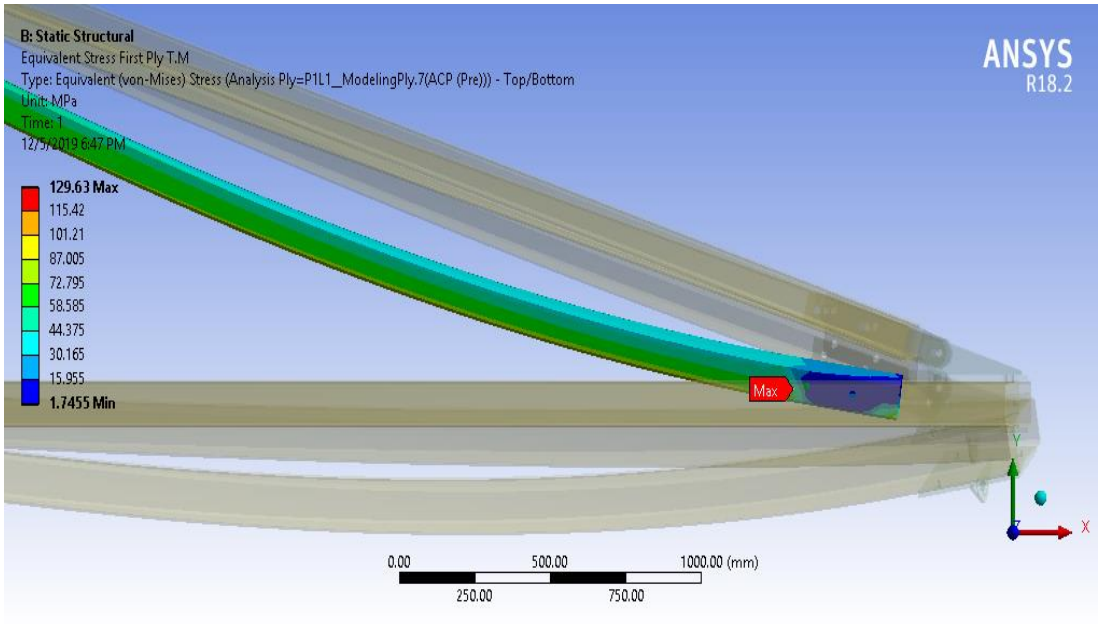

Figure 4.40 Equivalent stress ply first layer of tie member

4.4.2.4 Brand D Sample

Table 4.26 and 4.27 shows the results of parametric study for Brand D's GFRP crossarm in broken wire condition. Figure 4.41, 4.42, and 4.43 shows the maximum deformation, equivalent stress first ply for main member, and tie member of Brand D's GFRP crossarm for 1 x Working Load (WL). Based on the minimum strength of materials, it is found that the Factor of Safety (FOS) is 0.85 which mean Brand D's sample cannot withstand the working load even 1WL.

Table 4.26 Maximum load capacity and deformation of Brand D crossarm

Working load	Vertical load (N)	Transverse Load (N)	Longitudinal Load (N)	Deformation (mm)
1WL	16436	8667	25779	72.56

Table 4.27 Maximum stress in lamina of Brand D crossarm

Load	Deformation (mm)	Stress ply (N/mm^2) First Layer		Compressive Strength (N/mm^2)	Minimum Factor of Safety (Strength/Stress)
		Main	Tie		
1WL	72.56	333.67	58.53	284	0.85

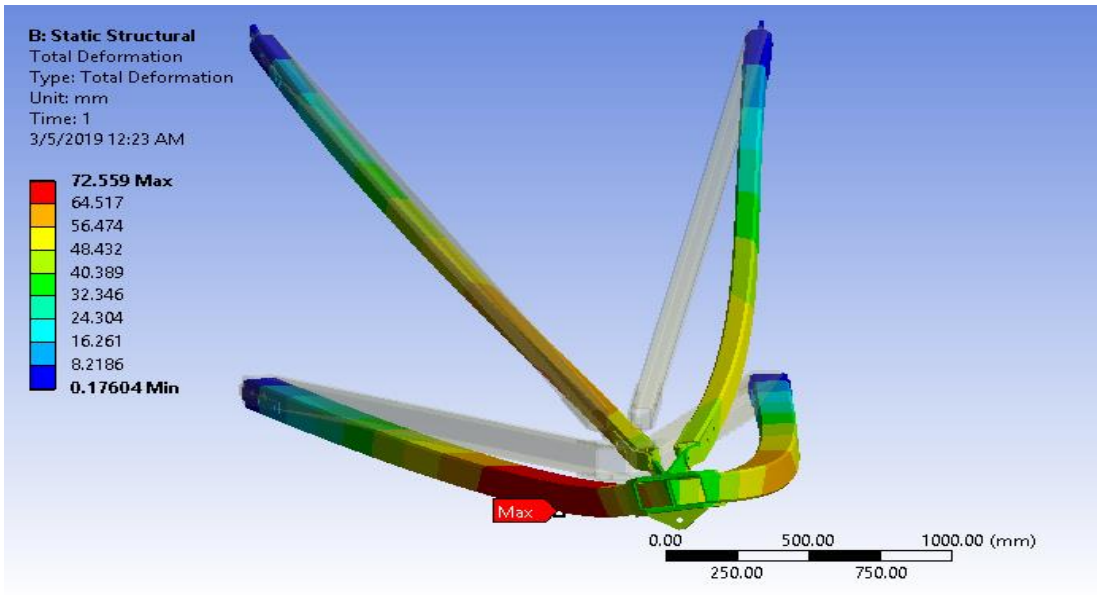

Figure 4.41 Maximum deformation of Brand D crossarm (Broken Wire Condition)

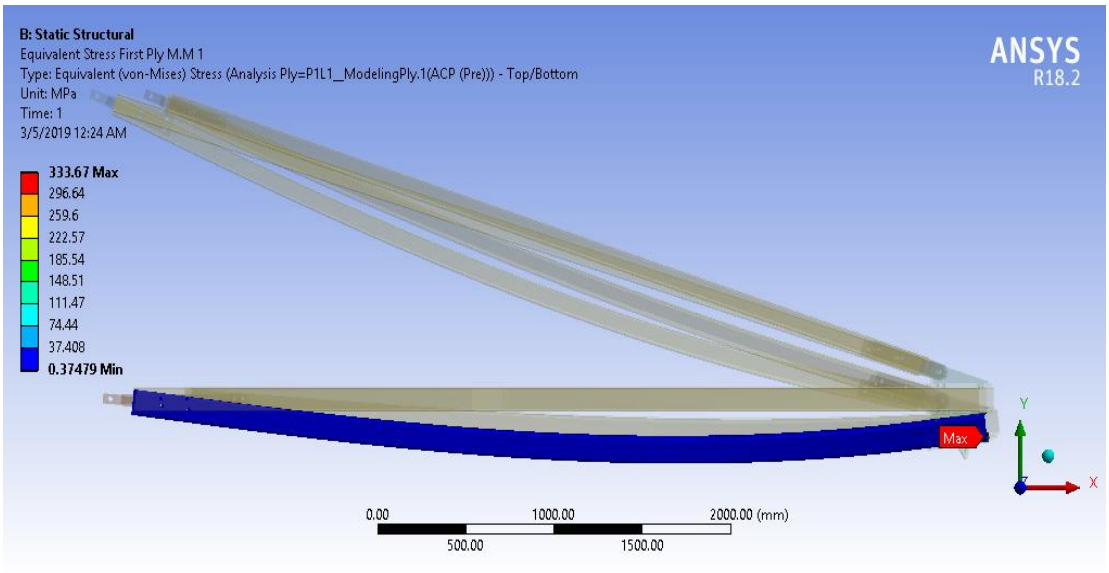

Figure 4.42 Equivalent stress ply first layer of main member

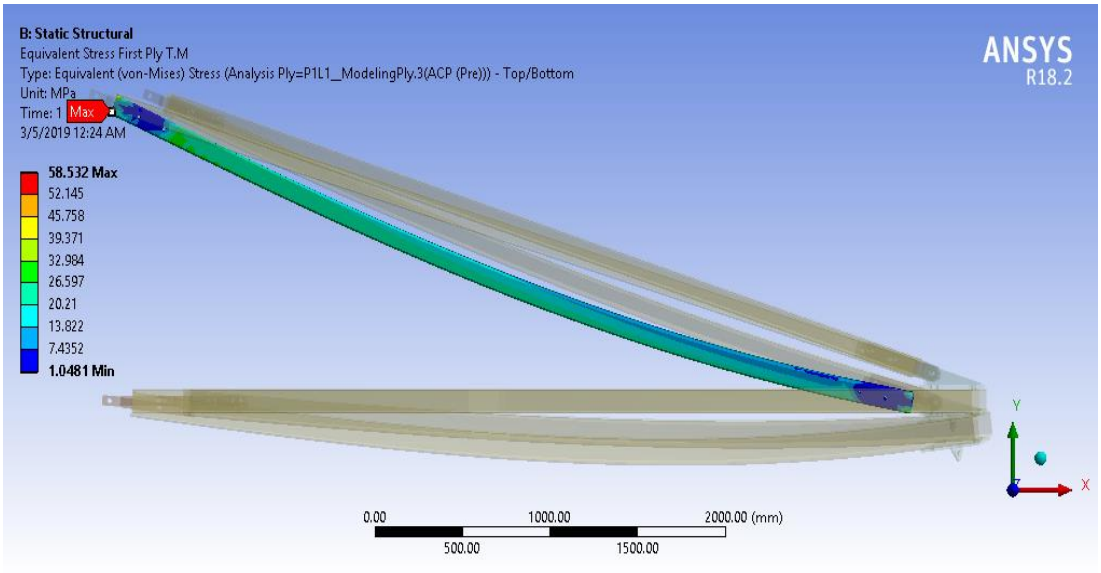

Figure 4.43 Equivalent stress ply first layer of tie member

4.4.3 Normal Condition vs Broken Wire Condition

GFRP crossarm of different brand fails at certain working load due to different material characterization of lamina. This section will be compared both condition of GFRP crossarm which is normal condition with broken wire condition for all brands of GFRP crossarm. Comparison of normal condition with broken wire condition were tabulated in Table 4.28, 4.29, 4.30 and 4.31.

Table 4.28 Comparison normal condition VS broken wire condition for Brand A crossarm

Load	Deformation (mm)		Minimum Factor of Safety (Strength/Stress)	
	Normal Condition	Broken Wire Condition	Normal Condition	Broken Wire Condition
1WL	49.60	55.07	5.16	3.22
2WL	93.77	109.05	2.66	1.64
3WL	137.96	162.42	1.79	1.10
4WL	182.15	215.79	1.35	0.82
5WL	226.35		1.08	
6WL	270.54		0.90	

It was discovered that Brand A crossarm was able to support up to 5 times Working Load (WL) for normal condition while 3WL for broken wire condition. Maximum deformation in normal condition for 1WL and 5WL are 49.60 mm and 226.35 mm respectively. Maximum deformation in broken wire condition for 1WL and 3WL are 55.07 mm and 162.42 mm. Minimum Factor of Safety (FOS) for normal condition is 1.08 at 5WL while for broken wire condition is 1.10 at 3WL.

Table 4.29 Comparison normal condition VS broken wire condition for Brand B crossarm

Load	Deformation (mm)		Minimum Factor of Safety (Strength/Stress)	
	Normal Condition	Broken Wire Condition	Normal Condition	Broken Wire Condition
1WL	64.76	82.825	0.67	0.40

Brand B crossarm was not able to support even up to 1 times Working Load (WL) for both normal and broken wire condition. Both conditions fail with minimum FOS below than 1.

Table 4.30 Comparison normal condition VS broken wire condition for Brand C crossarm

Load	Deformation (mm)		Minimum Factor of Safety (Strength/Stress)	
	Normal Condition	Broken Wire Condition	Normal Condition	Broken Wire Condition
1WL	148.40	201.76	4.60	2.75
2WL	283.76	393.79	2.34	1.37
3WL	419.12	585.86	1.56	0.91
4WL	554.50		1.18	
5WL	689.88		0.94	

Brand C crossarm was able to support up to 4 times Working Load (WL) for normal condition while 2WL for broken wire condition. Maximum deformation in normal condition for 1WL and 4WL are 148.40 mm and 554.50 mm respectively. Maximum deformation in broken wire condition for 1WL and 2WL are 201.76 mm and 393.79 mm. Minimum Factor of Safety (FOS) for normal condition is 1.18 at 4WL while for broken wire condition is 1.37 at 2WL.

Table 4.31 Comparison normal condition VS broken wire condition for Brand D crossarm

Load	Deformation (mm)		Minimum Factor of Safety (Strength/Stress)	
	Normal Condition	Broken Wire Condition	Normal Condition	Broken Wire Condition
1WL	56.29	72.56	1.36	0.85
2WL	106.27		0.72	

Brand D crossarm was able to hold up to 1 times Working Load (WL) for normal condition while Brand D crossarm was not able to hold up even to 1 times Working Load (WL) for broken wire condition. Maximum deformation in normal condition for 1WL is 56.29 mm. Minimum Factor of Safety (FOS) for normal condition is 1.36 at 1WL while for broken wire condition fails with minimum FOS below than 1.

4.4.4 Summary

GFRP crossarm of different brands fails at certain working load due to different material strength and stress of lamina. This section will be compared both condition of GFRP crossarm which is normal condition and broken wire condition for all brands of GFRP crossarm. Comparison of normal condition with different brand of crossarm were tabulated in Table 4.32 while for broken wire condition were tabulated in Table 4.33. Failure of crossarm was measured by the minimum factor of safety which is more than 1.0. Minimum Factor of Safety for GFRP crossarm can be calculated by using Equation 2.1.

Table 4.32 Comparison factor of safety for all brands of crossarm in normal condition

Load	Minimum Factor of Safety (Strength/Stress)			
	Brand A	**Brand B**	**Brand C**	**Brand D**
1WL	5.16	0.67	4.60	1.36
2WL	2.66		2.34	0.72
3WL	1.79		1.56	
4WL	1.35		1.18	
5WL	1.08		0.94	
6WL	0.90			

Figure 4.44 Factor of safety for all brands of crossarm in normal condition

It was discovered that Brand A crossarm was able to support up to 5 times Working Load (WL) for normal condition with minimum factor of safety 1.08 but Brand A have the highest factor of safety among all the brand of crossarm which is 5.16. Brand C crossarm have recorded a slightly lower value factor of safety than Brand A which is 4.6 and able to support up to 4 times Working Load (WL). Meanwhile, Brand D crossarm was able to support up to 1 times Working Load (WL) only for normal condition. It has been found that Brand B crossarm does not meet the requirements of having a minimum factor of safety which is more than 1.0.

Table 4.33 Comparison factor of safety for all brands of crossarm in broken wire condition

Load	Minimum Factor of Safety (Strength/Stress)			
	Brand A	Brand B	Brand C	Brand D
1WL	3.22	0.40	2.75	0.85
2WL	1.64		1.37	
3WL	1.10		0.91	
4WL	0.82			

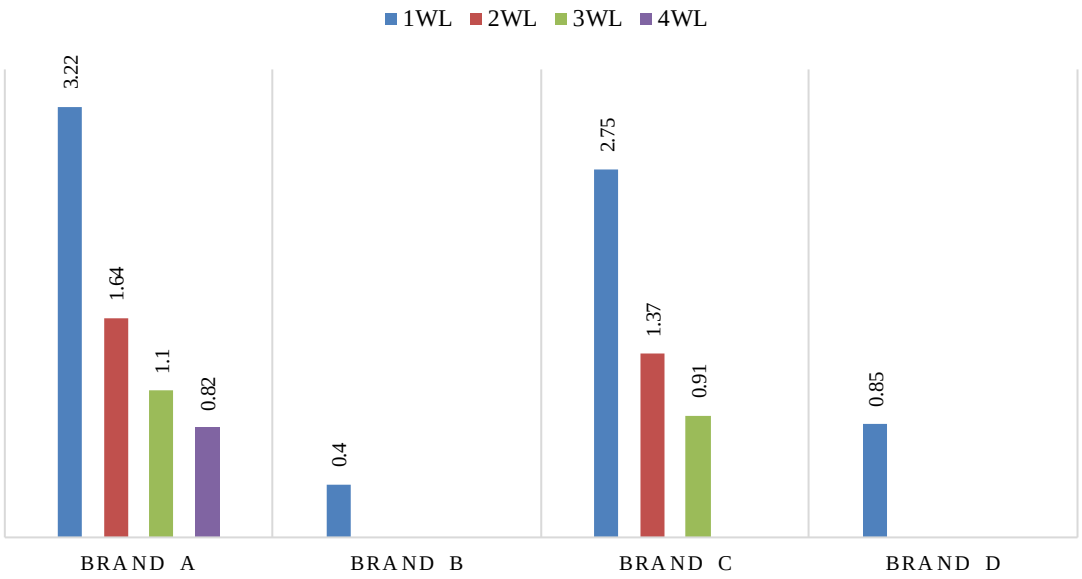

Figure 4.45 Factor of safety for all brands of crossarm in broken wire condition

It was discovered that for broken wire condition, Brand A crossarm was also able to support up to 3 times Working Load (WL) with minimum factor of safety 1.10, but as expected Brand A have the highest factor of safety among all the brand of crossarm which is 3.22. Brand C crossarm has recorded a slightly lower value than Brand A in factor of safety same as normal condition which is 2.75 and able to support up to 2 times Working Load (WL). Meanwhile, for both Brand D and Brand B crossarm was found does not meet the requirements of having a minimum factor of safety which is more than 1.0 in broken wire condition.

4.5 Failure Criteria

Failure criteria where more than one stress components have been used to evaluate the different failure modes. Failure indication for Hashin criteria comprised of fibre, matrix failures and involve four failure modes. The maximum stress criteria are used for transverse normal stress component in order to extend the criteria to three dimensional problems. This section will be compared both failure criteria of GFRP crossarm which is maximum stress criteria and hashin criteria for all brands of GFRP crossarm. Comparison of both criteria for all brands of crossarm were tabulated in Table 4.34, 4.36, 4.38, and 4.40 with different number of layer and different fiber orientation. Failure of crossarm using Hashin theory was measured by the strength ratio in ANSYS software. The strength ratio is evaluated by using both failure theories in order to check which lamina will fails first. The lamina of composite will fail if the value is equal or more than 1.0 as stated in Equation 3.8, 3.9, 4.0 and 4.1.

4.5.1 Brand A Crossarm

The results of strength ratio for Brand A's crossarm for both failure criteria were shown in Table 4.34. The plot of strength ratio versus angle of rotation for comparison of failure theories is plotted in Figure 4.46.

Table 4.34 Comparison strength ratio for Brand A crossarm in both failure criteria

Layer	Fiber Orientation	Maximum Stress	Strength Ratio Hashin (ANSYS)	Difference
1	0	0.50	0.50	0
2	45	0.26	0.30	0.04
3	0	0.38	0.38	0
4	-45	0.18	0.21	0.03
5	0	0.27	0.27	0
6	-45	0.21	0.24	0.03
7	0	0.37	0.37	0
8	45	0.23	0.25	0.02
9	0	0.47	0.48	0.01

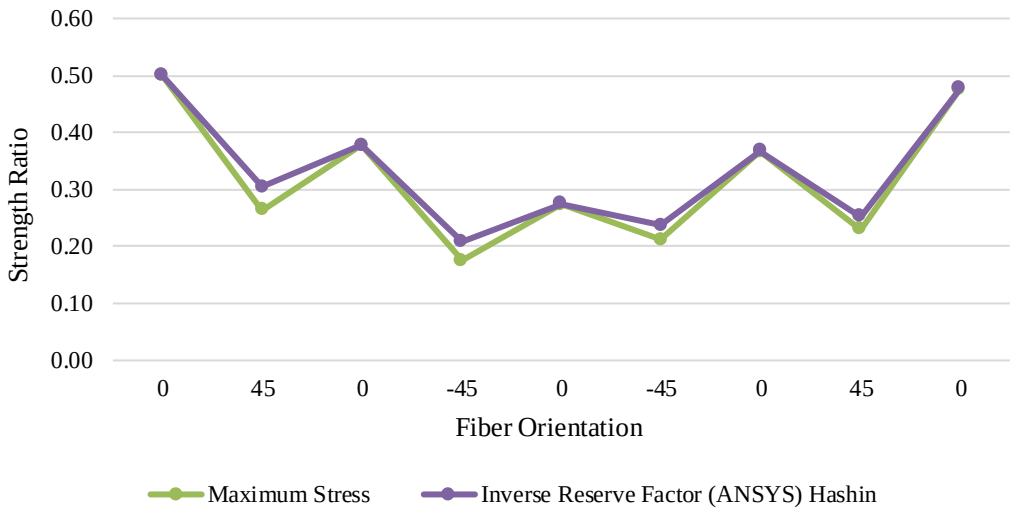

Figure 4.46 Comparison of strength ratio for Brand A Crossarm

It can be observed that the difference of the strength ratio between maximum stress and Hashin theory with error of less than 1.0. The lamina with value more than 1.0 that will fail first gives the First Ply Failure (FPF) load and the last lamina fails gives the Last Ply Failure (LPF) load.

Table 4.35 Strength ratio with different load for Brand A Crossarm

Lamina	Fiber Orientation	1WL	2WL	3WL	4WL	5WL	6WL
lamina 1	0	0.50	0.97	1.44	1.90	2.37	2.84
lamina 2	45	0.30	0.59	0.87	1.16	1.44	1.73
lamina 3	0	0.38	0.73	1.09	1.44	1.79	2.15
lamina 4	-45	0.21	0.40	0.60	0.80	0.99	1.19
lamina 5	0	0.27	0.53	0.79	1.05	1.30	1.56
lamina 6	-45	0.24	0.46	0.68	0.90	1.13	1.35
lamina 7	0	0.37	0.71	1.06	1.40	1.75	2.10
lamina 8	45	0.25	0.49	0.73	0.96	1.20	1.44
lamina 9	0	0.48	0.93	1.37	1.82	2.27	2.72

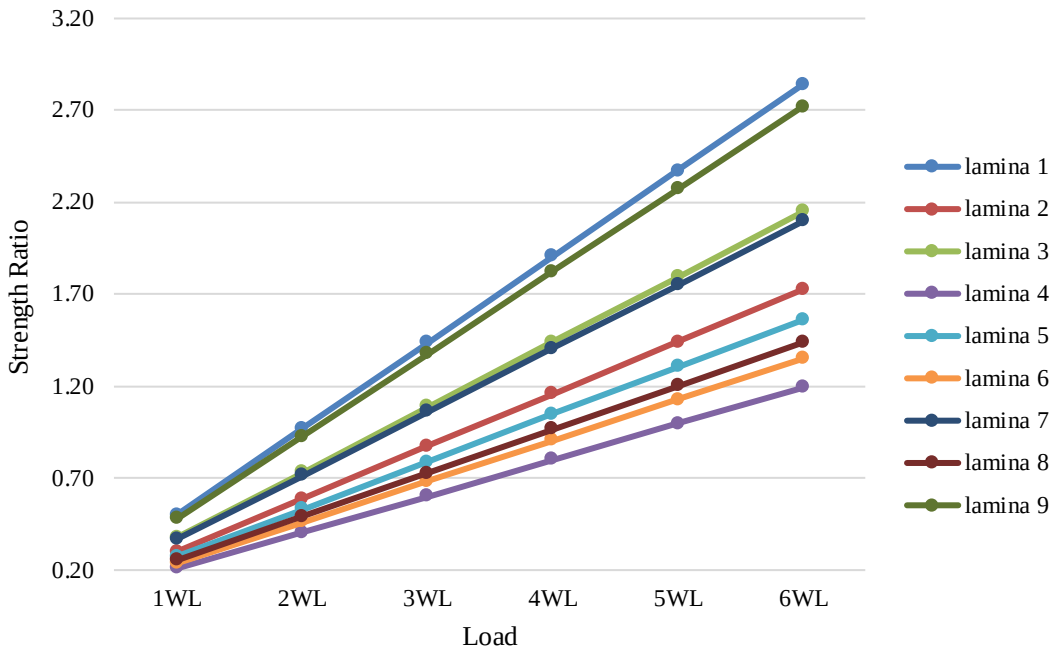

Figure 4.47 Strength ratio with different load for Brand A Crossarm

It was discovered that lamina 1, 3, 7, and 9 fails first at 3 times of Working Load (WL) with value of 1.44, 1.09, 1.06 and 1.37 and 0° fiber orientation. Brand A have an internal failure since most internal lamina will fail first for at least 3WL but the structure will not fail up until 5WL. It was observed that the lamina was failed due to the deflection at 0° fiber orientation. The failure will continue to the other degree of fiber orientation which is 45 °and 90° fiber orientation due to torsional effect of failure. Meanwhile, lamina 2 and lamina 5 fails at 4 times of Working Load (WL) with 1.16 and 1.05 strength ratio and 45° and 0° fiber orientation. At 5 times of Working Load (WL), lamina 6 and lamina 8 has been found fails with value of 1.13 and 1.20 respectively. The last lamina that fails is lamina 4 at 6 times of Working Load (WL) and -45° fiber orientation. The optimum design of GFRP can be achieved by improving the thickness of every lamina since the thinnest layer will fail first when the load was applied. Other than that, the choice of using accurate fiber orientation such as using 45 °and 90° also can be one of the factors that can minimize the failure of GFRP crossarm.

4.5.2 Brand B Crossarm

The results of strength ratio for Brand B's crossarm for both failure criteria were shown in Table 4.36. The plot of strength ratio versus angle of rotation for comparison of failure theories is plotted in Figure 4.48.

Table 4.36 Comparison strength ratio for Brand B Crossarm in both failure criteria

Layer	Fiber Orientation	Maximum Stress	Strength Ratio Hashin (ANSYS)	Difference
1	45	0.68	0.80	0.12
2	-45	0.89	1.07	0.18
3	90	0.87	0.91	0.04
4	0	0.68	0.65	-0.03
5	45	0.29	0.36	0.07

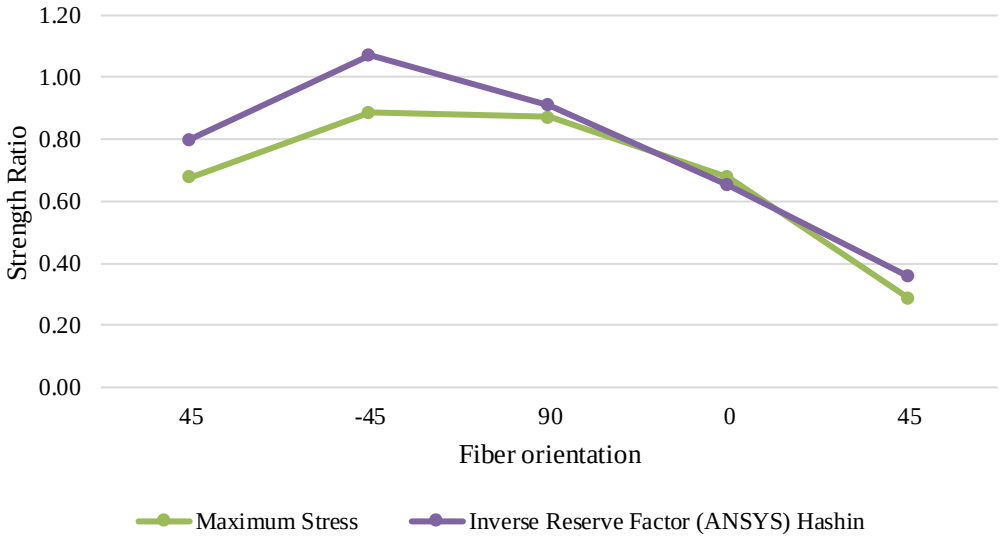

Figure 4.48 Comparison of Strength Ratio for Brand B Crossarm

It can be observed that the difference of the strength ratio between maximum stress and Hashin theory has an error of less than 1.0. However, lamina 1 and lamina 2 with 45° and -45° fiber orientation shows a slightly higher difference strength ratio value as shown in Figure 4.48.

Table 4.37 Strength ratio with different load for Brand B Crossarm

Lamina	Fiber Orientation	1WL	2WL	3WL	4WL	5WL	6WL
lamina 1	45	0.80	1.52	2.24	2.96	3.69	4.41
lamina 2	-45	1.07	2.04	3.00	3.97	4.93	5.89
lamina 3	90	0.91	1.73	2.55	3.37	4.19	5.01
lamina 4	0	0.65	1.24	1.83	2.41	3.00	3.58
lamina 5	45	0.36	0.70	1.04	1.38	1.72	2.07

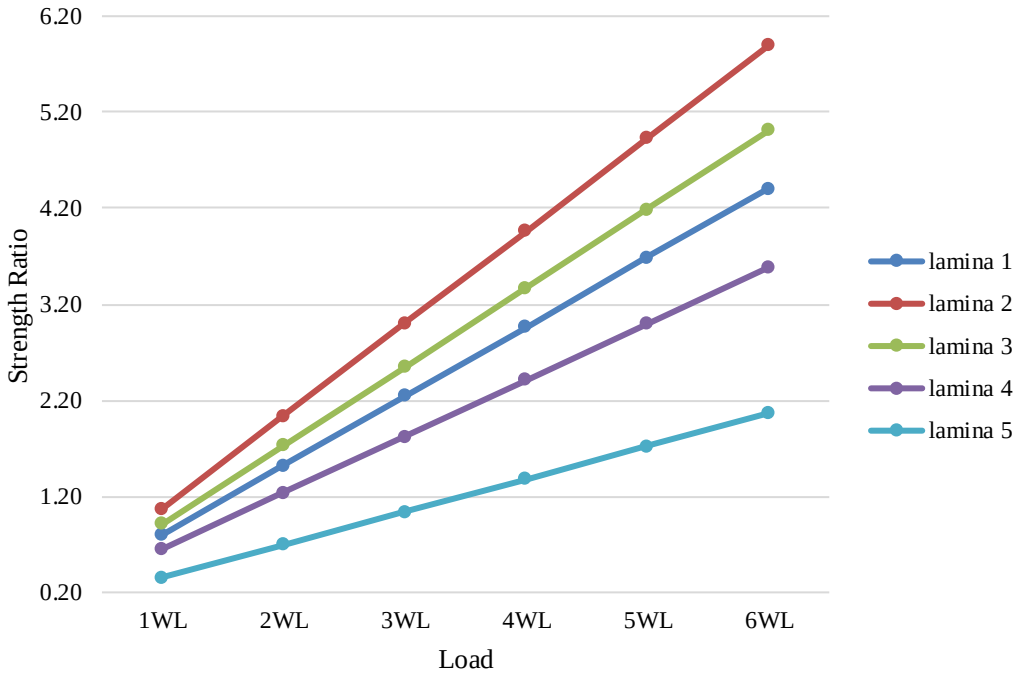

Figure 4.49 Strength ratio with different load for Brand B Crossarm

It was discovered that lamina 2 fails first at 1 times of Working Load (WL) with value of 1.07 and -45° fiber orientation. Lamina 1, 3 and lamina 4 fails at 2 times of Working Load (WL) with 1.52, 1.73, and 1.24 strength ratio and 45°, 90° and 0° fiber orientation. The last lamina fails is lamina 5 at 3 times of Working Load (WL) and 45° fiber orientation.

4.5.3 Brand C Crossarm

The results of strength ratio for Brand C's crossarm for both failure criteria were shown in Table 4.38. The plot of strength ratio versus angle of rotation for comparison of failure theories is plotted in Figure 4.50.

Table 4.38 Comparison strength ratio for Brand C Crossarm in both failure criteria

Layer	Fiber Orientation	Maximum Stress	Strength Ratio Hashin (ANSYS)	Difference
1	45	0.29	0.31	0.02
2	0	0.25	0.27	0.02
3	45	0.24	0.25	0.01

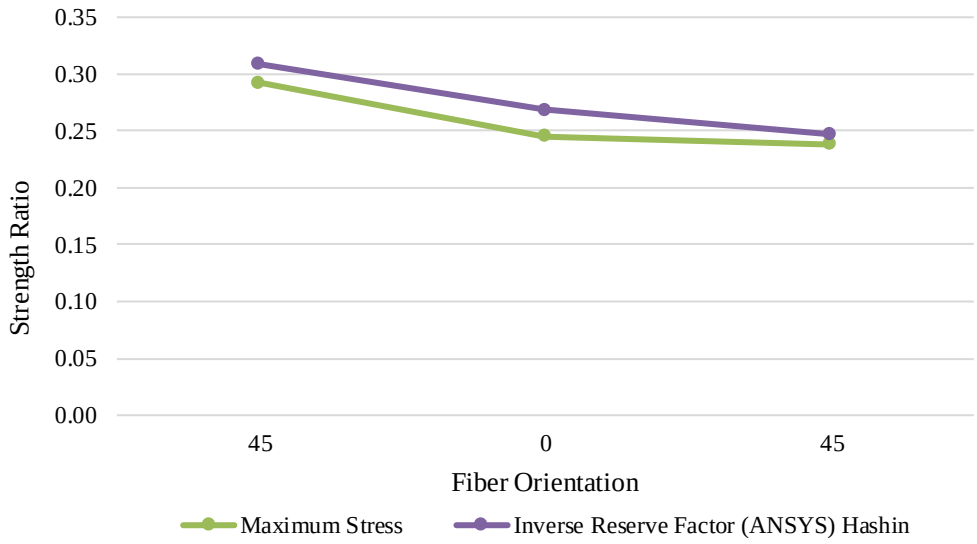

Figure 4.50 Comparison of strength ratio for Brand C Crossarm

It can be observed that the difference of the strength ratio between maximum stress and Hashin theory with error of less than 1.0.

Table 4.39 Strength ratio with different load for Brand C Crossarm

Lamina	Fiber Orientation	1WL	2WL	3WL	4WL	5WL	6WL
lamina 1	45	0.31	0.61	0.92	1.22	1.53	1.83
lamina 2	0	0.27	0.53	0.79	1.05	1.31	1.57
lamina 3	45	0.25	0.49	0.73	0.97	1.21	1.45

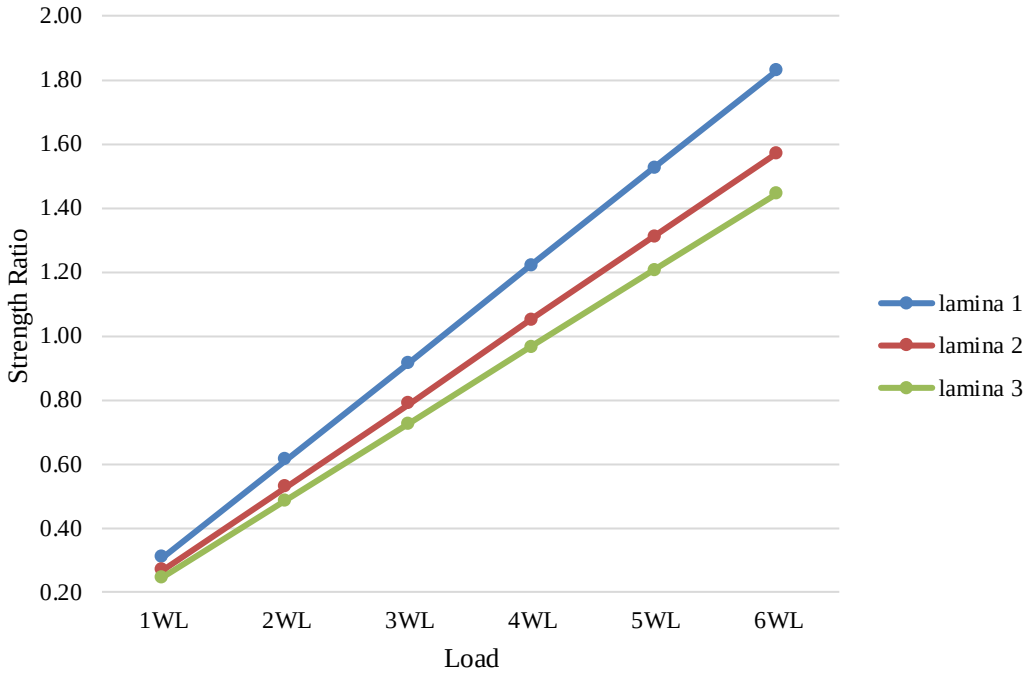

Figure 4.51 Strength ratio with different load for Brand C Crossarm

It was discovered that lamina 1 and lamina 2 fails first at 4 times of Working Load (WL) with value of 1.22 and 1.05 strength ratio and 45° and 0° fiber orientation. Meanwhile, the last lamina fails is lamina 3 at 5 times of Working Load (WL) and 45° fiber orientation as shown in Table 4.39 and Figure 4.51.

4.5.4 Brand D Crossarm

The results of strength ratio for Brand D crossarm for both failure criteria were shown in Table 4.40. The plot of strength ratio versus angle of rotation for comparison of failure theories is plotted in Figure 4.52.

Table 4.40 Comparison strength ratio for Brand D Crossarm in both failure criteria

Layer	Fiber Orientation	Maximum Stress	Strength Ratio Hashin (ANSYS)	Difference
1	45	0.81	0.87	0.06
2	-45	1.11	1.24	0.13
3	0	0.52	0.53	0.01
4	0	0.43	0.50	0.07
5	0	0.39	0.48	0.09
6	0	0.39	0.45	0.06
7	0	0.38	0.44	0.06
8	0	0.40	0.43	0.03
9	-45	0.61	0.61	0
10	45	0.35	0.39	0.04

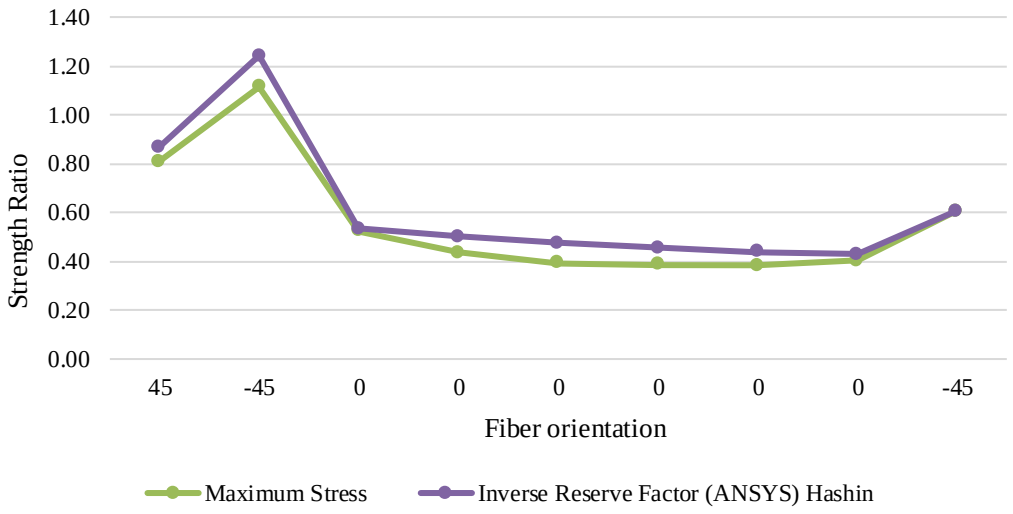

Figure 4.52 Strength ratio with different load for Brand D Crossarm

It can be observed that the difference of the strength ratio between maximum stress and Hashin theory with error of less than 1.0. However, lamina 2 with -45° fiber orientation shows a slightly higher difference strength ratio value as shown in Table 4.40.

Table 4.41 Strength ratio with different load for Brand D Crossarm

Lamina	Fiber Orientation	1WL	2WL	3WL	4WL	5WL	6WL
lamina 1	45	0.87	1.63	2.40	3.16	3.93	4.69
lamina 2	-45	1.24	2.34	3.43	4.53	5.62	6.72
lamina 3	0	0.53	1.00	1.47	1.94	2.41	2.88
lamina 4	0	0.50	0.94	1.38	1.82	2.26	2.70
lamina 5	0	0.48	0.89	1.31	1.73	2.15	2.56
lamina 6	0	0.45	0.85	1.25	1.65	2.05	2.45
lamina 7	0	0.44	0.82	1.21	1.60	1.98	2.37
lamina 8	0	0.43	0.81	1.19	1.56	1.94	2.32
lamina 9	-45	0.61	1.14	1.67	2.20	2.73	3.26
lamina 10	45	0.39	0.75	1.11	1.47	1.84	2.20

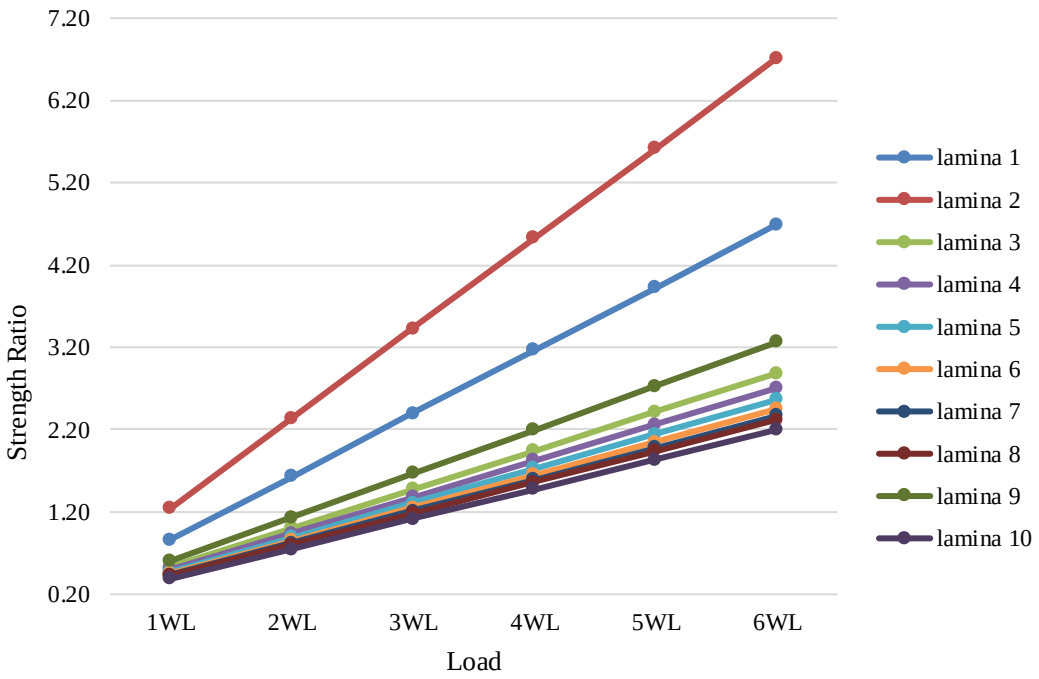

Figure 4.53 Strength ratio with different load for Brand D Crossarm

It has been found that lamina 2 fails first at 1 times of Working Load (WL) with value of 1.24 and -45° fiber orientation. Meanwhile, lamina 1, 3 and 5 fails at 2 times of Working Load (WL) with 1.63, 100 and 1.14 strength ratio and 45°, 0° and -45° fiber orientation. The last lamina fails is lamina 4, 5, 6, 7, 8 and 10 at 3 times of Working Load (WL) with 0° and -45° fiber orientation.

CHAPTER 5

CONCLUSION AND RECOMMENDATIONS FOR FUTURE WORK

5.1 Conclusion

This research was carried out to study the behaviour of glass fiber reinforced polymer (GFRP) crossarm subjected to static loading by using laboratory testing and numerical modelling. Material characterization of GFRP crossarm was conducted using four experimental testing comparing all brands of crossarms. Furthermore, forensic and experimental testing using full scale was conducted and compared with numerical modelling analysis. Numerical modelling using ANSYS has simulated different brand of crossarm with different working loads in two different condition which is normal condition and broken wire condition. Parametric study using numerical modelling was conducted to find the factor of safety and determine failure criteria of GFRP crossarm. All results and outcome of these studies will be concluded in this chapter.

a) Based on density and specific gravity test, the range of density for GFRP crossarm falls between the range of 1800 kg/m^3 - 2030 kg/m^3. The percent fibre mass fraction mostly ranging from 64% to 78% and for percent of void content falls in the range of 13% only. The thickness of GFRP crossarm was observed falls between range 5 mm to 6 mm at all side of crossarm. Higher fibre content coupled with low void content could be one of the possible reasons that contribute to superior mechanical performance of GFRP crossarm. Based on the result obtained from tensile test shown that the sufficient tensile strength for GFRP crossarm is between 500 MPa to 540 MPa and for tensile modulus is between 20 GPa to 30 GPa. Higher tensile strength is due to the higher content of continuous fiber roving used in fabricating the profiles. It was discovered from compressive strength test that the compressive stress value is between 165 MPa to 320 MPa and for compressive modulus is between 30 GPa to 36 GPa. Samples produced by Brand A displayed superior performance than samples produced by other manufacturers in terms of microstructure, physical, mechanical and durability properties.

b) It was found that the deformation of GFRP crossarm recorded the value of 7.7 cm to 12 cm. Meanwhile, it was discovered that during the experimental testing, the breaking load has been exceed until 80 kN. This proves that GFRP crossarm must has the ability to withstand highest working load in full assembly testing using vertical load in order to have a better performance. Allowable percentage difference between experimental and numerical analysis results must falls below 5% in order to consider acceptable according to studies by Gabriele (2016) [63].

c) Based on numerical simulation, it was found that GFRP crossarm was able to withstand load up to 5 times of working load (WL) in normal condition and 3WL for broken wire condition. From calculation using Equation 2.1, it was discovered that GFRP crossarm recorded Factor of Safety (FOS) ranging from 1.36 to 5.16 which meet the requirement of having FOS higher than 1 in normal condition. It was observed that for broken wire condition, the FOS is ranging between 2.75 to 3.22.

d) Failure criteria of GFRP crossarm using Hashin failure criteria theory was conducted to determine the micro-failure of GFRP crossarm. It was found that GFRP crossarm have an internal lamina failure since all brands of GFRP crossarm fails first at range of lamina 2 to lamina 8. Outer lamina of GFRP crossarms fails when the maximum load is reached. It was observed that the lamina was failed due to the deflection at 0° and -45° fiber orientation. The failure then continues to the other degree of fiber orientation which is 45° and 90° fiber orientation due to torsional effect of failure. Better fibre arrangement with high precision design and better process control facilitates during fabrication leading to consistent cross-section and uniform fibre content which can slow down the failure of GFRP crossarm.

5.2 Recommendation

The premature failure of GFRP crossarms became a crucial issue since it will affect production of electricity and incur high cost for repairing and maintenance. The premature failure of crossarms is mainly due to the poor quality of crossarms which was contributed by many factors such as choice of materials, precision and optimization processing parameters and design. The followings are some pertinent matters for consideration:

i) The types of testing and characterisations in this study is classified as full scale testing and is confine to static mechanical testing. In service, GFRP crossarms are being subjected to a more complex load such as transverse load, longitudinal load and mode of stresses (tensile, compression, bending, torsion). Thus, it is highly recommended to conduct those tests so as to gather more relevant data that can be used to predict the service behaviour of the GFRP crossarms since in this study conducted for vertical load only.

ii) Future research on the failure analysis and mode of failure in GFRP crossarm should be conducted by comparing all failure theories in composite by using numerical simulation. This is to evaluate the structural performance of GFRP crossarm in transmission tower.

REFERENCES

[1] N. Prasad Rao, G. M. Samuel Knight, S. J. Mohan, and N. Lakshmanan, "Studies on failure of transmission line towers in testing," *Eng. Struct.*, vol. 35, pp. 55–70, 2012.

[2] S. Grzybowski, L. Fellow, T. Disyadej, and S. Member, "Electrical Performance of Fiberglass Crossarm in Distribution and Transmission Lines," pp. 1–5, 2008.

[3] I. M. Rawi, M. S. A. Rahman, M. Z. A. Ab Kadir, and M. Izadi, "Wood and fiberglass crossarm performance against lightning strikes on transmission towers," *Int. Conf. Power Syst. Transient*, pp. 1–6, 2017.

[4] L. Prediction, O. F. Electrical, and P. Transmission, "ESDA2008-59490," pp. 1–11, 2008.

[5] N. Zawani and M. Faizuhar, "Modelling of 132kV Overhead Transmission Lines by Using ATP / EMTP for Shielding Failure Pattern Recognition," *Procedia Eng.*, vol. 53, pp. 278–287, 2013.

[6] O. O. Ochoa and J. N. Reddy, *Finite Element Analysis of Composite Laminates*. 1992.

[7] H. Xin, Y. Liu, A. S. Mosallam, J. He, and A. Du, "Evaluation on material behaviors of pultruded glass fiber reinforced polymer (GFRP) laminates," vol. 182, pp. 283–300, 2017.

[8] Z. Itam, Z. A. M. Ishak, Z. M. Yusof, N. Salwi, and M. Zainoodin, "Effect on the temperature behavior of glass fiber reinforced polymer (GFRP) in various application - A review," vol. 020026, no. November, p. 020026, 2018.

[9] S. Zhang, C. C. Caprani, and A. Heidarpour, "Strain rate studies of pultruded glass fibre reinforced polymer material properties : A literature review," vol. 171, pp. 984–1004, 2018.

[10] A. Syamsir, Z. A. M. Ishak, Z. M. Yusof, N. Salwi, and A. Nadhirah, "Durability control of UV radiation in glass fiber reinforced polymer (GFRP) - A review," vol. 020033, no. November, p. 020033, 2018.

[11] A. Kashi, A. A. Ramezanianpour, and F. Moodi, "Durability evaluation of retrofitted corroded reinforced concrete columns with FRP sheets in marine environmental conditions," *Constr. Build. Mater.*, vol. 151, pp. 520–533, 2017.

[12] M. Giampaoli, V. Terlizzi, M. Rossi, G. Chiappini, and P. Munafò, "Mechanical

performances of GFRP-steel specimens bonded with different epoxy adhesives , before and after the aging treatments," *Compos. Struct.*, vol. 171, pp. 145–157, 2017.

[13] Y. Fang *et al.*, "Monitoring of seawater immersion degradation in glass fi bre reinforced polymer composites using quantum dots," *Compos. Part B*, vol. 112, pp. 93–102, 2017.

[14] J. M. L. Reis, F. D. F. Martins, and H. S. Costa, "In fl uence of ageing in the failure pressure of a GFRP pipe used in oil industry," *EFA*, vol. 71, pp. 120–130, 2017.

[15] A. Kashi, A. Akbar, and F. Moodi, "Effect of cement based coatings on durability enhancement of GFRP-wrapped columns in marine environments," *Constr. Build. Mater.*, vol. 137, pp. 307–316, 2017.

[16] T. Wong, K. Lau, W. Tam, J. Leng, and J. A. Etches, "UV resistibility of a nano-ZnO / glass fibre reinforced epoxy composite," *J. Mater.*, vol. 56, pp. 254–257, 2014.

[17] S. Beddu, A. Syamsir, Z. Arifin, and M. Ishak, "Creep behavior of glass fibre reinforced polymer structures in crossarms transmission line towers," *AIP Conf. Proc.*, vol. 020039, no. November, 2018.

[18] V. Paolo, M. Perrella, L. Feo, and G. Cricrì, "Creep behavior of GFRP laminates and their phases : Experimental investigation and analytical modeling," *Compos. Part B*, vol. 122, pp. 136–144, 2017.

[19] M. F. Sá, A. M. Gomes, J. R. Correia, and N. Silvestre, "Creep behavior of pultruded GFRP elements – Part 1 : Literature review and experimental study," vol. 93, pp. 2450–2459, 2011.

[20] Y. A. Al-salloum and T. H. Almusallam, "Creep effect on the behavior of concrete beams reinforced with GFRP bars subjected to different environments," vol. 21, pp. 1510–1519, 2007.

[21] J. A. Gonilha *et al.*, "Static , dynamic and creep behaviour of a full-scale GFRP-SFRSCC hybrid footbridge," vol. 118, pp. 496–509, 2014.

[22] L. Ascione, V. P. Berardi, and A. D. Aponte, "Creep phenomena in FRP materials," *Mech. Res. Commun.*, vol. 43, pp. 15–21, 2012.

[23] W. Wang, M. Sain, and P. A. Cooper, "SCIENCE AND Study of moisture absorption in natural fiber plastic composites," vol. 66, pp. 379–386, 2006.

[24] B. C. Ray, "Temperature effect during humid ageing on interfaces of glass and

carbon fibers reinforced epoxy composites," vol. 298, pp. 111–117, 2006.

[25] J. Wang, H. Gangarao, R. Liang, and D. Zhou, "Durability of glass fiber-reinforced polymer composites under the combined effects of moisture and sustained loads," no. 30, 2015.

[26] Y. Hu, X. Li, A. W. Lang, Y. Zhang, and S. R. Nutt, "Water immersion aging of polydicyclopentadiene resin and glass fi ber composites," *Polym. Degrad. Stab.*, vol. 124, pp. 35–42, 2016.

[27] P. Böer, L. Holliday, and T. H. Kang, "Independent environmental effects on durability of fiber-reinforced polymer wraps in civil applications : A review," *Constr. Build. Mater.*, vol. 48, pp. 360–370, 2013.

[28] G. Carra and V. Carvelli, "Ageing of pultruded glass fibre reinforced polymer composites exposed to combined environmental agents," *Compos. Struct.*, vol. 108, pp. 1019–1026, 2014.

[29] A. Zafar, F. Bertocco, and J. C. Rauhe, "Investigation of the long term effects of moisture on carbon fibre and epoxy matrix composites," *Compos. Sci. Technol.*, vol. 72, no. 6, pp. 656–666, 2012.

[30] K. Aniskevich, A. Aniskevich, A. Arnautov, and J. Jansons, "Mechanical properties of pultruded glass fiber-reinforced plastic after moistening," *Compos. Struct.*, vol. 94, no. 9, pp. 2914–2919, 2012.

[31] X. Jiang, H. Kolstein, and F. S. K. Bijlaard, "Composites : Part B Moisture diffusion in glass – fiber-reinforced polymer composite bridge under hot / wet environment," *Compos. Part B*, vol. 45, no. 1, pp. 407–416, 2013.

[32] A. Pegoretti and A. Penati, "Recycled poly (ethylene terephthalate) and its short glass fibres composites : effects of hygrothermal aging on the thermo-mechanical behaviour," vol. 45, pp. 7995–8004, 2004.

[33] I. Nishizaki and S. Meiarashi, "Long-Term Deterioration of GFRP in Water and Moist Environment," vol. 6, no. February, pp. 21–27, 2002.

[34] N. Sateesh, P. S. Rao, D. V Ravishanker, and K. Satyanarayana, "Effect of Moisture on GFRP Composite Materials," *Mater. Today Proc.*, vol. 2, no. 4–5, pp. 2902–2908, 2015.

[35] M. Heshmati, R. Haghani, and M. Al-emrani, "Durability of bonded FRP-to-steel joints : Effects of moisture , de-icing salt solution , temperature and FRP type," *Compos. Part B*, vol. 119, pp. 153–167, 2017.

[36] H. Xin, Y. Liu, A. Mosallam, and Y. Zhang, "Moisture diffusion and

hygrothermal aging of pultruded glass fi ber reinforced polymer laminates in bridge application," *Compos. Part B*, vol. 100, pp. 197–207, 2016.

[37] S. Eslami, A. Honarbakhsh-raouf, and S. Eslami, "Effects of moisture absorption on degradation of E-glass fiber reinforced Vinyl Ester composite pipes and modelling of transient moisture diffusion using finite element analysis," *Corros. Sci.*, vol. 90, pp. 168–175, 2015.

[38] A. Manalo, G. Maranan, S. Sharma, W. Karunasena, and Y. Bai, "Temperature-sensitive mechanical properties of GFRP composites in longitudinal and transverse directions : A comparative study," *Compos. Struct.*, vol. 173, pp. 255–267, 2017.

[39] V. Carvelli, M. A. Pisani, and C. Poggi, "Composites : Part B High temperature effects on concrete members reinforced with GFRP rebars," *Compos. Part B*, vol. 54, pp. 125–132, 2013.

[40] M. Robert and B. Benmokrane, "Behavior of GFRP Reinforcing Bars Subjected to Extreme Temperatures," vol. 14, no. August, pp. 353–360, 2010.

[41] M. Berry, J. Johnson, and K. Mcdevitt, "Cold Regions Science and Technology Effect of cold temperatures on the behavior and ultimate capacity of GFRP-reinforced concrete beams," *Cold Reg. Sci. Technol.*, vol. 136, pp. 9–16, 2017.

[42] D. Baggio, K. Soudki, and M. Noël, "Strengthening of shear critical RC beams with various FRP systems," *Constr. Build. Mater.*, vol. 66, pp. 634–644, 2014.

[43] R. H. Haddad, N. Al-mekhlafy, and A. M. Ashteyat, "Repair of heat-damaged reinforced concrete slabs using fibrous composite materials," *Constr. Build. Mater.*, vol. 25, no. 3, pp. 1213–1221, 2011.

[44] I. Shaw and B. Andrawes, "Repair of damaged end regions of PC beams using externally bonded FRP shear reinforcement," *Constr. Build. Mater.*, vol. 148, pp. 184–194, 2017.

[45] A. Kaya, M. Dawood, and B. Gencturk, "Repair of corroded and buckled short steel columns using concrete-filled GFRP jackets," *Constr. Build. Mater.*, vol. 94, pp. 20–27, 2015.

[46] E. Aydin and M. Aktas, "Thin-Walled Structures Obtaining a permanent repair by using GFRP in steel plates reformed by heat-treatment," *Thin Walled Struct.*, vol. 94, pp. 13–22, 2015.

[47] I. Mahfouz, S. Sarkani, and T. Rizk, "REPAIRING AND STRENGTHENING REINFORCED CONCRETE STRUCTURES USING FIBER- REINFORCED

PLASTICS."

[48] M. Yaqub and C. G. Bailey, "Cross sectional shape effects on the performance of post-heated reinforced concrete columns wrapped with FRP composites," *Compos. Struct.*, vol. 93, no. 3, pp. 1103–1117, 2011.

[49] M. Selvaraj, S. Kulkarni, and R. R. Babu, "Analysis and experimental testing of a built-up composite cross arm in a transmission line tower for mechanical performance," *Compos. Struct.*, vol. 96, pp. 1–7, 2013.

[50] "See discussions, stats, and author profiles for this publication at: https://www.researchgate.net/publication/303517627," no. May 2016, pp. 3–6.

[51] W. Grodzki and K. Le, "MODELLING OF UAV ' S COMPOSITE STRUCTURES AND PREDICTION," pp. 67–75.

[52] S. Kaewunruen, K. Goto, and L. Xie, "Materials Today : Proceedings Failure modes of fibre reinforced foamed urethane composite beams : Full-scale experimental determination," *Mater. Today Proc.*, vol. 29, no. November 2018, pp. 11–15, 2020.

[53] B. R. Producers and N. Bureau, "A theory of the yielding and plastic flow of anisotropic metals," pp. 281–297, 1947.

[54] S. W. Tsai and E. M. Wu, "Theory of Strength for Anisotropic Materials," vol. 5, no. January 1971, 2016.

[55] F. Composites, "Failure Criteria for Unidirectional Mr !," vol. 47, no. June, pp. 329–334, 1980.

[56] A. Puck and H. Schu, "Failure analysis of FRP laminates by means of physically based phenomenological models," vol. 62, pp. 1633–1662, 2002.

[57] R. Koh and B. Madsen, "Mechanics of Materials Strength failure criteria analysis for a fl ax fi bre reinforced composite," *Mech. Mater.*, vol. 124, no. April, pp. 26–32, 2018.

[58] X. Li *et al.*, "Assessment of failure criteria and damage evolution methods for composite laminates under low-velocity impact," vol. 207, no. July 2018, pp. 727–739, 2019.

[59] R. M. Christensen, "Failure criteria for fiber composite materials , the astonishing sixty year search , definitive usable results," *Compos. Sci. Technol.*, vol. 182, no. July, p. 107718, 2019.

[60] M. J. Hinton, A. S. Kaddour, and P. D. Soden, *A comparison of the predictive capabilities of current failure theories for composite laminates , judged against*

experimental evidence, vol. 62. 2002.

[61] R. H. Lopez, M. A. Luersen, and E. S. Cursi, "Composites : Part B Optimization of laminated composites considering different failure criteria," *Compos. Part B*, vol. 40, no. 8, pp. 731–740, 2009.

[62] M. Muttashar, A. Manalo, W. Karunasena, and W. Lokuge, "Flexural behaviour of multi-celled GFRP composite beams with concrete infill : Experiment and theoretical analysis," *Compos. Struct.*, vol. 159, pp. 21–33, 2017.

[63] S. Amministrativa, I. I. Indirizzo, E. Ciclo, P. C. Coordinatore, and L. Rossetto, "Aero-Structural Optimization of Vertical Axis Wind Turbines." Ph.D dissertation, Dept. Industrial Eng., University of Padova, Padova, 2016.

[64] A. De Luca and F. Caputo, "A review on analytical failure criteria for composite materials," vol. 4, no. August, pp. 1165–1185, 2017.

[65] Jawaid, M., Thariq, M., & Saba, N. (Eds.). (2018). *Mechanical and Physical Testing of Biocomposites, Fibre-Reinforced Composites and Hybrid Composites*. Woodhead Publishing. [Online]. Available : https://doi.org/10.1016/B978-0-08-102292-4.00007-2.

[66] Kadhim, Hussein, M R Ishak, S M Sapuan, N Yidris, and Arash Fattahi. "Experimental and Numerical Investigation of the Mechanical Behavior of Full-Scale Wooden Cross Arm in the Transmission Towers in Terms of Load-Deflection Test." *Integrative Medicine Research* 9 (4): 7937–46. https://doi.org/10.1016/j.jmrt.2020.04.069, 2020.

[67] A. Alhayek, A. Syamsir, V. Anggraini, Z. C. Muda, and N. M. Nor, "Numerical Modelling of Glass Fiber Reinforced Polymer (GFRP) Cross Arm," *Int. J. Recent Technol. Eng.*, vol. 8, no. 4, pp. 6484–6489, 2019.

APPENDIX A: DETAIL DRAWING OF 275KV GFRP CROSSARM

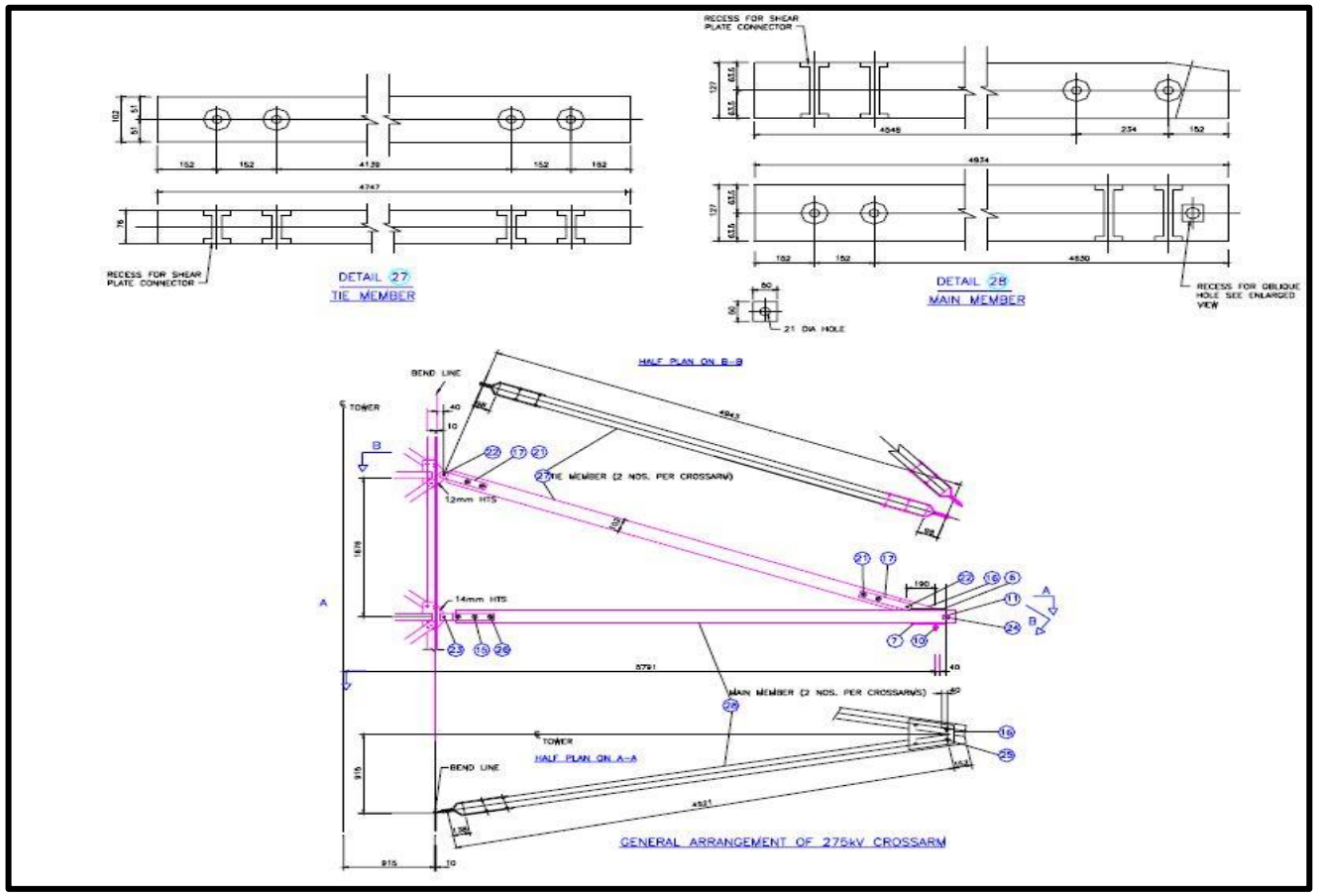

Figure A.1 General Arrangement of 275 kV Composite Crossarm for 24L.

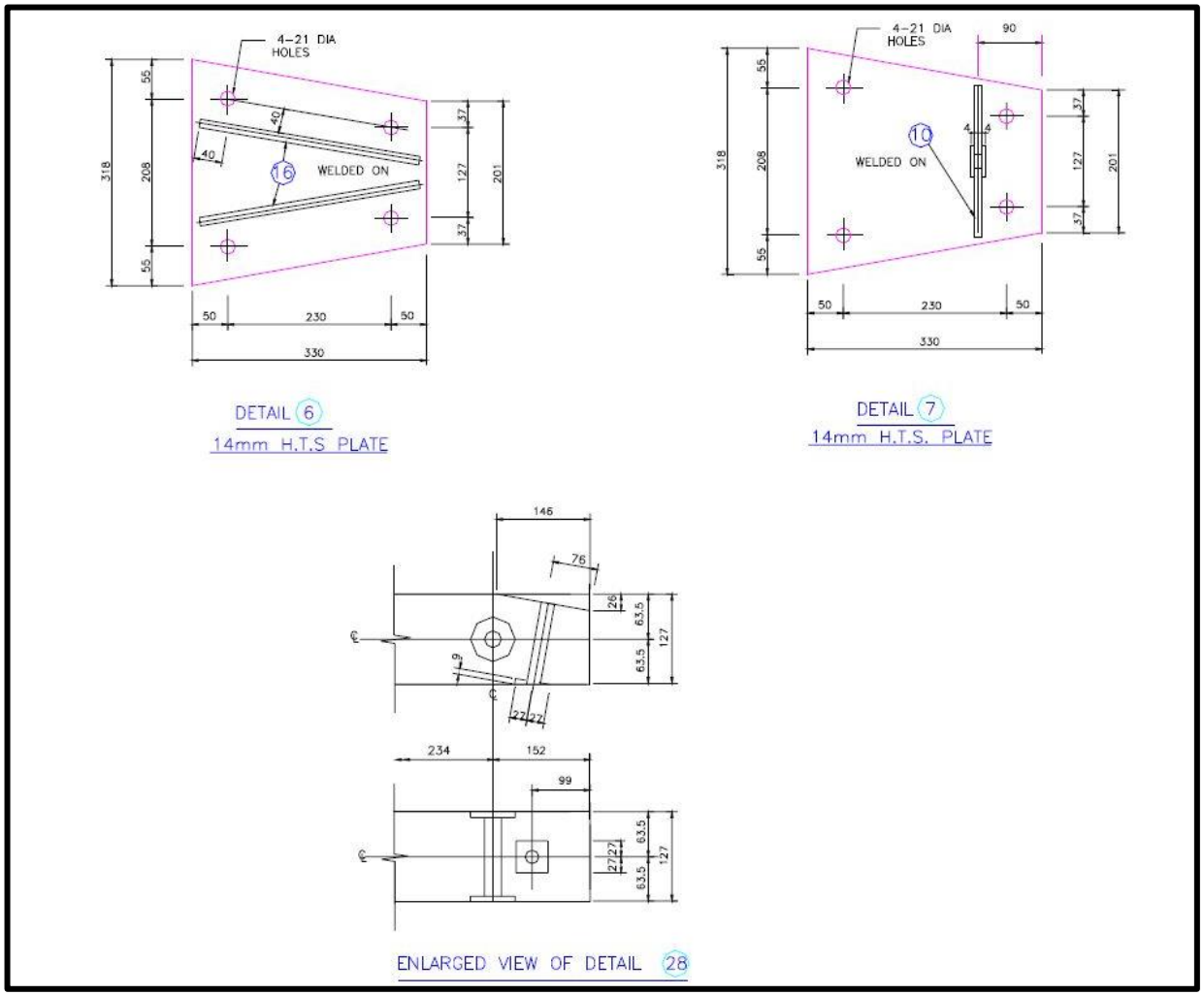

Figure A.2 Detail 6,7 and Enlarged View Detail 28 of 275kV Composite Crossarm.

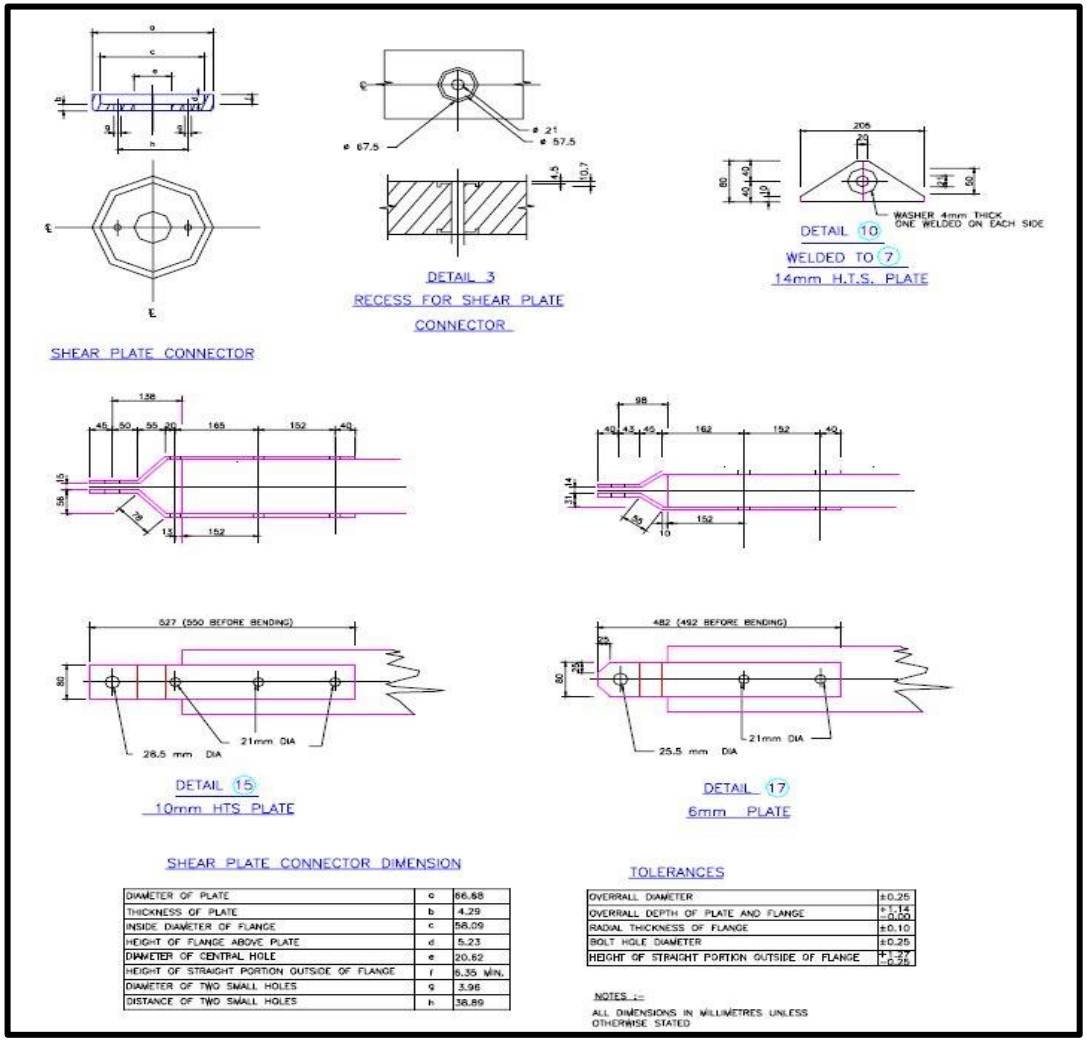

DIAMETER OF PLATE	a	66.68
THICKNESS OF PLATE	b	4.29
INSIDE DIAMETER OF FLANGE	c	58.09
HEIGHT OF FLANGE ABOVE PLATE	d	5.23
DIAMETER OF CENTRAL HOLE	e	20.62
HEIGHT OF STRAIGHT PORTION OUTSIDE OF FLANGE	f	6.35 MIN.
DIAMETER OF TWO SMALL HOLES	g	3.96
DISTANCE OF TWO SMALL HOLES	h	38.89

OVERRALL DIAMETER	±0.25
OVERRALL DEPTH OF PLATE AND FLANGE	+1.14 −0.00
RADIAL THICKNESS OF FLANGE	±0.10
BOLT HOLE DIAMETER	±0.25
HEIGHT OF STRAIGHT PORTION OUTSIDE OF FLANGE	+1.27 −0.25

Figure A.3 Detail Drawing of 275kV Composite Crossarm (Shear Plate Connector).

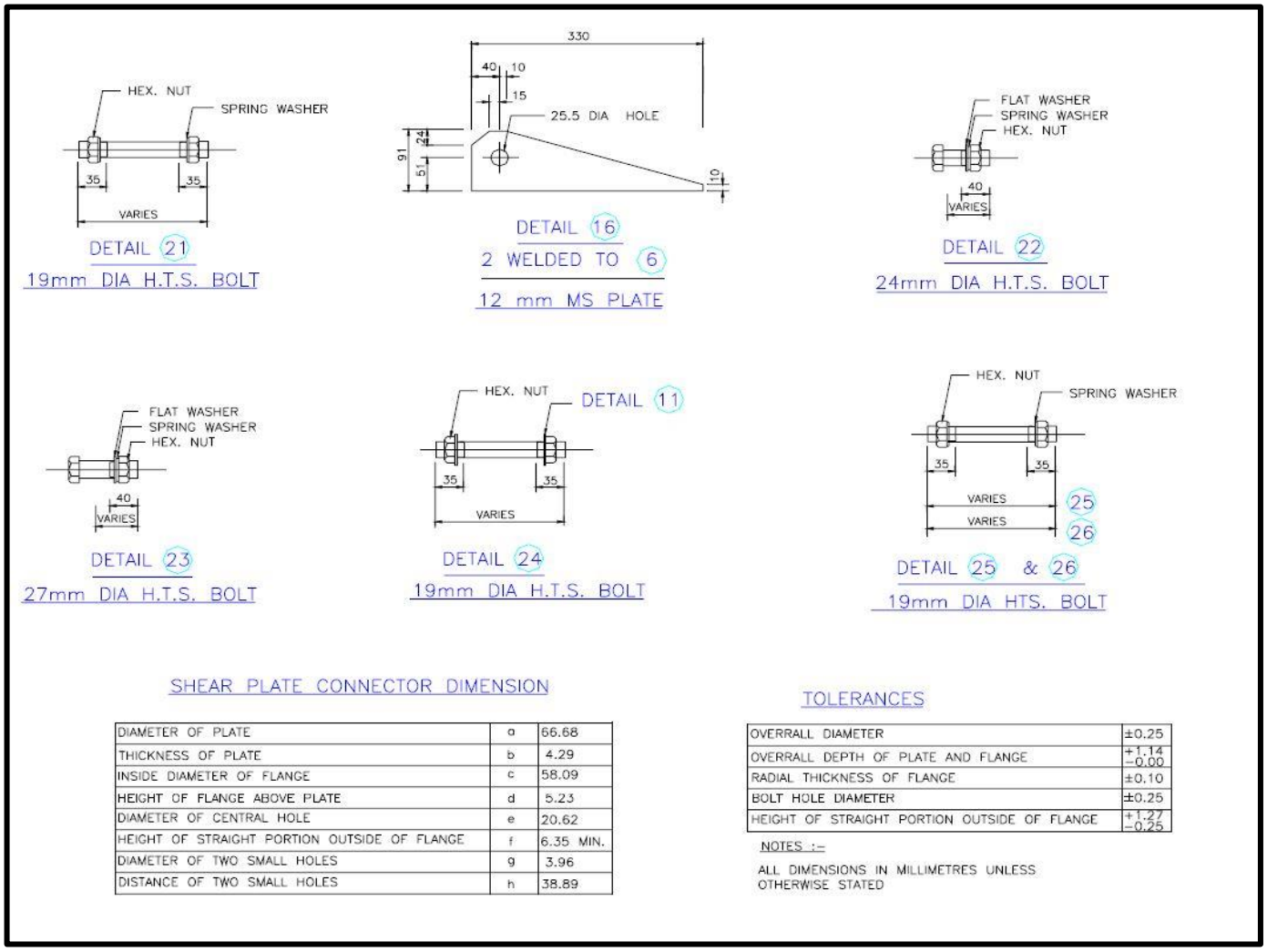

Figure A.4 Detail Drawing of 275kV Composite Crossarm (H.T.S Bolt).